Catalytic Transformation of Greenhouse Gases in a Membrane Reactor

Anil Prabhu

Dissertation submitted to the Faculty of the
Virginia Polytechnic Institute and State University
in partial fulfillment of the requirements for the degree of

DOCTOR OF PHILOSOPHY
in
Chemical Engineering

Dr. S. Ted Oyama, Chair
Dr. David F. Cox
Dr. Richey M. Davis
Dr. Eva Marand
Dr. Brian E. Hanson

March 13, 2003
Blacksburg, VA 24061

Keywords: Dry Reforming, Nickel and Rhodium Catalysts, Membrane Reactor, Vycor Membrane, Hydrogen Selective Nanosil Membrane, Mathematical Model

Catalytic Transformation of Greenhouse Gases in a Membrane Reactor

Anil K. Prabhu

(Abstract)

Supported Ni and Rh catalysts were developed for the reforming of two greenhouse gases, methane and carbon dioxide to syngas (a mixture of hydrogen and carbon monoxide). This is an endothermic, equilibrium limited reaction. To overcome the thermodynamic limitations, a commercially available porous membrane (Vycor glass) was used in a combined reactor-separator configuration. This was to selectively remove one or more of the products from the reaction chamber, and consequently shift the equilibrium to the right. However, the separation mechanism in this membrane involved Knudsen diffusion, which provided only partial separations. Consequently, there was some transport of reactants across the membrane and this led to only marginal improvements in performance. To overcome this limitation, a new membrane was developed by modifying the Vycor substrate by the chemical vapor deposition of a silica precursor. This new membrane, termed Nanosil, provided high selectivity to hydrogen at permeabilities comparable to the support material. Application of this membrane in the combined reactor-separator unit provided higher conversions than that obtained using the Vycor membrane.

ACKNOWLEDGEMENTS

First and foremost, I wish to thank Professor S. Ted Oyama for being my advisor through this journey. He provided the right support and guidance during all times while here at Tech. What I appreciate the most is his welcoming me back with open arms upon return to Tech after a long hiatus to formally complete my dissertation defense. This is something I can never forget and will forever remain indebted to him for this gesture.

My committee members deserve special thanks for providing me with the opportunity to conduct research in this area. I wish to acknowledge the help received from all members to include Professors David Cox, Eva Marand, Richey Davis, Brian Hanson and William Conger. Andy the glassblower deserves special mention for making the membrane tubes.

The laboratory where this work was completed had excellent individuals who assisted me in many ways during my stay. They include Rakesh Radhakrishnan, Todd St. Clair, Wei Li, Balamurugan Dhandapani, Rajat Kapoor, Celine Sayag, Sasanghan Ramanathan, Toby Lucy, Mark Abee, Viviane Schwartz, Paul Clark, and Doohwan Lee. The contributions of Lale Gokbudak, Kristin Jasinkiewicz and Ashley Liu with the mathematical model developed here is also greatfully acknowledged. I will forever cherish the memories of the good times I had in this laboratory.

I dedicate this work to my wife Chitra, who stood by me through all times here in Blacksburg and beyond. Her love, support and understanding deserve special mention and this work would not have been complete without her.

TABLE OF CONTENTS

LIST OF TABLES

LIST OF FIGURES

1. INTRODUCTION

This study deals with two topics of great current importance. The first topic is the catalytic transformation of two greenhouse gases, carbon dioxide and methane, into a commercially important feedstock. The conversion of the reactants in this reaction is, however, limited by thermodynamic equilibrium. Limitations in conversion can be overcome by selective removal of one or more of the product(s) as they are generated. The second topic deals with the testing and development of separation membranes to bring about the selective removal of one of the products, hydrogen, thereby providing improved performance.

1.1 Historical Perspective

The catalytic conversion of CH_4 to synthesis gas or syngas (a mixture of $CO + H_2$) is very important from an industrial point of view since it forms the feedstock for many commercially important processes. Some of the uses for syngas include methanol synthesis and Fischer-Tropsch syntheses for the production of liquid fuels, oxygenates and olefins. The hydrogen in syngas can also be separated and used for other applications such as fuel cells. The steam reforming of methane (1) is the current dominant commercial

$$CH_4 + H_2O \rightarrow CO + 3H_2 \qquad \Delta H^0_{298} = 225.4 \text{ kJ mol}^{-1} \qquad (1)$$

method for the production of syngas [1,2]. However, the poor selectivity for CO is unsuitable for the methanol and Fischer-Tropsch syntheses [3]. The process is operated with excess CO_2 to promote the reverse water-gas shift reaction so as to obtain lower H_2/CO ratios [1,2]. Many researchers [4-16] have focused on the partial oxidation of CH_4 (2) as an alternative route for

$$CH_4 + 0.5O_2 \rightarrow CO + 2H_2 \qquad \Delta H^0_{298} = -22.6 \text{ kJ mol}^{-1} \qquad (2)$$

syngas production. This process has high activity and selectivity towards CO [6,17,18]. However, the exothermic nature of the methane combustion process leads to the generation of localized hot spots in the catalyst bed [19,20]. For example, the use of Co/MgO for the partial oxidation of CH_4 results in high temperatures during reaction [21]. The removal of heat from the reactor is very difficult, particularly from large scale equipment and consequently the process is very difficult to control [19, 20]. A breakthrough in this area was achieved using noble metals on a monolithic support at very short contact time conditions [*22*]. CH_4 reforming with CO_2 (3) offers advantages of more suitable H_2/CO ratios.

$$CH_4 + CO_2 \rightarrow 2CO + 2H_2 \qquad \Delta H^0_{298} = 247 \text{ kJ mol}^{-1} \qquad (3)$$

Fischer and Tropsch [23] were the first to propose this route for methane conversion to syngas. In recent years, there has been renewed interest in studying this reaction as a feasible alternative to other methods of syngas production, particularly with concern over global warming due to the greenhouse effect (see Figure 1.1).

Figure 1.2 from Mackenzie and Mackenzie [24] shows the contribution to the greenhouse effect resulting from anthropogenic activities (contributions from water vapor was not included). It is evident that contributions from methane and carbon dioxide account for three quarters of the total effect. The reforming reaction studied here provides a route to convert these into syngas, an industrially important feedstock. Figure 1.3 shows some of the existing and potential routes for syngas conversion to commercially important chemicals. Cornils [25] has provided a comprehensive list of the current and future potential for syngas conversion.

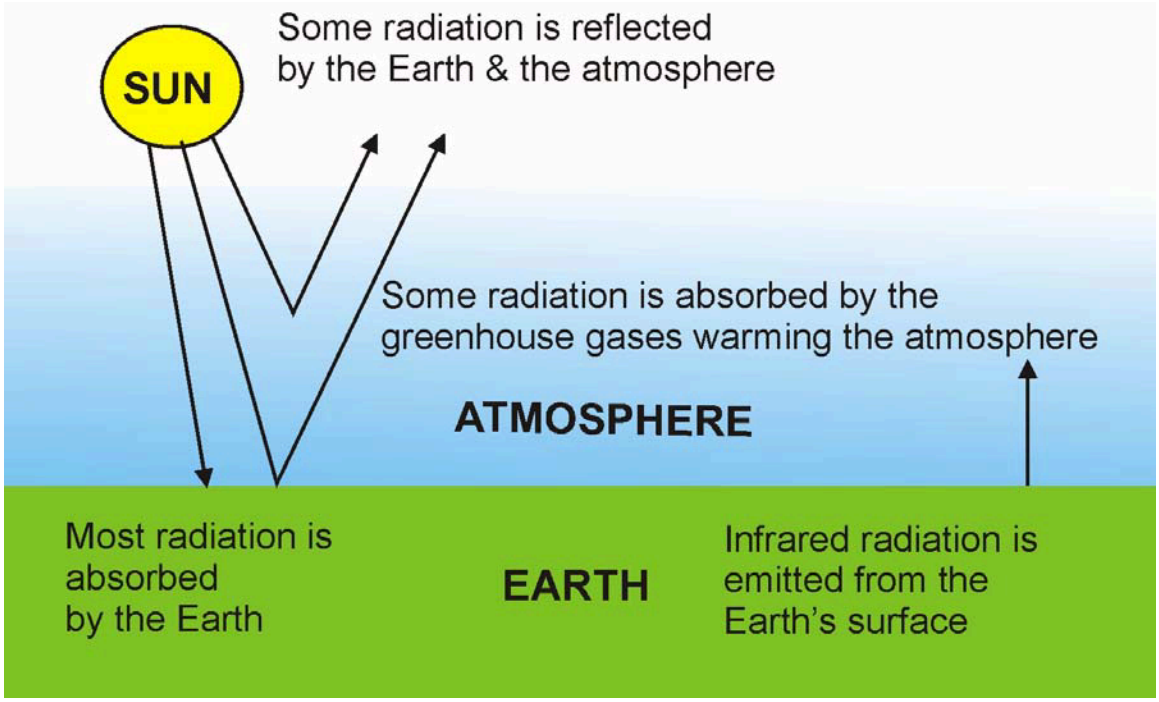

Figure 1.1 The Greenhouse Effect

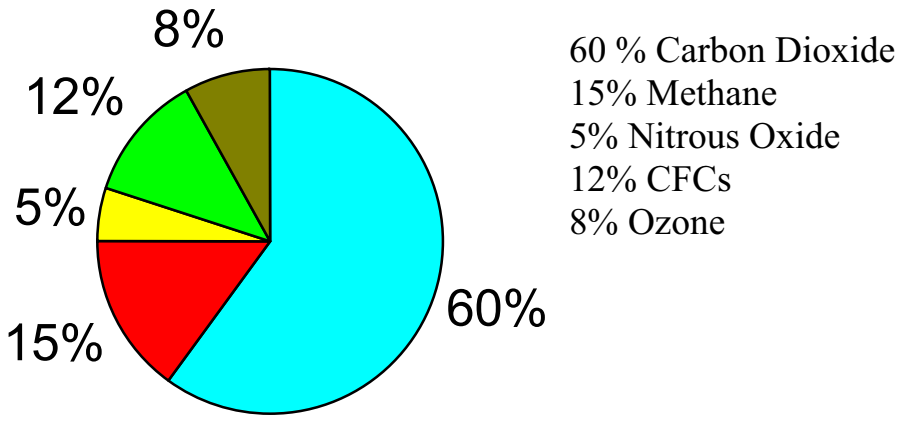

Figure 1.2 Contribution to the Greenhouse Effect

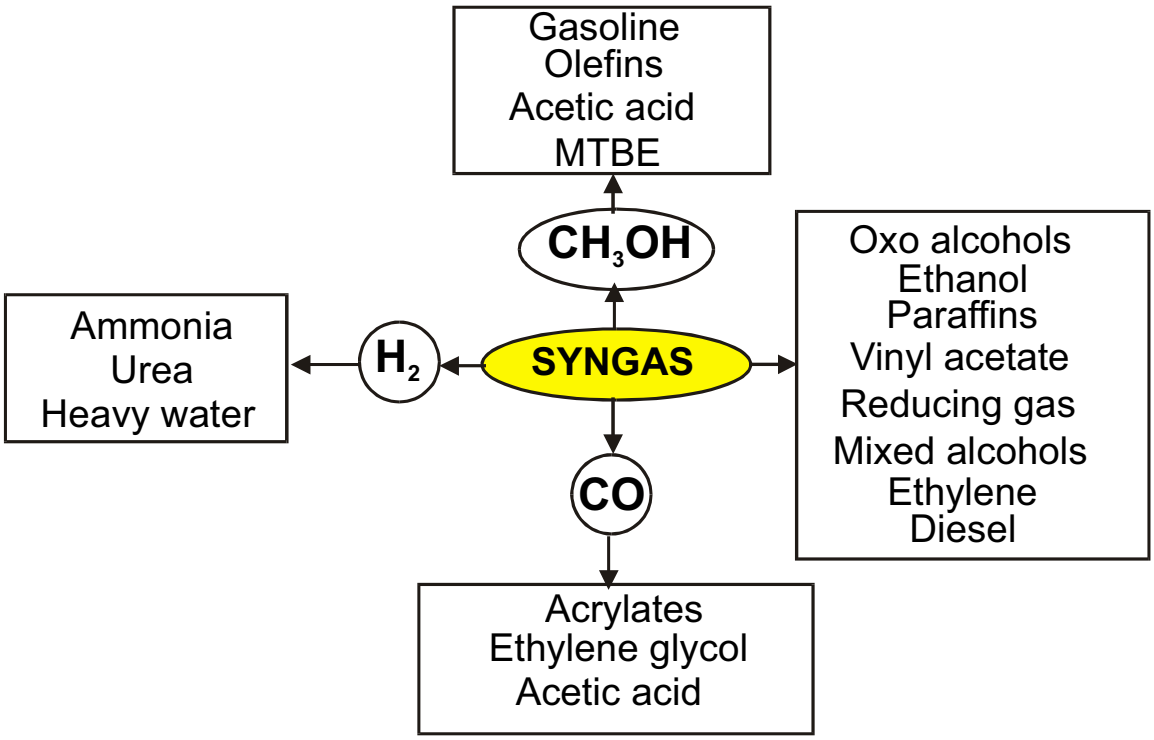

Figure 1.3 Existing and Potential Routes for Syngas Conversion

1.2 Necessity for a Membrane Reactor

The reversibility of the reforming reaction limits the maximum conversion of methane in the fixed bed mode of operation. Equilibrium conversions in such thermodynamically limited reactions can be overcome by the preferential removal of one or more of the products during reaction. In recent years, membrane reactors have become increasingly studied as a means to overcome such equilibrium limitations. They have also been used in applications where controlled introduction of reactant(s) is necessary to reduce hot spots in the catalyst bed or to avoid undesirable side reactions. Membrane reactors offer advantages over conventional fixed bed reactors that include higher energy efficiency, lower capital and operating costs, compact modular construction, low maintenance cost, and ease of scale-up [26]. Hsieh [27,28,29], Armor [30,31], Falconer et al. [32], Saracco and Specchia [33], and Zaman and Chakma [34] have prepared a comprehensive review of publications in the area of ceramic membrane reactors. A summary of membrane applications has been provided by Julbe et al. [35] and Koros and Fleming [36] with discussions about the opportunities that exist for commercialization of existing technologies in the future.

1.3 Prior Research in Methane Reforming

Many researchers have explored the CO_2 reforming of CH_4 for syngas production [18-86]. Several studies have focused on developing Ni and noble metal catalysts for the reforming reaction. Studies have been reported with Ni on several supports like SiO_2 [37,39,54,72,76,77], Al_2O_3 [50,54,63,70,78-82], NaY [54], MgO [3,37,39,68,74], CeO_2 [50], CaO [3], SrO [3], BaO [3], ZrO_2 [39,40,81], La_2O_3 [39,41], TiO_2 [39,76,83], Al_2O_3-SiO_2 [39], K/SiO_2 [39], Cu/SiO_2 [39], MgO-CaO [46], activated carbon [37], zeolite and zeolite promoted with K or Ca [84] and perovskites [73]. Co and Fe have been utilized on TiO_2 [66,76] and SiO_2 [44,76] while only Co has been used on MgO [44,57]and CaO [44]. Supported noble metal catalysts studied included Ir on Al_2O_3 [85], TiO_2 [76], Rh on Al_2O_3[41,44,83,85,86], ZrO_2 [41], ZrO_2/SiO_2[85], yttria-stabilized ZrO_2 [86], TiO_2 [41,76,83,86], SiO_2[41,76,83,86], La_2O_3 [41,69,86], MgO [41,69,83,86], Y_2O_3 [41,69], Ta_2O_5 [41,69], CeO_2 [41], and Nb_2O_5 [41], Ru on Al_2O_3 [44,71,75], TiO_2 [75,76], C[75], La_2O_3 [71], Y_2O_3 [71], ZrO_2 [71], ZrO_2/SiO_2 [85], NaY [64], HY [64], Pd on NaY [54], SiO_2 [76], TiO_2 [76], Pt on NaY [54], TiO_2 [67,76], ZrO_2 [44,51,61,65,67,81], SiO_2 [76], CeO_2 [51], Al_2O_3 [44,51,52,65,67,72,81] and ZrO_2/Al_2O_3 [65]. β - Mo_2C and WC have also been used for this reaction [87]. Many investigators have reported low stability of the Ni catalysts and deactivation due to carbon deposition for poorly dispersed catalysts [3,37,39,77-82,84]. Noble metal catalysts were usually less sensitive to coking [44,54,65,67,81,83,85,86]. However, deactivation has been observed on a Pt/Al_2O_3 catalyst [44,51,52,65,67,81] and a similar loss of activity over time has been reported for Rh on CeO_2 [41], Nb_2O_5 [41], ZrO_2 [41], TiO_2 [41,86]and MgO [86]. Excellent stability and activity of Mo_2C has been reported [87] but only at high pressures (8 bar). Good activity has been obtained with Pt, Pd and Rh promoted $Ni_{0.03}Mg_{0.97}O$ [88]. To address some of the activity and deactivation issues, recent research has focused on incorporating promoters into traditional supported catalysts. The promoters have included $CoAl_2O_4$ on Pt/Al_2O_3 [60], MgO on Ru/C [56], Na_2O [70], MgO [70], MgO/CeO_2 [63], CaO [70], La_2O_3 [70], and CeO_2 [70] on Ni/Al_2O_3, Y_2O_3 [50] on Ni/CeO_2, CeO_2 [51,61] and La_2O_3 [61] on Pt/ZrO_2, Mordenite on Ru/CeO_2 [37] and Rh on Ni-Pt/Ce_2O_3 [49]. The picture here was mixed too, with some reporting better performance with the addition of promoters [37,49,50,51,56,60,61,63,70], while others reported deterioriation or no improvements with addition of Na_2O [70], MgO [70] and Y_2O_3 [50]. Comprehensive summaries of catalysts used in the carbon dioxide reforming of methane has been reported [89-92]. A main conclusion from these studies is that most of the current nickel catalysts have been ineffective primarily due to their coking and subsequent deactivation of the catalysts. The results from studies with noble metal catalysts have provided a mixed picture. Some have deactivated (mostly platinum) while others were reasonably resistant to coking.

1.4 Present Work

In the first part of this study, the suitability of two Ni based catalysts (5 wt. % Ni/MgO and 2 wt. % Ni/La_2O_3) and a Rh based (1 wt. % Rh/Al_2O_3) catalyst was investigated for the methane reforming reaction. Our study focused on developing high activity catalysts which are resistant to coking and do not deactivate with time. The conversions were chosen to be at or close to thermodynamic equilibrium levels to test the effect of a membrane to overcome these limitations.

The details are provided in Chapter 2 titled “Catalyst Development and Testing”. In the second part of this study, a commercially available porous Vycor glass was tested in a reactor-separator configuration. This was to selectively remove one or more of the products and bring about a shift in thermodynamic equilibrium with the possibility of improved methane conversions. The details are provided in Chapter 3 titled “Permeable Membrane Reactor Studies”. To overcome the limitations of the Vycor membrane, several attempts were made to modify the selectivity of this substrate. A new membrane termed Nanosil was developed which proved to be the culmination of our efforts to develop a selective yet highly permeable membrane. Incorporation of this new membrane in the reactor-separator configuration provided improved performance. The details are provided in Chapter 4 titled “New Membrane Development and Testing”. A mathematical model was developed to simulate the operation of the three different reactor configurations employed here: fixed bed, Vycor membrane and Nanosil membrane. Theoretical results were compared to experimental results from Chapters 2-4. The details are provided in Chapter 5 titled “Mathematical Model Development”. Conclusions and suggestions for future work are listed in Chapter 6 titled “Conclusions and Future Work”.

REFERENCES:

[1] D. L. Trimm, Catal. Rev.-Sci. Eng. 16 (1977) p. 155.
[2] J. R. Rostrup-Nielsen, in J. R. Anderson, M. Boudart (Eds.), Catalysis Science and Technology, Springer, NY, USA Vol. 5 (1984) p. 1.
[3] E. Ruckenstein, Y. H. Hu, Appl. Catal. A: 133 (1995) p. 149.
[4] V. R. Choudhary, S. D. Samsare, A. S. Mammam, Appl. Catal. A: 90 (1992) p. L1.
[5] R. H. Jones, A. T. Ashcroft, D. Waller, A. K. Cheetham, J. M. Thomas, Catal. Lett. 8 (1991) p. 169.
[6] D. A. Hickman, L. D. Schmidt, Science 259 (1993) p. 343.
[7] A. T. Ashcroft, A. K. Cheetham, J. S. Foord, M. L. H. Green, C. P. Grey, A. J. Murrell, P. D. F. Vernon, Nature 344 (1990) p. 319.
[8] V. R. Choudhary, A. M. Rajput, B. J. Prabhakar, J. Catal. A: 139 (1993) p. 326.
[9] Y. H. Hu, C. T. Au, H. L. Wan, Chin. Sci. Bull. 40(4) (1995) p. 303.
[10] Y. H. Hu, E. Ruckenstein, Catal. Lett. 34 (1995) p. 41.
[11] C. T. Au, Y. H. Hu, H. L. Wan, Catal. Lett. 27 (1992) p. 199.
[12] D. Dissanayake, M. P. Rosynek, K. C. C. Kharas, J. H. Lunsford, J. Catal. 132 (1991) p. 117.
[13] J. K. Hochmuth, Appl. Catal. B: 1 (1992) p. 89.
[14] P. D. F. Vernon, M. L. H. Green, A. K. Cheetham, A. T. Ashcroft, Catal. Lett. 6 (1990) p. 181.
[15] M. G. Poirier, J. Trudel, D. Guay, Catal. Lett. 21 (1993) p. 99.
[16] P. M. Torniainen, X. Chu, L. D. Schmidt, J. Catal. 146 (1994) p. 1.
[17] S. Tenner, Hydrocarb. Proc. 66(7) (1987) p. 52.
[18] A. T. Ashcroft, A. K. Cheetham, M. L. H. Green, P. D. F. Vernon, Nature 352 (1991) p. 225.
[19] D. Dissanayake, M. P. Rosynek, L. H. Lunsford, J. Phys. Chem. 97 (1993) p. 3644.
[20] V. R. Choudhary, A. M. Rajput, B. P. Prabhakar, Angew. Chem. Int. Ed. Engl. 33 (1994) p. 2104.
[21] Y. F. Chang, H. Heinemann, Catal. Lett. 21 (1993) p. 215.
[22] M. Huff, L. D. Schmidt, J. Catal. 149 (1994) p. 127.
[23] F. Fischer, H. Tropsch, Brennstoff Chem. 3(9) (1928) p. 39.
[24] Mackenzie, F. T. and Mackenzie, J. A., Our Changing Planet, Prentice-Hall, Upper Saddle River, NJ, USA (1995) p. 288.
[*25*] B. Cornils, Chemicals from Coal: New Processes, Ed. K. R. Payne in Technical Reports on Applied Chemistry, John Wiley & Sons, Chicester, Great Britain Vol. 14 (1987) p. 4.
[26] A. Sengupta, K. K. Sircar, in R. D. Noble, S. A. Stern (Eds.), Membrane Separations Technology, Principles and Applications, Elsevier Science, Amsterdam (1995) p. 499.
[27] H. P. Hsieh, AIChE Sym. Series 84(261) (1988) p. 1.
[28] H. P. Hsieh, Catal. Rev.-Sci. Eng. 33 (1991) p. 170.
[29] H. P. Hsieh, Inorganic Membranes for Separation and Reaction, Elsevier Science, Amsterdam (1996).
[30] J. N. Armor, Appl. Catal. 49 (1989) p. 1.

[31] J. N. Armor, Catal. Today 25 (1995) p. 199.
[32] J. L. Falconer, R. D. Noble and D. P. Sperry, Catalytic membrane reactors, in R. D. Noble and S. A. Stern (Eds.), Membrane Separations Technology, Principles and Applications, Elsevier Science B. V. (1995) p. 669.
[33] G. Saracco, V. Specchia, Catal. Rev.-Sci. Eng. 36 (1994) p. 305.
[34] J. Zaman, A. Chakma, J. Memb. Sci. 92 (1994) p. 1.
[35] A. Julbe, D. Farrusseng, C. Guizard, J. Memb. Sci. 181 (2001) p. 3.
[36] W. J. Koros, G. K. Fleming, J. Memb. Sci. 83 (1993) p.1.
[37] K. Hashimoto, S. Watase, N. Toukai, Catal. Lett. 80 (2002) p. 147.
[38] M. C. J. Bradford, M. A. Vannice, Appl. Catal. A: 142 (1996) p. 73.
[39] J. Wei, B. Xu, J. Li, Z. Cheng, Q. Zhu, Appl. Catal. A: 196 (2000) p. L167.
[40] H. M. Swaan, V. C. H. Kroll, G. A. Martin, C. Mirodatos, Catal. Today 21 (1994) p. 571.
[41] H. Wang, E. Ruckenstein, Appl. Catal. A: 204 (2000) p. 143.
[42] V. A. Tsaipouriari, X. E. Verykios, Catal. Today 64 (2001) p. 83.
[43] Z. Zhang, X. E. Verykios, Appl. Catal. A: 138 (1996) p. 109.
[44] K. Nagaoka, K. Seshan, J. A. Lercher, K. Aika, Catal. Lett. 70 (2000) p. 109.
[45] J. T. Richardson, S. A. Paripatyadar, Appl. Catal. 61 (1990) p. 293.
[46] K. Hwang, H. Y. Zhu, G. Q. Lu, Catal. Today 68 (2001) p. 183.
[47] O. Yamazaki, T. Nozaki, K. Omata, K. Fujimoto, Chem. Lett. (1992) p. 1953.
[48] A. M. Gadalla, M. E. Sommer, Chem. Eng. Sci. 44 (1989) p. 2825.
[49] T. Inui, Catal. Today 51 (1999) p. 361.
[50] J. B. Wang, Y. Tai, W. Dow, T. Huang, Appl. Catal. A: 218 (2001) p. 69.
[51] F. B. Noronha, E. C. Fendley, R. R. Soares, W. E. Alvarez, D. E. Resasco, Chem. Engg. J. 82 (2001) p. 21.
[52] K. Nagaoka, K. Seshan, K. Aika, J. A. Lercher, J. Catal. 197 (2001) p. 34.
[53] A. M. Gadalla, B. Bower, Chem. Eng. Sci. 43 (1988) p. 3049.
[54] G. J. Kim, D. S. Cho, K. H. Kim, J. H. Kim, Catal. Lett. 28 (1994) p. 41.
[55] J. S. Chang, S. E. Park, K. W. Lee, M. J. Choi, Stud. Surf. Sci. Catal. 84 (1994) p. 1587.
[56] Y. Schuurman, C. Mirodatos, P. Ferreira-Aparicio, I. Rodriguez-Ramos, A. Guerrero-Ruiz, Catal. Lett. 66 (2000) p. 33.
[57] H. Y. Wang, E. Ruckenstein, Appl. Catal. A: 209 (2001) p. 207.
[58] E. Ruckenstein, H. Y. Wang, Catal. Lett. 73 (2001) p. 99.
[59] Z. Zhang, X. E. Verykios, Chem. Soc., Chem. Commun. (1995) p. 71.
[60] L. Mo, Xiaoming, C. Huang, J. Fei, Catal. Lett. 80 (2002) p. 165.
[61] S. M. Stagg-Williams, F. B. Noronha, G. Fendley, D. E. Resasco, J. Catal. 194 (2000) p. 240.
[62] S. Sharma, S. Hilaire, J. M. Vohs, R. J. Gorte, H. W. Jen, J. Catal. 190 (2000) p. 199.
[63] R. G. Ding, Z. F. Yan, Catal. Today 68 (2001) p. 135.
[64] U. L. Portugal Jr., C. M. P. Marques, E. C. C. Araujo, E. V. Morales, M. V. Giotto, J. M. C. Bueno, Appl. Catal. A: 193 (2000) p. 173.
[65] M. M. V. M. Souza, D. A. G. Aranda, M. Schmal, J. Catal. 204 (2001) p. 498.
[66] K. Nagaoka, K. Takanabe, K. Aika, Chem. Comm. (2002) p. 1006.
[67] J. H. Bitter, K. Seshan, J. A. Lercher, J. Catal. 183 (1999) p. 336.
[68] K. Tomishige, Y. Chen, K. Fujimoto, J. Catal. 181 (1999) p. 91.
[69] E. Ruckenstein, H. Y. Wang, J. Catal. 190 (2000) p. 32.

[70] S. Wang, G. Q. Lu, J. Chem. Tech. and Biotech. 75 (2000) p. 589.
[71] N. Matsui, K. Anzai, N. Akamatsu, K. Nagakawa, N. Ikenaga, T. Suzuki, Appl. Catal. A: 179 (1999) p. 247.
[72] M. Ito, T. Tagawa, S. Goto, Appl. Catal. A: 177 (1999) p. 15.
[73] T. Hayakawa, S. Suzuki, J. Nakamura, T. Uchijima, S. Hamakawa, K. Suzuki, T. Shishido, K. Takehira, Appl. Catal. A: 183 (1999) p. 273.
[74] B. Xu, J. Wei, H. Wang, K. Sun, Q. Zhu, Catal. Today 68 (2001) p. 217.
[75] M. C. J. Bradford, M. A. Vannice, J. Catal. 183 (1999) p. 69.
[76] M. C. J. Bradford, M. A. Vannice, Catal. Today 50 (1999) p. 87.
[77] T. Sodesawa, A. Dobaschi, F. Nozaki, React. Kinet. Catal. Lett. 12 (1979) p. 107.
[78] T. A. Chubb, Solar Energy 24 (1980) p. 341.
[79] T. A. Chubb, J. H. McCrary, G. E. McCrary, J. J. Nemecek, D. E. Simmons, Proc. Meet. Am. Sect. Int. Sol. Eng. Soc. 4 (1981) p. 166.
[80] R. Blom, I. M. Dahl, A. Slagtern, B. Sortland, A. Spjelkavik, E. Tangstad, Catal. Today 21 (1994) p. 535.
[81] K. Seshan, H. W. ten Barge, W. Hally, A. N. J. van Keulen, J. R. H. Ross, in H. E. Curry-Hide, R. F. Howe (Eds.), Natural Gas Conversion II, Elsevier Science B. V. (1994) p. 285.
[82] Y. Sakai, H. Saito, T. Sodesawa, F. Nozaki, React. Kinet. Catal. Lett. 24 (1984) p. 253.
[83] A. Erdöhelyi, J. Cserenyi, F. Solymosi, J. Catal. 141 (1993) p. 287.
[84] J. Chang, S. Park, H. Chon, Appl. Catal. A: 145 (1996) p. 111.
[85] M. F. Mark, W. F. Maier, J. Catal. 164 (1996) p. 122.
[86] Z. L. Zhang, V. A Tsipouriari, A. M. Efstathiou, X. E. Verykios, J. Catal. 158 (1996) p. 51.
[87] A. P. E. York, J. B. Claridge, A. J. Brungs, S. C. Tsang, M. L. H. Green, Chem. Comm. (1997) p. 39.
[88] Y. Chen, O. Yamazaki, T. Tomishige, K. Fujimoto, Catal. Lett. 39 (1996) p. 91.
[89] S. Wang, G. Q. Lu, G. J. Millar, Energy and Fuels 10 (1996) p. 896.
[90] R. Ding, Z. Yan, L. Linhua, X. Liu, J. Nat. Gas Chemistry 10(3) (2001) p. 237.
[91] M. C. J. Bradford, M. A. Vannice, E. Ruckenstein, Cat. Rev.-Sci. and Engg. 41(1) (1999) p. 1.
[92] G. Q. Lu, S. Wang, Chem. Tech. 29(1) (1999) p. 37.

2. CATALYST DEVELOPMENT AND TESTING

2.1 Introduction

CH_4 reforming with CO_2 (1) offers advantages of high CO selectivity as discussed in Chapter 1. The reaction is also highly endothermic and is favored by high temperatures and low pressures (see Figure 2.1). From the stoichiometry of reaction (1), a H_2/CO ratio of 1.0 is expected.

$$CH_4 + CO_2 \rightarrow 2CO + 2H_2 \qquad \Delta H^0_{298} = 247 \text{ kJ mol}^{-1} \qquad (1)$$

But the reverse water-gas shift reaction (RWGS) (2),

$$CO_2 + H_2 \rightarrow CO + H_2O \qquad \Delta H^0_{298} = 41 \text{ kJ mol}^{-1} \qquad (2)$$

which occurs in parallel with the methane reforming reaction, leads to H_2/CO ratios being less than 1.0. The occurrence of the RWGS reaction has been confirmed in several studies [1-18]. Different hydrogen to carbon monoxide ratios for different catalysts have been reported [5]. At low methane conversions, the H_2/CO ratio was less than one and at higher methane conversions, this ratio approached unity. It was concluded that the activity of the catalyst for the reaction controls the RWGS and hence the final product composition. It has also been reported that at lower temperatures, the ratio was less than 1.0 due to the RWGS reaction [10]. The results of two studies [12,19] however, are contradictory to other investigations. It is claimed that no contribution from the RWGS reaction [1013 K - 1053 K] occurs on supported Ni and noble metals.

In the first part of this project, the suitability of two Ni based catalysts, $Ni_{0.03}Mg_{0.97}O$ (designated here as 5 wt. % NiMgO) and 2 wt. % Ni/La_2O_3, was investigated for the methane reforming reaction. A 1 wt. % Rh/Al_2O_3 catalyst was also included in the study because of its high activity and resistance to coking. $Ni_{0.03}Mg_{0.97}O$ [20] was reported to be tolerant to coking, while the Ni/La_2O_3 catalyst produced mixed results. One study [5] reported coking and subsequent deactivation while another [21] reported no appreciable deactivation. Our study focused on testing high activity catalysts which are resistant to coking and do not deactivate with time. This study did not test the effects of different operational parameters on reactor efficiency. High conversions, close to equilibrium, were chosen in order to more readily assess the occurrence of coking. Also, the latter part of the study (incorporation of a membrane) required operation close to equilibrium conditions.

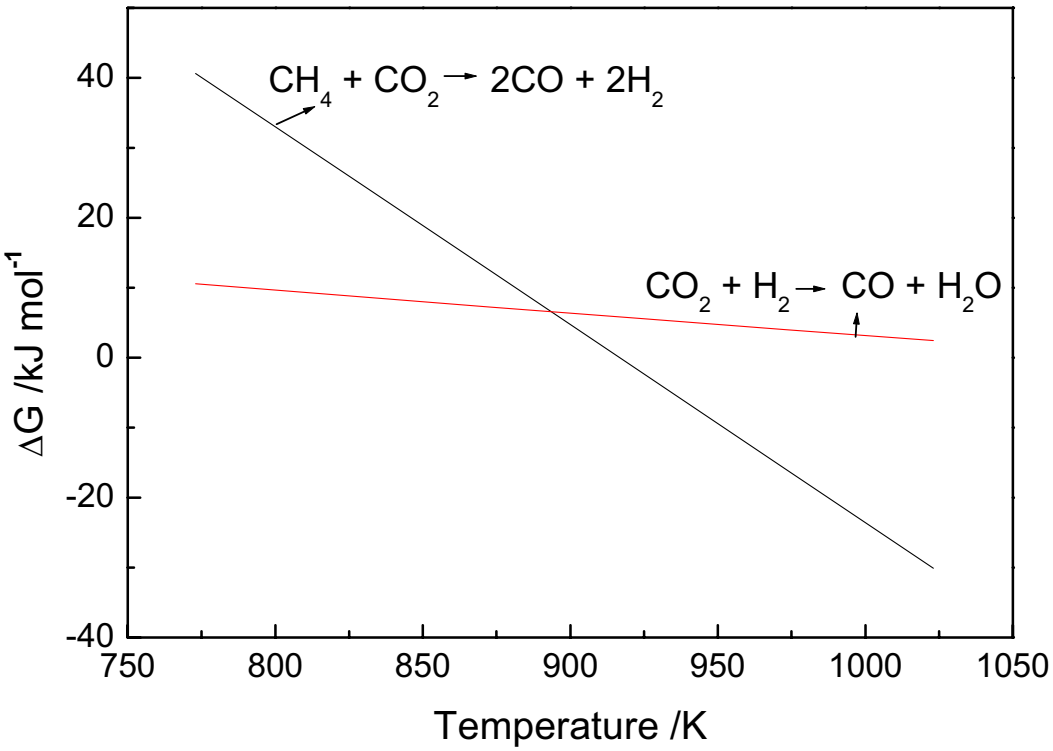

Figure 2.1 Thermodynamics of the Reforming and RWGS Reactions

2.2 Catalyst Preparation

A Ni/MgO catalyst was prepared as reported by Fujimoto's group [22] in Japan. It was a solid solution with a composition of $Ni_{0.03}Mg_{0.97}O$ and corresponded to 5 wt. % Ni (hence designated as 5 wt. % Ni/MgO). Both designations are used to represent this catalyst in this dissertation. It was prepared by co-precipitating an aqueous solution of nickel acetate and magnesium nitrate with potassium carbonate, in which the concentrations of nickel ion, magnesium ion and potassium ion were 0.02 M, 0.59 M and 0.61 M respectively. The solution was maintained at 348 K for 1 h to complete the precipitation. The filtered precipitate was washed with deionized water at 353 K, dried overnight at 393 K, and finally calcined in air at 1123 K for 10 h. The catalyst was pelletized and sieved to 30/120 mesh (0.6-0.12 mm).

The Ni/La_2O_3 was prepared by the wet impregnation technique using lanthanum oxide (Alfa, 99.99%) and nickel nitrate hexahydrate (Alfa, 99.99%). For the 2 wt. % catalyst, 2.0 g of nickel nitrate hexahydrate was dissolved in 10 cm^3 of water. This was added to 19.7 g of La_2O_3 with constant stirring. The mixture was dried at 403 K (β = 0.03 K s^{-1}, 18 h soak) and calcined at 773 K (β = 0.03 K s^{-1}, 6 h soak) in a muffle furnace (NEY, Vulcan 3-550). The catalyst was pelletized and sieved as described above.

The nominal 0.8 wt. % (designated in the rest of the document as 1 wt. %) Rh/Al_2O_3 catalyst was prepared by the incipient wetness technique using 0.11 g of $RhCl_3 \bullet 3H_2O$ (99.9 % Alfa-Aesar) dissolved in 6.1 cm^3 of distilled water and 4.97 g of Al_2O_3 (Aluminumoxid C, Degussa, calcined to 1173 K). The mixture was dried at 383 K (β = 0.08 K s^{-1}, 2 h soak) and calcined at 723 K (β = 0.08 K s^{-1}, 3 h soak) in a muffle furnace (NEY, Vulcan 3-550). The catalyst was pelletized and sieved as described above.

2.3 Catalyst Characterization

The specific surface area (S_g) of the catalysts and supports was determined in a Micromeritics ASAP 2000 series volumetric unit. The sample (typically 0.2-0.5 g) was first degassed at 473 K in vacuum for 2 h. It was then cooled and transferred in the sample holder to the analysis station without exposure to air. A standard 5 point BET using P/P_0s of 0.05, 0.1, 0.15, 0.2, and 0.3 was selected from the analysis software. Hydrogen and CO chemisorption were also measured in this volumetric unit using a high temperature of pretreatment identical to the highest employed in the reactivity determination. The process involved evacuating the sample at 1123 K (1023 K for Ni/La_2O_3 and 723 K for Rh/Al_2O_3) in vacuum, flowing H_2 at 1123 K (as listed above for the other two catalysts) to reduce the nickel, evacuating the reactor at 1023 K to remove residual H_2, and dosing H_2 or CO in two steps at 308 K. The first step measured both strong (irreversible) and weak (reversible) sorption data in combination, while the second step measured only the weak sorption by the sample. The difference between the two measurements was the uptake of the given sample. These measurements were performed on the supports and the catalyst samples before and after reaction.

X-ray diffraction was used to determine the crystalline phases for all the fresh and spent catalyst samples. An ASC (007 model) diffractometer using CuK_α radiation (45 kV, 40 mA) was used to scan the samples from 2θ angles of 10° to 110° degrees at a rate of 2° min^{-1}. Elemental analysis was conducted using the elemental analyzer (Carlo Erba EA 1108 Elemental Analyzer), which consisted of a combustion train coupled with a gas chromatograph and a packed column (Porapak QS).

2.4 Experimental Details

The reactor assembly (Figure 2.2) consisted of two concentric quartz tubes with the catalyst packed in a 4 cm section on the outer shell side to allow for good heat transfer. The larger external tube had an outside diameter of 16 mm with a wall thickness of 1 mm. The inner tube had an outside diameter of 10 mm and a wall thickness of 1 mm. The shell and tube sides were isolated from each other by Swagelock fittings equipped with Teflon fittings. Appropriate conduits using 1/8" tubing were welded on to the fittings for introducing feed gases and removing the outlet stream. The central part of the reactor was heated in a tubular furnace

(Hoskins) while the Swagelock fittings were kept outside and cooled with fans. A schematic of the experimental system is also shown in Figure 2.2. For some initial experiments, gas flow was controlled using calibrated capillary restrictors. Mass flow controllers (Brooks model 5850E) were later used to obtain more accurate flow control. Shell and tube side pressure was monitored using pressure gauges. Pure Ar (AIRCO, 99.999%) was passed through a gas purifier (AllTech) to remove moisture, oil and other impurities. CH_4 (AIRCO, 99.99%) was purified from possible sulfur impurities using Ni on calcium silicate/bentonite clay/alumina support (Ni-3266 E 1/16, Engelhard Corp), activated according to the manufacturer's directions. CO_2 (AIRCO, 99.99%)

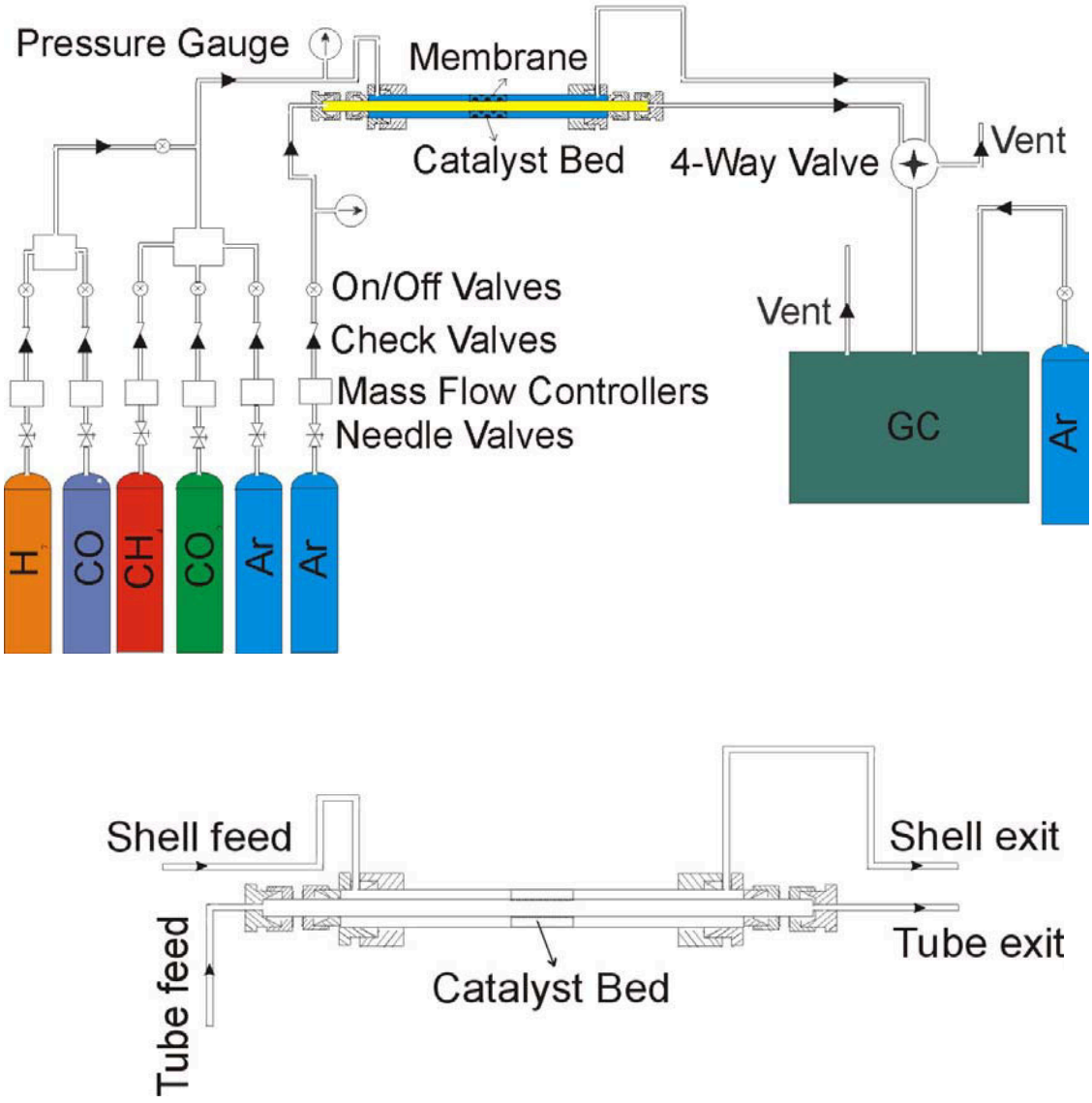

Figure 2.2 Experimental Set-up

was purified using an indicating Oxy-Trap (Alltech). A mixture of Ar, CH_4 and CO_2 was the inlet feed to the shell side. The outlet gases were separated using a Carbosphere packed column (Alltech) and analyzed online using a gas chromatograph (SRI 8610B).

Typically, a quantity of 0.5 g of catalyst (30/120 mesh) was mixed with an appropriate amount of quartz chips (30/120 mesh) to make up the 4 cm bed on the shell side. The reactor was then sealed with the Swagelock fittings. A leak test was performed by pressurizing the shell side to 10 psi (and tube side for membrane studies) and making sure that the pressure did not drop over 2 h. The catalyst was first heated to the highest temperature used in the studies (1123, 1023, and 773 K for Ni/MgO, Ni/La_2O_3 and Rh/Al_2O_3 respectively) with only the Ar flow (27 μmol s^{-1}), then reduced in H_2 (24 μmol s^{-1}) for 0.5 h (Flow rates in μmol s^{-1} can be converted to cm^3 (NTP) min^{-1} by multiplication by 1.5). The feed consisting of CH_4 (24 μmol s^{-1}), CO_2 (24 μmol s^{-1}), and Ar (27 μmol s^{-1}) was then introduced at the high temperature. GC traces of the outlet gases were taken periodically until the CH_4 conversion indicated a steady-state value and this process was repeated for lower temperatures.

Tests were also conducted to demonstrate the stability of these catalysts tested above. Initially, tests were conducted at the highest temperature and reactor exit gases sampled regularly to determine reactant conversion. The temperature was then changed to the next lower value and sampling was conducted as above. This was repeated for several different temperatures. Finally, the reactor temperature was raised to the initial value and reactant conversion calculated as above to determine any loss in activity after cycling through the range of temperatures.

2.5 Results and Discussion

The BET specific surface areas (S_g) of the supports and catalysts used in this study are reported in Table 2.1 Due to the high temperature of calcination, the S_g values are moderately small except for the Rh catalyst due to the high initial surface area of the Al_2O_3 support. The surface areas of the samples decreased after reaction due to sintering at the high temperatures of reaction. The catalysts were exposed to the highest temperature at the start of the measurement, and activity remained stable, indicating that the loss of S_g probably occurred during the activation period.

Table 2.1 Specific Surface Area (S_g) results from N_2 Physisorption

Sample	Ni (wt. %)	S_g (Before Rxn) ($m^2\ g^{-1}$)	S_g (After Rxn) ($m^2\ g^{-1}$)
MgO	0	26	22
La_2O_3	0	15	4
Al_2O_3	0	99	87
$Ni_{0.03}Mg_{0.97}O$	5	25	22
Ni/La_2O_3	2	9	2
Rh/Al_2O_3	1	91	74

The CO and H_2 chemisorption measurements are summarized in Tables 2.2 and 2.3.

Table 2.2 CO Uptake Determinations

Sample	Ni (wt. %)	Reduction Temperature (K)	Uptake (Before Rxn) ($\mu mol\ g^{-1}$)	Uptake (After Rxn) ($\mu mol\ g^{-1}$)
MgO	0	1123	0.1	0.0
La_2O_3	0	1023	5.7	0.0
Al_2O_3	0	723	0.0	0.0
$Ni_{0.03}Mg_{0.97}O$	5	1123	0.2	0.0
Ni/La_2O_3	2	1023	61.0	3.2
Rh/Al_2O_3	1	723	60	48

Table 2.3 H_2 Uptake Determinations

Sample	Ni (wt. %)	Reduction Temperature (K)	Uptake (Before Rxn) ($\mu mol\ g^{-1}$)	Uptake (After Rxn) ($\mu mol\ g^{-1}$)
MgO	0	1123	0.0	0.0
La_2O_3	0	1023	0.1	0.0
Al_2O_3	0	723	0.0	0.0
$Ni_{0.03}Mg_{0.97}O$	5	1123	0.6	0.0
Ni/La_2O_3	2	1023	1.0	0.0
Rh/Al_2O_3	1	723	45.0	28.0

Hydrogen uptakes for the fresh and the spent supported Ni catalysts were negligible. Low H_2 uptakes on the $Ni_{0.03}Mg_{0.97}O$ have been attributed to the formation of a solid solution [20]. The elements Ni and Mg fit almost perfectly the Hume-Rothery criterion for the formation of a perfect solid solution since both cations have similar ionic radii (0.078 nm), the same bulk-oxide

structure and the same oxidation state (2+). The formation of a solid solution likely prevents reduction of the bulk Ni leading to the observed low chemisorption uptakes for this material. Low chemisorption for Ni supported on MgO has also been reported elsewhere [3,11,23,24]. Recently, the formation of a solid solution has also been documented for a CoO/MgO catalyst [25,26]. The H_2 uptakes were also low for this catalyst. The H_2 uptake was also low for the La_2O_3 supported catalyst. The activity of these low H_2 uptake catalysts suggests the presence of a dispersed nickel oxide surface species that participates in the reaction, but which does not chemisorb hydrogen. High activity of certain supported Ni catalysts with low uptakes has been attributed to their unreduced activated nickel oxide phase [*27*]. H_2 uptake was moderate on the supported Rh catalyst. These samples after reaction experienced a modest reduction in chemisorption capacity. CO uptake was negligible on the Ni/MgO catalyst but significantly higher on the other two catalysts. This could be for the same reason discussed above. These cations have dissimilar ionic radii and different oxidation states and hence do not satisfy the Hume-Rothery criteria for the formation of a solid solution. Studies [28-31] have confirmed the formation of $Ni(CO)_4$ during CO chemisorption measurements on supported Ni catalysts at 298 K. The formation of the volatile carbonyl species during chemisorption could result in higher uptakes for supported Ni catalysts. The post reaction CO uptakes are generally much lower than the fresh catalysts. The supported Rh catalyst suffered only modest reduction in chemisorption capacity after reaction while the lanthanum supported Ni catalyst suffered drastic reduction in CO uptake following the reaction. This was due to the latter's propensity to form surface carbon, although during reaction, no significant deactivation or loss of activity was observed due to the dynamic nature of the reaction process. We hypothesize that upon completion of the reaction study, during the cooling process of the catalytic bed, surface carbon may have interacted with the reduced Ni metal and undergone irreversible changes reducing the metal's capacity for CO chemisorption.

X-ray diffraction (XRD) was used to examine the bulk structure of the pre and post reaction samples. No phases due to bulk Ni or NiO were observed on any of the Ni samples. Fig. 2.3 shows the pattern for the $Ni_{0.03}Mg_{0.97}O$ catalyst. Both the fresh and spent catalyst samples showed dominant support peaks indicating that the nickel was probably well dispersed on the surface and in the bulk. The formation of a solid solution for this catalyst caused the Ni to be embedded in the MgO matrix. This coupled with the low loading of Ni led to no contribution to the pattern. Fig. 2.4 compares the XRD patterns of the La_2O_3 support and the Ni/La_2O_3 catalysts before and after reaction to standards from the diffraction files.

The calcined support shows the characteristic lines of bulk La_2O_3. The fresh and spent Ni/La_2O_3 samples showed that a substantial portion of the lanthanum oxide was converted to a mixture of two $La_2O_2CO_3$ species. The presence of such oxycarbonate species has been documented in an earlier study [21]. For the 1wt.% Rh/Al_2O_3 catalyst (Figure 2.5), no phases due to Rh or Rh_2O_3 were observed on any of the samples consistent with the high dispersion indicated by the chemisorption results. Hashimoto et al. [15] and Wang and Ruckenstein [19] have also reported no contributions from Rh for their low loading (< 1.0 wt.%) supported Rh catalysts. Both the fresh and spent catalyst samples just showed dominant support peaks.

Table 2.4 shows the results from the elemental analysis on the fresh and spent samples. The fresh $Ni_{0.03}Mg_{0.97}O$ shows a small amount of carbon content, probably due to carbonate contamination in the surface layers. The spent $Ni_{0.03}Mg_{0.97}O$ sample did not indicate any coking occurring during the reaction. The Ni/La_2O_3 spent sample indicated the presence of about 8 % carbon (the oxycarbonate species contributes about 3 % carbon to the fresh sample). The effects of coking were probably negligible since the catalysts were stable and active for extended periods of operation. The Rh/Al_2O_3 catalyst also did not indicate any coking behavior consistent with the observation of Richardson and Paripatyadar [6].

Table 2.4 Carbon Analysis using the Elemental Analyzer

Catalyst	Fresh sample	Spent sample
$Ni_{0.03}Mg_{0.97}O$	2.0	2.0
Ni/La_2O_3	3.0	8.0
Rh/Al_2O_3	0.0	0.0

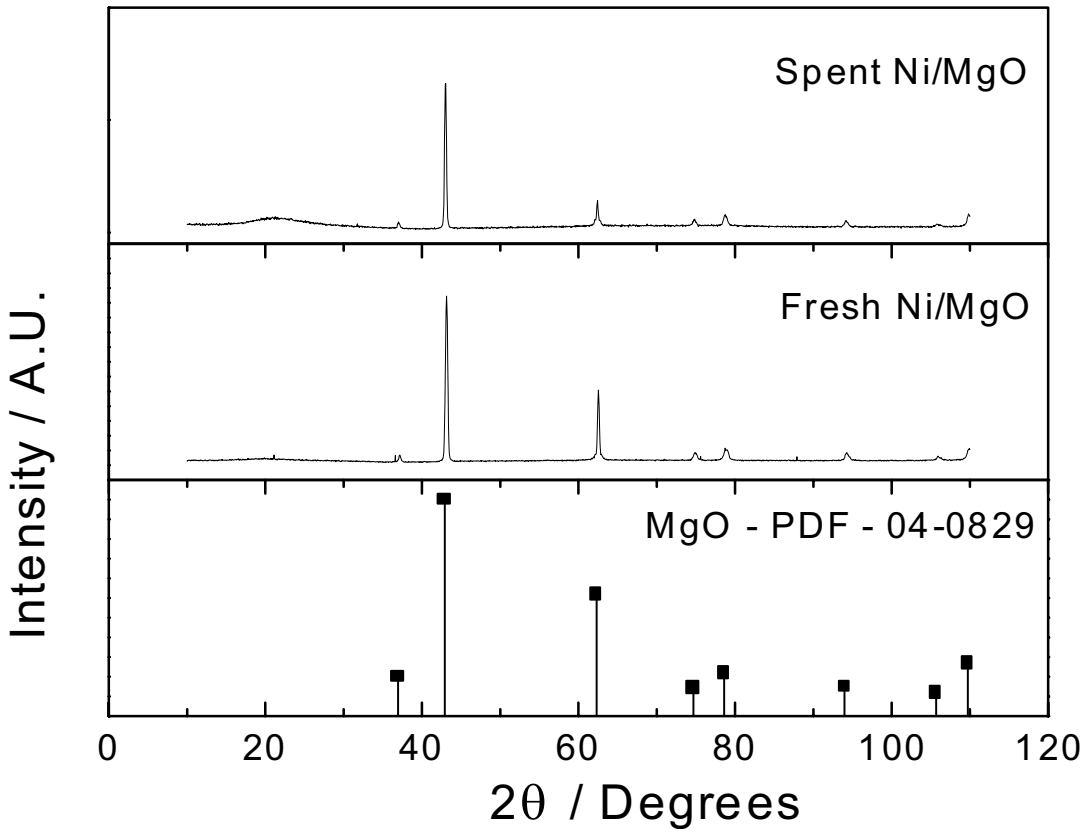

Figure 2.3 XRD Patterns for the Ni/MgO Catalyst

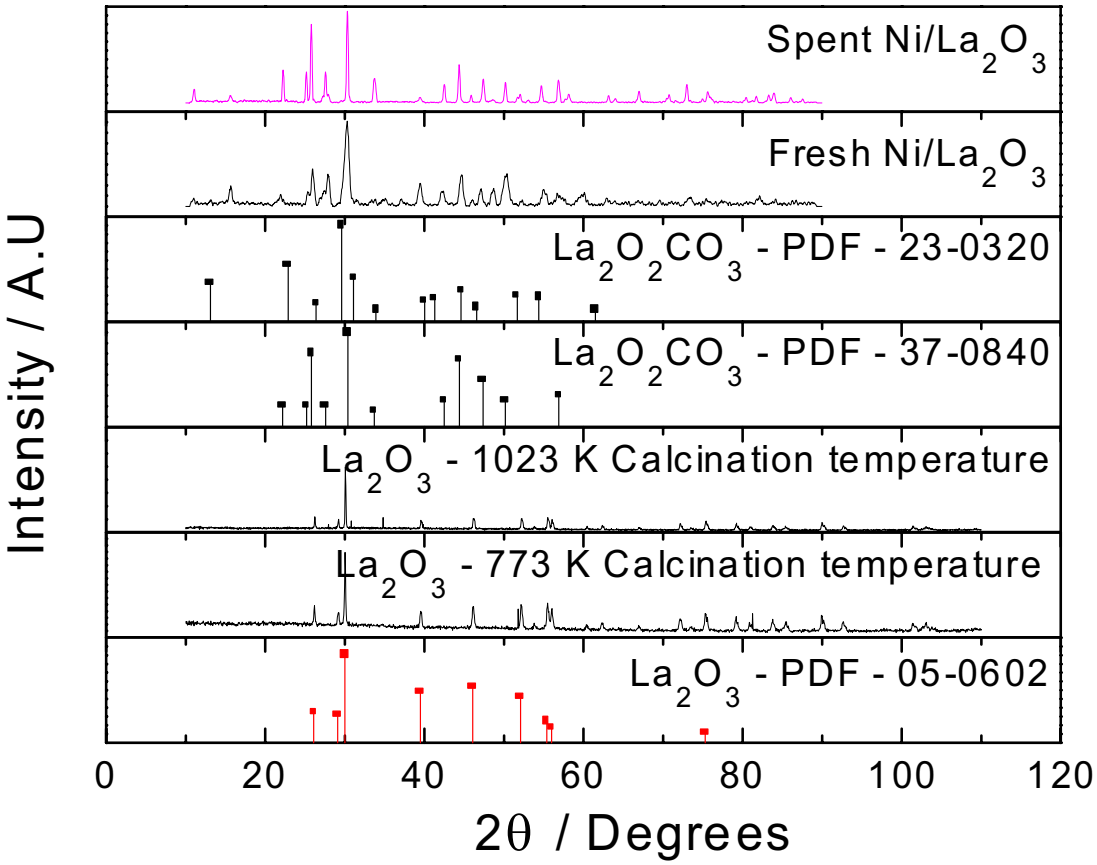

Figure 2.4 XRD Patterns for the Ni/La_2O_3 Catalyst

In the present study, the RWGS reaction affected the final product composition for all the catalysts studied. The effect of this reaction has been considered in calculating reactant conversions in all measurements. Calculations were performed by assigning X_1 to be the conversion of CO_2 from reaction (1) and X_2 to be the conversion of CO_2 from reaction (2). A mole balance was carried out to include all species (including the inert) and solved for X_1 and X_2 from the outlet concentrations. The water exit concentration was difficult to quantify due to the low thermal response of water and was estimated from the calculated value of X_2. A carbon balance calculation was also performed to determine loss of carbon due to coking if any.

Tables 2.5- 2.7 compare experimental conversion values with maximum theoretical conversion from thermodynamic calculations for the three catalysts. They also provide carbon balance results for all the catalysts. The methane conversion in the tables corresponds to X_1 and the difference between CO_2 conversion and CH_4 conversion corresponds to X_2 (the extent of the RWGS). Errors in the experimental values range from 1.3 to 1.6 %.

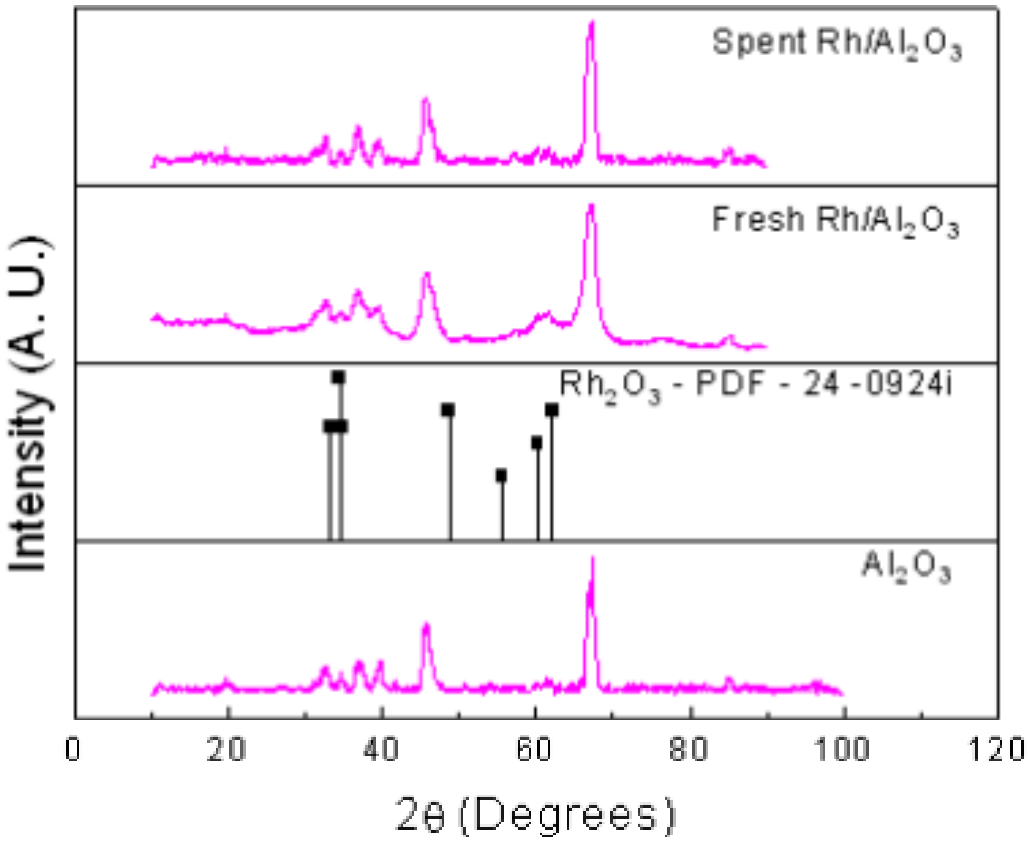

Figure 2.5 XRD Patterns for the Rh/Al_2O_3 Catalyst

Table 2.5 Comparison of Experimental Conversions with Theoretical Conversions for Ni/MgO

Flow Rates: CH_4= 24 μmol s^{-1}, Ar = 27 μmol s^{-1}, CO_2 = 24 μmol s^{-1}

Temp (K)	CH_4 Conv. (%)	CO_2 Conv. (%)	Theoretical CH_4 Conv. (%)	Theoretical CO_2 Conv. (%)	$\Sigma C_{out}/\Sigma C_{in}$
898	52.3	66	54.2	65.6	0.99
923	62.1	73.5	62.5	73.0	0.98
948	68.6	80.1	70.0	79.6	0.97
973	77.1	85.3	76.6	84.9	0.99
998	82.1	91.2	82.0	88.9	0.99

Error in experimental value was between 1.3 to 1.6 %

Table 2.6 Comparison of Experimental Conversions with Theoretical Conversions for Ni/La_2O_3

Flow Rates: CH_4= 24 μmol s^{-1}, Ar = 27 μmol s^{-1}, CO_2 = 24 μmol s^{-1}

Temp (K)	CH_4 Conv. (%)	CO_2 Conv. (%)	Theoretical CH_4 Conv. (%)	Theoretical CO_2 Conv. (%)	$\Sigma C_{out}/\Sigma C_{in}$
898	54.1	65.1	54.2	65.6	0.97
923	62.9	72.9	62.5	73.0	0.96
973	74.2	83.4	76.6	84.9	0.98
998	80.4	88.2	82.0	88.9	0.92
1023	86.0	92.1	86.3	91.6	0.94

Error in experimental value was between 1.3 to 1.6 %

Table 2.7 Comparison of Experimental Conversions with Theoretical Conversions for Rh/Al_2O_3

Flow Rates: CH_4= 24 μmol s^{-1}, Ar = 27 μmol s^{-1}, CO_2 = 24 μmol s^{-1}

Temp (K)	CH_4 Conv. (%)	CO_2 Conv. (%)	Theoretical CH_4 Conv. (%)	Theoretical CO_2 Conv. (%)	$\Sigma C_{out}/\Sigma C_{in}$
923	62.6	73.2	62.5	73.0	0.97
948	70.2	80.0	70.0	79.6	0.96
973	76.8	85.4	76.6	84.9	0.99
998	82.3	89.3	82.0	88.9	0.96
1023	86.5	92.1	86.3	91.6	0.98

Error in experimental value was between 1.3 to 1.6 %

Fig 2.6 shows the vant Hoff plot for the Ni/MgO catalyst, which was a basis for concluding that the steady state conversions obtained from the experimental data were indeed the equilibrium conversions. The figure provides equilibrium constant values K_1 for reaction (1), where K_1 was calculated from $\frac{y_{CO}^2 y_{H_2}^2}{y_{CH_4} y_{CO_2}}$. The linear fit of the experimental points and the slope (257 kJ mol^{-1}) being comparable to the heat of reaction ΔH_{rxn} (247 kJ mol^{-1}), indicated that the reaction was in equilibrium. The low thermal response of water did not permit the calculation of accurate values for its exit concentration. Hence, a vant Hoff plot for the RWGS reaction has not been provided. However, an estimate of water concentrations was consistent with the RWGS being in equilibrium.

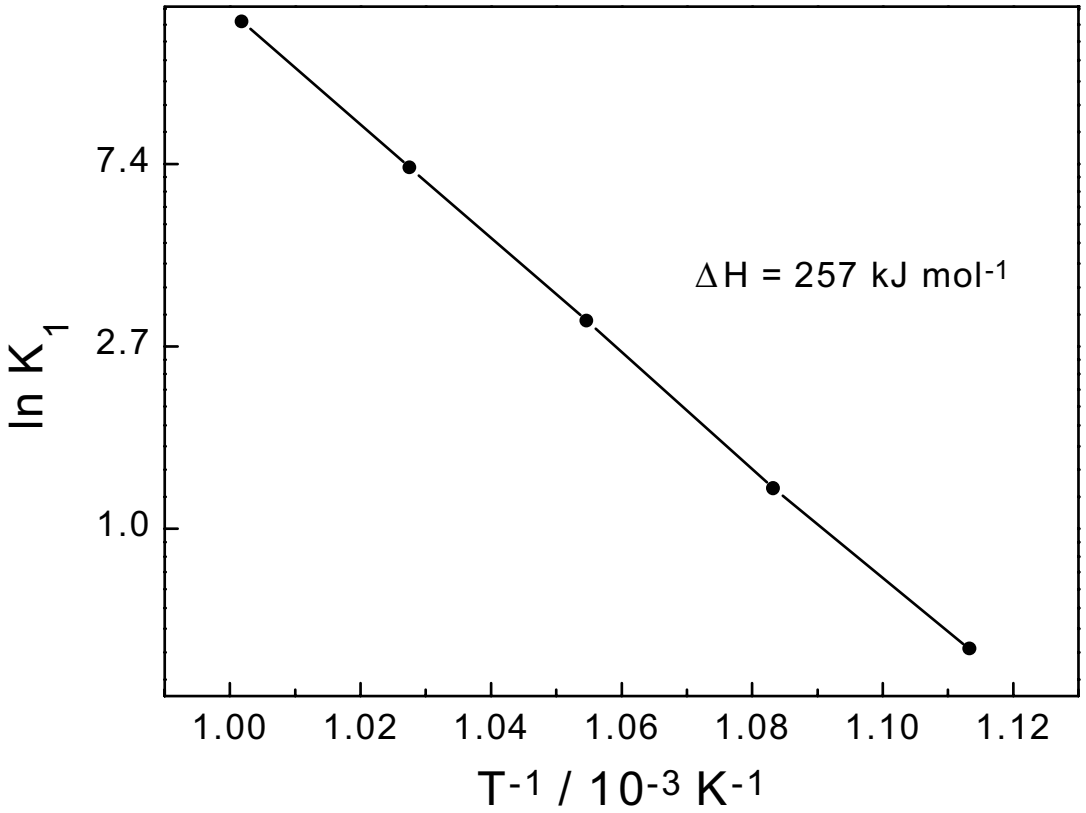

Figure 2.6 Vant Hoff Plot for the Ni/MgO Catalyst

Studies by [5,6,20] indicate the RWGS to be in equilibrium while those by [7,20,32] do not. The plot for the other two catalysts was similar. We could not determine the activation energy since the reforming reaction was close to equilibrium for both the catalysts. An E_a of 69 kJmol^{-1} [11] and 92 kJmol^{-1} [20] has been reported for Ni/MgO. An E_a of 63 kJmol^{-1} for Ni/SiO_2 [33] and 40 kJmol^{-1} and 43 kJmol^{-1} for Ni/SiO_2 and Ni/Al_2O_3 catalysts respectively have been reported [34]. A recent study [35] reported a value of 55 kJmol^{-1} for a Ni/La_2O_3 catalyst. A literature review revealed that there was a wide scatter in reported activation energy values from different studies.

Tests were also conducted to demonstrate the stability of the catalysts tested above. Figure 2.7 shows the activity plot for the Ni/La_2O_3 catalyst. The catalyst was cycled through a temperature range of 898-1023 K. As can be seen from Figure 2.7, the catalyst was stable for over 100 hours of operation without any deactivation. The other two catalysts behaved similarly with no appreciable change in activity upon cycling through the range of temperatures.

2.6 Conclusions

Both the low Ni loading and the supported Rh catalysts tested in this experimental study were resistant to carbon deposition. They were stable for extended periods (> 100 h) of operation

without significant deactivation. All three catalysts exhibited high activity and provided high CH_4 conversions. XRD patterns of the pre and post reaction samples did not show any trace of Ni or Rh. Elemental analysis of the catalysts indicated some carbon deposition on the Ni/La_2O_3 catalyst. Experimental data for these catalysts suggests that the methane reforming reaction (1) was in equilibrium.

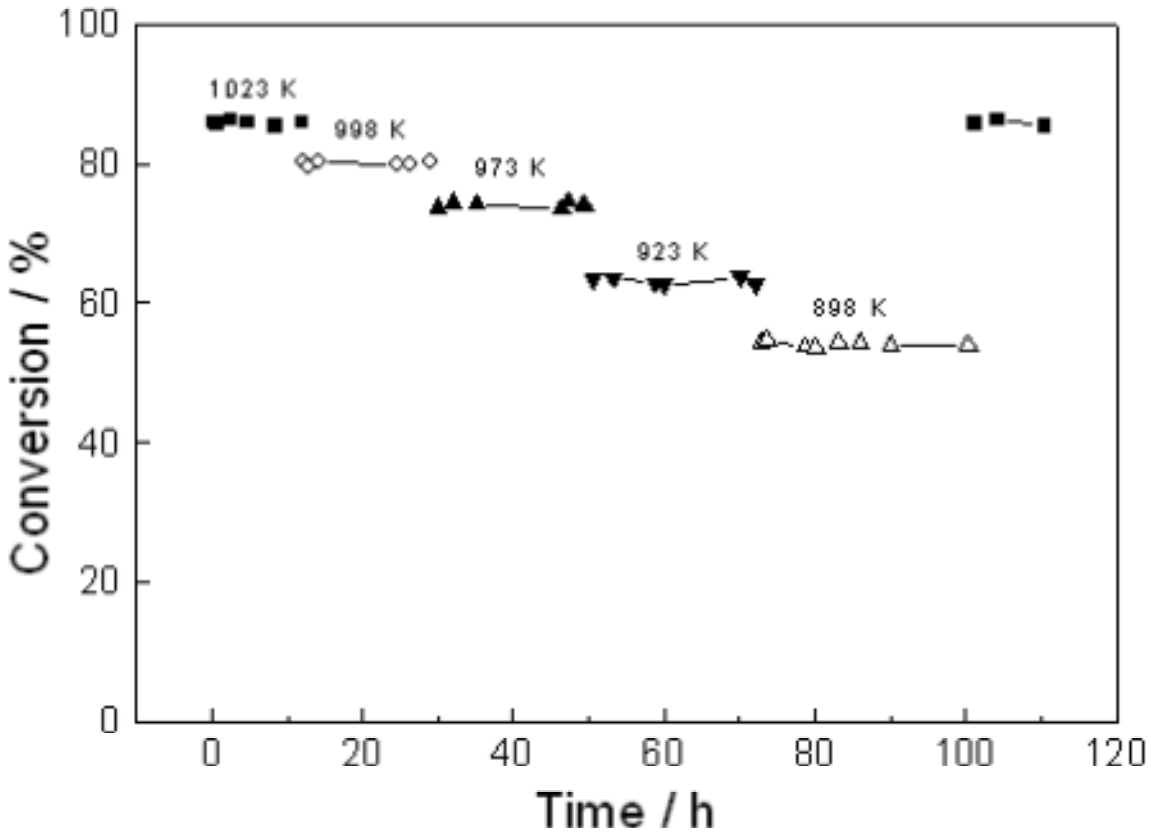

Figure 2.7 Stability Tests on the Ni/La_2O_3 Catalyst

REFERENCES:

[1] D. L. Trimm, Catal. Rev.-Sci. Eng. 16 (1977) p. 155.

[2] J. R. Rostrup-Nielsen, in J. R. Anderson, M. Boudart (Eds.), Catalysis Science and Technology, Springer, NY Vol. 5 (1984) p. 1.

[3] E. Ruckenstein, Y. H. Hu, Appl. Catal. A: 133 (1995) p. 149.

[4] A. T. Ashcroft, A. K. Cheetham, M. L. H. Green, P. D. F. Vernon, Nature 352 (1991) p. 225.

[5] H. M. Swaan, V. C. H. Kroll, G. A. Martin, C. Mirodatos, Catal. Today 21 (1994) p. 571.

[6] J. T. Richardson, S. A. Paripatyadar, Appl. Catal. 61 (1990) p. 293.

[7] A. M. Gadalla, M. E. Sommer, Chem. Eng. Sci. 44 (1989) p. 2825.

[8] A. M. Gadalla, B. Bower, Chem. Eng. Sci. 43 (1988) p. 3049.

[9] R. Blom, I. M. Dahl, A. Slagtern, B. Sortland, A. Spjelkavik, E. Tangstad, Catal. Today 21 (1994) p. 535.

[10] Z. L. Zhang, V. A Tsipouriari, A. M. Efstathiou, X. E. Verykios, J. Catal. 158 (1996) p. 51.

[11] Y. Chen, O. Yamazaki, T. Tomishige, K. Fujimoto, Catal. Lett. 39 (1996) p. 91.

[12] O. Takayasu, E. Hirose, N. Matsuda, I. Matsuura, Chemistry Express 6 (1991) p. 447.

[13] M. C. J. Bradford, M. A. Vannice, Appl. Catal. A 142 (1996) p. 97.

[14] J. R. Rostrup-Nielsen, J. H. Bak Hansen, J. Cat. 144 (1993) p. 38.

[15] K. Hashimoto, S. Watase, N. Toukai, Catal. Lett. 80 (2002) p. 147.

[16] J. Wei, B. Xu, J. Li, Z. Cheng, Q. Zhu, Appl. Catal. A: 196 (2000) p. L167.

[17] Y. Schuurman, C. Mirodatos, P. Ferreira-Aparicio, I. Rodriguez-Ramos, A. Guerrero-Ruiz, Catal. Lett. 66 (2000) p. 33.

[18] M. M. V. M. Souza, D. A. G. Aranda, M. Schmal, J. Catal. 204 (2001) p. 498.

[19] H. Wang, E. Ruckenstein, Appl. Catal. A: 204 (2000) p. 143.

[20] M. C. J. Bradford, M. A. Vannice, Appl. Catal. A 142 (1996) p. 73.

[21] Z. Zhang, X. E. Verykios, Appl. Catal. A 138 (1996) p. 109.

[22] K. Fujimoto, Private Communication (1996).

[23] Y. H. Hu, E. Ruckenstein, Catal. Lett. 34 (1995) p. 41.

[24] A. Parmaliana, F. Arena, F. Frusteri, N. Giordano, J. Chem. Soc. Faraday Trans. 86 (1990) p. 2663.

[*25*] H. Y. Wang, E. Ruckenstein, Appl. Catal. A: 209 (2001) p. 207.

[*26*] E. Ruckenstein, H. Y. Wang, Catal. Lett. 73 (2001) p. 99.

[27] P. W. Selwood, J. Catal. 42 (1976) p. 148.

[28] C. H. Barthlomew, R. B. Pannell, J. Catal. 65 (1980) p. 390.

[29] G. C. A. Schuit, L. L. van Reyen, Advan. in Catal. 10 (1958) p. 242.

[30] T. R. Hughes, R. J. Houston, R. P. Seig, Ind. Eng. Chem. Process Des. Develop. 1 (1962) p. 96.

[31] J. E. Germain, M. Ostyn, J. P. Benunfils, J. Chem. Phys. 61 (1964) p. 686.

[32] A. M. Gadalla, M. E. Sommer, Comm. of the Am. Ceram. Soc. 72 (1989) p. 4.

[33] Y. Sakai, H. Saito, T. Sodesawa, F. Nozaki, React. Kinet. Catal. Lett. 24 (1984) p. 253.

[34] A. Takano, T. Tagawa, S. Goto, J. Chem. Eng. Japan 27 (1994) p. 723.

[35] V. A. Tsipouriari, X. E. Verykios, Catal. Today 64 (2001) p. 83.

3. PERMEABLE MEMBRANE REACTOR STUDIES

3.1 Necessity for a Membrane Configuration

As discussed in the previous chapter, several catalysts were developed to provide high activity and stable operation during the methane dry reforming reaction (1):

$$CH_4 + CO_2 \rightarrow 2CO + 2H_2 \qquad \Delta H^0_{298} = 247 \text{ kJ mol}^{-1} \qquad (1)$$

The reforming reaction is reversible and limits the maximum conversion of methane in the fixed bed mode of operation. Table 3.1 lists the theoretical maximum conversions possible at different temperatures.

Table 3.1 Methane Equilibrium Conversions at Different Temperatures

Temperature / K	Equilibrium CH_4 Conversion / %
773	17.5
823	29.8
873	45.7
923	62.5
973	76.6
1023	86.3

Equilibrium conversions in such thermodynamically limited reactions can be overcome by the preferential removal of one or more of the products during reaction. In recent years, membranes for selective separation in chemical reactors have become increasingly studied as a means to overcome such equilibrium limitations. They have also been used in applications where controlled introduction of reactant(s) is necessary to reduce hot spots in the catalyst bed or to avoid undesirable side reactions. Membrane reactors offer advantages over conventional fixed bed reactors that include higher energy efficiency, lower capital and operating costs, compact modular construction, low maintenance cost, and ease of scale-up [1]. Membrane reactors have been broadly classified as inert membrane reactors and catalytic membrane reactors.

Inert Membrane Reactors:
In this type of operation, the membrane effects the separation/removal of components and does not participate in the actual reaction. The catalyst is usually packed on either the shell or tube side of the reactor.

Catalytic Membrane Reactors:
In this type of operation, the membrane serves as either the catalyst or as a support for the catalyst which is impregnated in the pores of the membrane. The effect on the reaction occurs in addition to the effect of separation/removal of components from the reaction chamber.

Some of the earliest studies on membrane reactor applications used noble metal membranes for several hydrogenation and dehydrogenation reactions and high conversions together with good selectivities were reported [2-6]. Later studies have focused on inorganic ceramic membranes. Studies of H_2S decomposition [7-9] in a porous-glass membrane reactor provided selective separation of H_2 from a reacting mixture and conversion twice as high as equilibrium. The methane steam reforming reaction was studied using metal dispersed alumina [10,11] and regular alumina [12] membrane reactors. Chai et al. [10] reported conversions 200 % higher than equilibrium conversions while Tsotsis et al. [12] obtained only 20 % higher conversions. Ethane dehydrogenation was studied in an alumina membrane reactor and conversions greater than twice the equilibrium level was reported by using the membrane mode of operation [12]. A recent study [13] on the dehydrogenation of methylcyclohexane to toluene in a porous Vycor reactor provided improved yields by controlling the operating parameters. Oxidative dehydrogenation of propane was studied by Ramos et al. [14] and they obtained good selectivity by controlled addition of one of the reactants. Good reviews of several research reports in the area of catalytic membrane reactors have been provided by Falconer et al. [15] and Hsieh [16,17,18]. A comprehensive review of patents and publications in the area of catalytic ceramic membranes has been compiled by Armor [19,20]. Several authors [21-24] have complied summaries that provide details about membrane developments and applications with discussions about the opportunities that exist for commercialization of existing technologies in the future.

Knudsen diffusivity (K_i) is defined as [25]:

$$K_i = \frac{2r\varepsilon_p}{3\tau RTd}\sqrt{\frac{8000RT}{\pi M_i}} \qquad (2)$$

This mode of separation prevails when the mean free path of a molecule λ, given by:

$$\lambda = \frac{3.2\mu}{P}\sqrt{\frac{RT}{2\pi M_i}} \qquad (3)$$

is much larger than the pore size of the membrane. For this study, the ratio of the mean free path of the gaseous species (CH_4, CO_2, CO, H_2O and H_2) and the pore size of the membrane (3.6 nm) was in the range of 50-110 (at 873 K, 0.1MPa) [26]. The mean free paths of the gaseous species were much larger than the pore size of the Vycor membrane, and the diffusion was described by the Knudsen mechanism.

At these conditions, the probability of a molecule colliding with the walls of the pore are much higher than that of colliding with another gas phase species. Also, the diffusivity is inversely proportional to the square root of the molecular weight of the gaseous species so that lighter species will diffuse faster than heavier species. In this study, commercially available porous Vycor glass (7930 glass, Corning Inc.) was tested as a selectively permeable membrane to bring about a shift in thermodynamic equilibrium with the possibility of improved methane conversions. This study did not test the effects of different operational parameters on reactor

efficiency. High conversions, close to equilibrium, were chosen in order to more readily assess and test the effect of the membrane.

3.2 Experimental Details

3.2.1 Membrane Characterization

A commercial porous Vycor glass (7930 glass, Corning, Inc.) of tubular geometry and nominal pore size of 4 nm was used in these studies. The fresh and used membranes were characterized by N_2 physisorption in a volumetric unit (Micromeritics ASAP 2000 series) using 0.4-0.6 g of the sample. The sample was first degassed under vacuum at 393 K. This was followed by measurement of both the adsorption and desorption amounts of N_2 at 77 K up to a $P/P_0 \sim 0.99$. The pore size distribution was determined from the desorption isotherm using the Barrett, Joyner and Halenda (BJH) method [27] (the desorption curve represents the thermodynamically stable adsorbate).

3.2.2 Permeability Measurements

The experimental setup for permeability measurements was the same as used for reactivity studies (described in chapter 2) but using inert quartz chips as bed material (as opposed to catalyst material) packed in the 4 cm porous section of the reactor. Individual gas permeabilities were determined by flowing 20 μmol s^{-1} of the pure gas at 123 kPa in the shell side and measuring the tube side (at atmospheric pressure) flow rate using a sensitive bubble flow meter. Permeability coefficients were calculated from:

$$P_i = \frac{Q_i}{A\Delta P} \qquad (4)$$

3.2.3 Reactivity and Membrane Studies

The reactor assembly (schematic shown in Figure 3.1) consisted of two concentric quartz tubes with the catalyst packed on the outer shell side in a 4 cm section to allow for good heat transfer (for more detailed information refer to Chapter 2). For the membrane configuration, quartz tubing of the same diameter (O. D. = 10 mm, I. D. = 8 mm) was glassblown to the ends of a piece of Vycor glass so as to leave a section 4 cm long of the membrane material in the center. The larger external tube had an outer diameter of 16 mm and an inner diameter of 14 mm. A mixture of Ar, CH_4 and CO_2 was the inlet feed to the shell side. Ar was introduced in the tube side as the sweep gas in all membrane reactor experiments. The outlet gases were separated using a Carbosphere packed column (Alltech) and analyzed online using a gas chromatograph (SRI 8610B). Catalyst loading, leak testing and operational conditions have been described in Chapter 2. For the membrane configuration, shell and tube side streams were mixed downstream of the reactor before sampling by the GC, to obtain total exit gas concentrations.

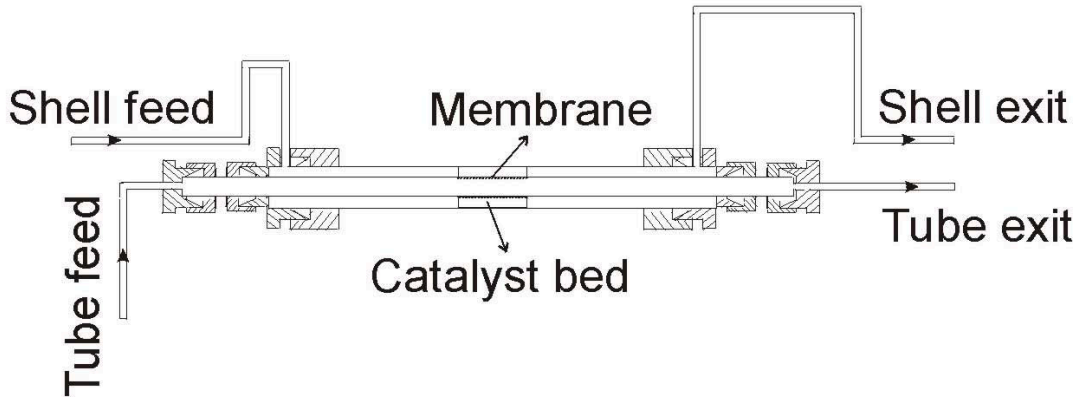

Figure 3.1 Membrane reactor configuration

3.3 Results and Discussion

The permeability coefficients for the different gases was determined by flowing the pure gas on the shell side under pressure and measuring the tube side flow rate as described in the experimental section. The hydrogen permeability coefficient Q_{H_2} for the Vycor sample was 1.8×10^{-8} mol m^{-2} s^{-1} Pa^{-1} at 873 K. However, in the literature values of 2.4×10^{-8} [28], 3.6×10^{-8} [29], 4.0×10^{-8} [30], 4.0×10^{-8} [31] and 5.4×10^{-8} mol m^{-2} s^{-1} Pa^{-1} [32] have been reported for Vycor at 873 K (values in mol m^{-2} s^{-1} Pa^{-1} can be converted to cm^3 cm^{-2} s^{-1} Pa^{-1} by multiplying by 2.24). Boyd and Thompson [33] have reported a value of 0.90×10^{-14} mol m^{-2} s^{-1} Pa^{-1} for solid glass at this temperature. As will be discussed, the slightly lower value obtained in our study can be accounted for by a slightly narrow pore size in our membrane batch. Separation factor is a measure of the preferential separation of one species as compared to another. The separation factors were determined by the ratios of individual gas permeability coefficients and are listed in Table 3.2. The experimental values were close to those predicted by theoretical Knudsen diffusion values in the temperature range 300 - 973 K.

Figure 3.2 shows the adsorption and desorption isotherms for the fresh and used porous glass samples. The volume of nitrogen adsorbed (per gram of sample) at 77 K is given as a function of the relative pressure, P/P_0. The initial rapid rise in the adsorption curve is due to the formation of a monolayer of N_2 on the walls of the pores. This was complete at about P/P_0 =0.3. At higher pressures, the increase in the slope was attributed to an increased uptake of adsorbate due to the formation of multilayers followed by filling of the pores with liquefied N_2. These steps were retraced during desorption except in the region of capillary condensation, where considerable hysteresis was observed. The isotherms can be classified as Type IV, a characteristic of porous materials with pores in the range 1.5 – 100 nm [34]. The hysteresis can be classified as Type A, which is exhibited by materials with cylindrical pores open at both ends [34]. Figure 3.3 shows the pore size distribution for the fresh and used samples. Both the samples had very narrow pore size distributions with an average pore size of 3.6 nm compared to the manufacturer's reported

nominal value of 4 nm. The lower pore size of our membrane batch could account for the slightly lower permeability values reported earlier.

Table 3.2 Separation Factors determined from Individual Gas Permeabilities of the Porous Vycor Membrane

Ratio	Theoretical	Experimental
H_2/CH_4	2.83	2.76
H_2/CO	3.74	3.62
H_2/CO_2	4.69	4.26

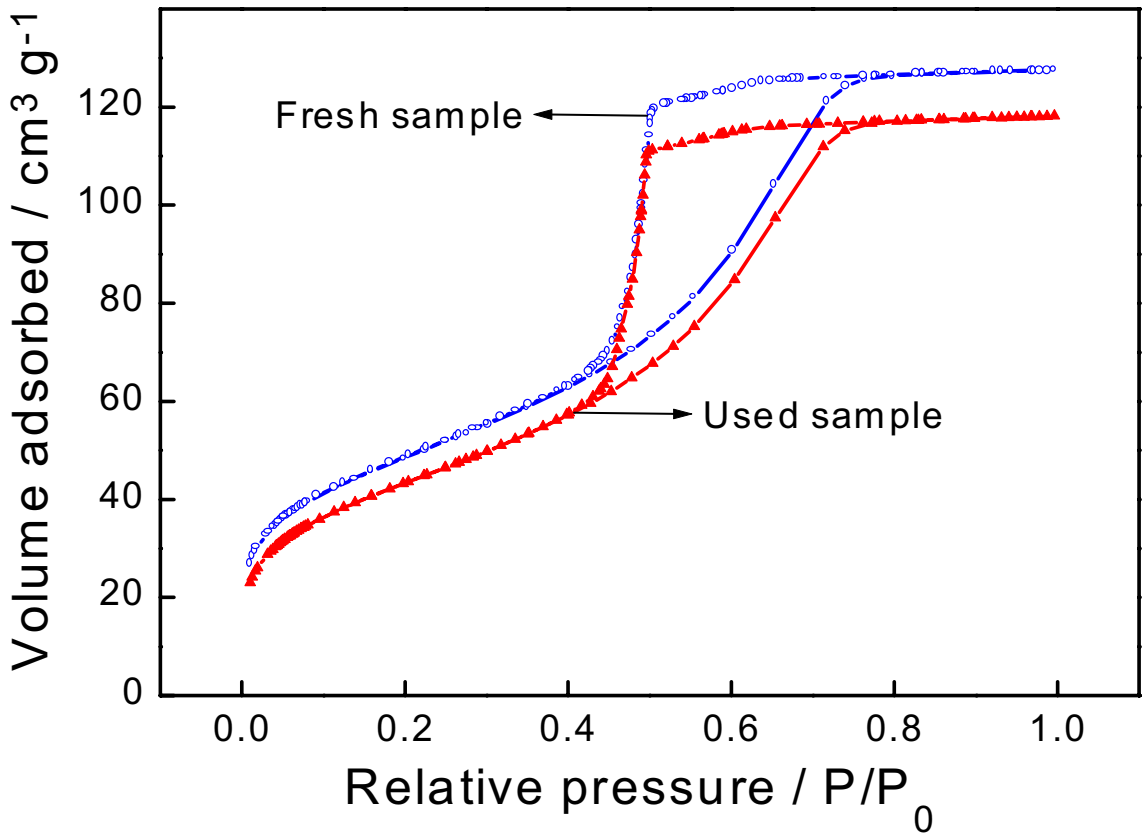

Figure 3.2 Adsorption-Desorption Isotherms for the Porous Glass Membrane

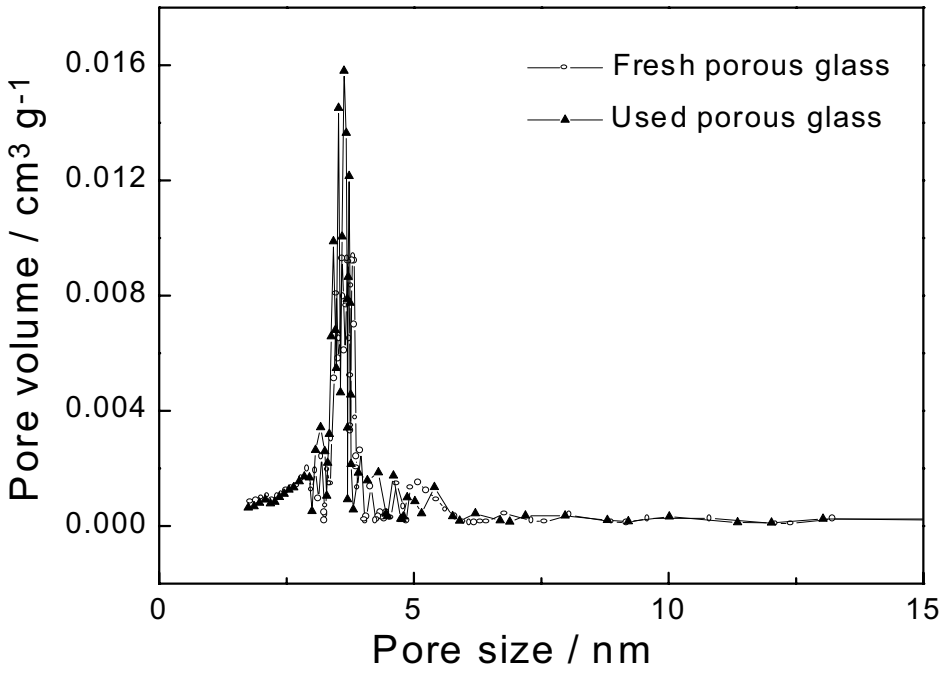

Figure 3.3 Pore Size Distributions using the BJH Method for Porous Glass

The RWGS reaction affected the final product composition for all the catalysts studied and this has been considered in calculating reactant conversions in all measurements. Calculations were performed by assigning X_1 to be the conversion of CO_2 from reaction (1) and X_2 to be the conversion of CO_2 from reaction (2).

$$CH_4 + CO_2 \rightarrow 2CO + 2H_2 \qquad \Delta H^0_{298} = 247 \text{ kJ mol}^{-1} \qquad (1)$$

$$CO_2 + H_2 \rightarrow CO + H_2O \qquad \Delta H^0_{298} = 41 \text{ kJ mol}^{-1} \qquad (2)$$

Figures 3.4 – 3.6 compare methane conversion in the fixed bed and membrane configurations for the Ni/La_2O_3, Ni/MgO and Rh/Al_2O_3 catalysts respectively. The dotted lines indicate the equilibrium conversion levels for methane (conversion X_1). The fixed bed provided methane conversions close to thermodynamic equilibrium levels. The use of the membrane configuration resulted in improved conversions of methane with both the catalysts. This could be attributed to the preferential removal of hydrogen during reaction which thereby shifted the equilibrium to the right. However, there was some loss of reactants to the tube side by Knudsen diffusion. This lowered the overall conversion of methane possible in the membrane reactor. This limitation can be overcome by incorporating a membrane that has selectivity for only hydrogen and with permeability comparable to the porous glass matrix.

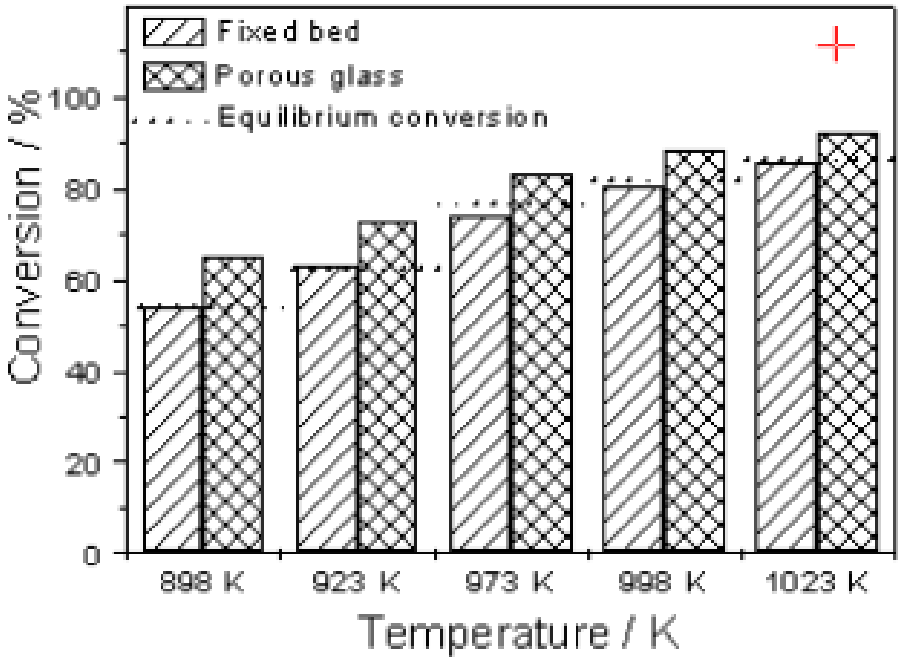

Figure 3.4 Methane Conversions with the Ni/La_2O_3 Catalyst

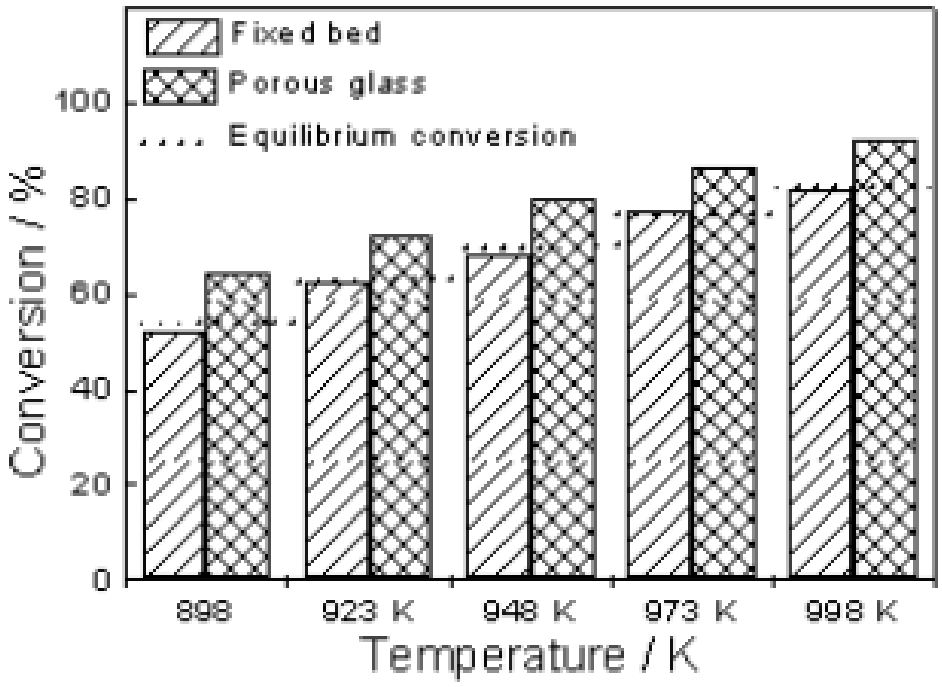

Figure 3.5 Methane Conversions with the Ni/MgO Catalyst

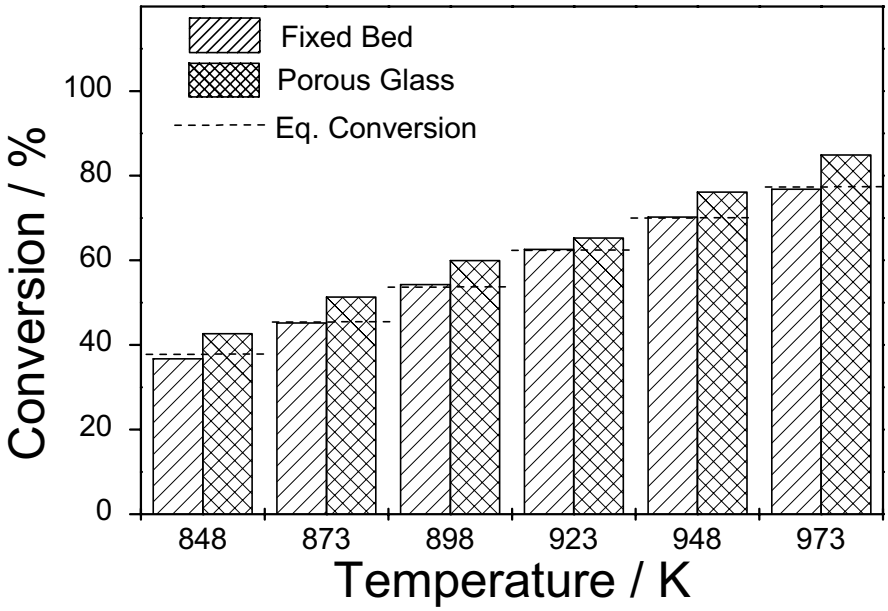

Figure 3.6 Methane Conversion with the Rh/Al_2O_3 Catalyst

This study does not attempt to make a rigorous comparison between the membrane reactor and the flow reactor. Issues relating to such comparisons have been well covered in recent publications which point out that increases in conversion can be due to dilution by the purge gas rather than equilibrium shifting [35,36]. A precise comparison between membrane and plug flow operation requires the use of two separate plug flow reactors [36], while here the catalyst part of the membrane reactor and the plug flow reactor are operated with the same flow rates and catalyst amounts.

The permeability of the Vycor glass membrane was moderate and the question arises about the practicality of the system. Recently, the usage of an areal time yield (ATY) has been suggested to assess the performance of a membrane system [37]. The ATY in units of mol m^{-2} s^{-1}, is obtained from the space time yield (STY) in units of mol m^{-3} s^{-1} by dividing by the surface to volume ratio (S/V) of the reactor. At 898 K for the Ni/MgO catalyst the STY for H_2 production is 7.82 mol m^{-3} s^{-1}. For the geometry employed in this study S/V = 320.0 m^{-1}, giving rise to an ATY of 0.024 mol m^{-2} s^{-1}. In comparison to this, at 873 K the hydrogen permeability is 1.80×10^{-3} mol m^{-2} s^{-1}. This value, lower than the ATY, indicates that H_2 transport through the membrane limits the performance of the membrane reactor. However, in terms of the Weisz criterion [38] for commercial viability, STY = 1.0 mol m^{-3} s^{-1}, the acceptable permeability for this system is 1.0/320.0 = 3.1 x 10^{-3} mol m^{-2} s^{-1}, which is close to the value found.

3.4 Conclusions

Experimental data for these catalysts suggests that the methane reforming reaction (1) is in equilibrium. The use of a porous glass membrane provided improvements in methane conversion compared to the fixed bed configuration. However, Knudsen diffusion being the dominant separation mechanism, diffusion of reactants to the tube side occurs. This loss of

reactants to the tube side (with no catalyst bed for reaction) potentially lowers the overall conversion possible in such a configuration. An obvious solution to this would be to eliminate (or minimize) diffusion of reactants to the tube side. This could be achieved by developing a selectively permeable membrane (to hydrogen only) for separation purposes. The next chapter discusses the different methods used to modify the porous glass membrane used here and results from using these modified membranes and applicability to the reforming system.

3.5 Nomenclature

K_i = effective permeability of species i (mol m^{-2} Pa^{-1} s^{-1})
r = pore radius of the membrane (m)
ε_p = porosity of the membrane
τ = tortuosity of the membrane
R = gas constant (Pa m^3 mol^{-1} K^{-1})
T = temperature (K)
d = membrane thickness (m)
M_i = molecular weight of species i (g mol^{-1})
P = pressure (Pa)
P_i = permeability coefficient (mol m^{-2} s^{-1} Pa)
Q_i = flow rate on the tube side (cm^3 s^{-1})
A = cross sectional area of the membrane available for diffusion (m^2)
ΔP = pressure difference between the shell and tube side (Pa)
λ = mean free path (m)
μ = viscosity of the gas (N s m^{-2})

REFERENCES:

[1] A. Sengupta, K. K. Sircar, in R. D. Noble, S. A. Stern (Eds.), Membrane Separations Technology, Principles and Applications, Elsevier Science, B. V. (1995) p. 499.

[2] A. P. Mischenko, V. M. Gryaznov, M. E. Sarylova, V. A. Bednyakova, Br. Pat. Appl., 2 187 759A (1987).

[3] N. L. Basov, V. M. Gryaznov, Memb. Katal. (1985) p. 117.

[4] A. P. Mischenko, V. M. Gryaznov, V. S. Smirnov, E. D. Senina, I. L. Parbuzina, N. R. Roshan, V. P. Polyakova, E. M. Savitsky, U. S. Patent 4 179 470 (1979).

[5] V. M. Gryaznov, M. G. Slin'ko, Discuss. Faraday Soc. (1982) p. 73.

[6] M. E. Sarylova, A. P. Mischenko, V. M. Gryaznov, V. S. Smirnov, Izv. Akad. Nauk SSSR, Ser Khim. 190 (1970) p. 144.

[7] T. Kamayema, M. Dokiya, M. Fujishige, H. Yokokawa, K. Fukuda, Ind. Eng. Chem. Fund. 20 (1981) p. 97.

[8] T. Kamayema, K. Fukuda, M. Fujishige, H. Yokokawa, M. Dokiya, Adv. Hydrogen Energy Proc. 2 (1981) p. 569.

[9] K. Fukuda, M. Dokiya, T. Kamayema, Y. Kotera, Ind. Eng. Chem. Fund. 17 (1978) p. 243.

[10] M. Chai, M. Machida, K. Eguchi, H. Arai, Appl. Catal. A: 110 (1994) p. 239.

[11] E. Kikuchi, Catal. Today 56 (2000) p. 97.

[12] T. T. Tsotsis, A. M. Champagnie, S. P. Vasileiadis, Z. D. Ziaka, R. G. Minet, Sep. Sci. Tech. 28 (1993) p. 397.

[13] P. Ferreira-Aparicio, I. Rodriguez-Ramos, A. Guerrero-Ruiz, J. Catal. 212 (2002) p. 182.

[14] R. Ramos, M. Menendez, J. Santamaria, Catal. Today 56 (2000) p. 239.

[15] J. L. Falconer, R. D. Noble, D. P. Sperry, in R. D. Noble, S. A. Stern (Eds.), Membrane Separations Technology, Principles and Applications, Elsevier Science B. V. (1995) p. 669.

[16] H. P. Hsieh, AIChE Sym. Series 84 (1988) p. 1.

[17] H. P. Hsieh, Inorganic Membranes for Separation and Reaction, Elsevier Science, Amsterdam (1996).

[18] H. P. Hsieh, Catal. Rev.-Sci. Eng. 33 (1991) p. 170.

[19] J. N. Armor, Appl. Catal. 49 (1989) p. 1.

[20] J. N. Armor, Catal. Today 25 (1995) p. 199.

[21] W. J. Koros, G. K. Fleming, J. Memb. Sci. 83 (1993) p. 1.

[22] A. Julbe, D. Farrusseng, C. Guizard, J. Memb. Sci. 181 (2001) p. 3.

[23] J. Coronas, J. Santamaria, Catal. Today 51 (1999) p. 377.

[24] J. Zaman, A. Chakma, J. Memb. Sci. 92 (1994) p. 1.

[25] J. C. S. Wu; P. K. T. Liu, Ind. Eng. Chem. Res. 31 (1992) p. 322.

[26] M. Mulder, Basic Principles of Membrane Technology, Kluwer Aacdemic, Dordrecht (1996) p. 227.

[27] E. P. Barrett, L. G. Joyner, P. P. Halenda, J. Amer. Chem. Soc. 73 (1951) p. 373.

[28] D. Lee, S. T. Oyama, J. Memb. Sci. 210 (2002) p. 291.

[29] M. Tsapatsis, G. Gavalas, J. Memb. Sci. 87 (1994) p. 281.

[30] S. Kitao, M. Asaeda, Key Engg. Materials 61 & 62 (1991) p. 267.

[31] S. Jiang, Y. Yan, G. R. Gavalas, J. Membr. Sci. 103 (1995) p. 211.

[32] S. W. Nam, G. R. Gavalas, AIChE Symp. Series 85(268) (1989) p. 68.

[33] D. C. Boyd, D. A. Thompson, Glass, in Kirk-Othmer Encyclopedia of Chemical Technology, 3rd Ed., Vol. 11, Wiley, NY (1980) p. 807.

[34] S. Lowell, J. E. Shields, Powder Surface Area and Porosity, 3rd Edition, Chapman and Hall, New York, NY (1991) p. 52.

[35] C. M. Reo, L. A. Bernstein, C. R. F. Lund, AIChE J. 43 (1997) p. 495.

[36] C. M. Reo, L. A. Bernstein, C. R. F. Lund, Chem. Eng. Sci. 52 (1997) p. 3075.

[37] M. Boudart, Cattech. Dec. (1997) p. 94.

[38] P. Weisz, ChemTech (1992) p. 424.

4. NEW MEMBRANE DEVELOPMENT AND TESTING

4.1 Background on Membrane Modification

The commercially available Vycor membrane provided for simultaneous separation and reaction resulting in enhanced methane conversions (above equilibrium levels). However, reactant species were also removed from the shell side (the effect was more pronounced at the beginning of the catalyst bed where the reactant concentration was higher compared to the products). This provided only marginal improvements in methane conversion. The objective of this part of the research was to develop a membrane that was selective only to hydrogen which would offer two advantages:

1) Increased conversion due to shift in equilibrium with no loss of reactants.
2) Potential use of the permeate stream enriched in pure hydrogen for other applications (such as fuel cells) requiring the use of pure hydrogen.

Several studies have focused on the development of membranes that provide high selectivity by suitably modifying a porous ceramic support. Sol-gel processing and CVD have been the methods of choice by most researchers. Sol-gel modification provides good selectivity and permeability as opposed to CVD methods where increases in selectivity are accompanied by loss of permeability. The sol-gel method however, suffers from a lack of reproducibility. CVD methods usually require substantial capital investment and controlled conditions of deposition. The table below summarizes the work in this area by several researchers.

Support	Method	Selectivity	H_2 Permeance $/10^{-8}$ cm^3 cm^{-2} s^{-1} Pa^{-1}	E_a / kJ mol^{-1}	Effect of water on permeability	Ref
Vycor	$SiCl_4$ +H_2O Alternating reactant deposition	H_2/N_2 = 500-1000 at 873 K	5.0 at 873 K	17-26	20-30% lower	1
Vycor	$SiCl_4$ +H_2O One-sided reactant deposition	H_2/N_2 = 500-1000 at 873 K	5.0 at 873 K	17-26	70-80% lower	1
Alumina	Sol-gel and CVD	$He/N_2 > 300$	12 at 500 K	12.2	No report	2
Alumina	Sol-gel	H_2/N_2 = 185	No report	8.3	No report	3
Porous glass	CVD of Boron Nitride at 523 K	H_2/N_2 = 2200	0.82 at 573 K	48.0	No report	4
Alumina	TEOS at 873 K	H_2/N_2 = 1000	2.2 at 873 K	-	No report	5

Porous glass	$SiH_4 + O_2$	H_2/N_2 = 2000-3000	3.2 at 873 K	35.0	80% lower	6
Porous glass	TEOS, TEOS+O_2, $SiCl_4$	H_2/N_2 = 500-3000	6.6 at 973 K	6.0	50% lower	7
Porous glass	$SiCl_4 + H_2O$	H_2/N_2 = 200-300	3.6 at 873 K	16	50% lower	8
α-Alumina tube	CVD of TEOS by evacuation (873-973 K)	H_2/N_2 = 100-1000	9.0 at 873 K	9-13	Dropped by 50% (873 K)	9
Vycor glass	$SiCl_4 + H_2O$	H_2/N_2 > 500	5.0 at 873 K	10-15	Dropped by more than 60 %	10
Vycor glass	Temporary carbon barrier before $SiCl_4 + H_2O$	H_2/N_2 = 350	8.8 at 873 K	14-21	Expected drop in permeability	11
Vycor glass	$SiH_4 + O_2$	H_2/N_2 = 2000-3000	3.3 at 873 K	6-30	lower	12
Ceramic support	Microporous glass coating	Removes only H_2 from a H_2/H_2O mixture	13 at 773 K	-	No report	13
Porous glass	TEOS + O_2 at 473 K	He/O_2 = 6	0.9 at 473 K	5.3	No report	14, 15
Porous glass	CVD of SiO_2, TiO_2, Al_2O_3, B_2O_3	H_2/N_2 = 1000-5000	1.6 – 5.0 at 723 K	37	Lowering of permeability	16
Porous substrate	deposited thin Ni and Pd films	-	-	-	Film brittle due to α-β transitions	17
Porous glass	Electroless plating of Pd film	-	168 at 673 K	10.7	Film brittle due to α-β transitions below 573 K	18
Porous glass	Pd film stabilized by Cu or Ag	-	50 at 673 K	15.5	Film stable but lowered permeability	19
Alumina	CVD of silica	H_2/N_2 = 12-72 at 873 K	0.76 – 478 at 873 K	6-20	> 60 % lower in first 2 h	20
Alumina	CVD of TEOS (at 673-873 K)	H_2/N_2 > 1000.	2 – 22 at 873 K	28	7% moisture at 773 K did not degrade the stability	21
alumina	CVD of TEOS (873 – 923 K)	Knudsen selectivity	2.2 at 873 K.	6-25	Reduced by 50% in 24h (773 K)	22

Micropo rous membra nes	Sol-gel modified	H_2/CH_4 = 40-200 (423-573 K)	336 at 373 K	17-22 (with aging reduced to 3)	No report	23, 24
Alumina	Dip coating under clean room conditions	H_2/CH_4 = 5000	112 at 473 K.	-	No report	25

Silica modified membranes reported by several researchers suffer from loss of permeability on exposure to moisture (as much as 50% or greater in the first 12 h). This has been attributed to the removal of Si-OH groups leading to the formation of Si-O-Si bonds which close the channel [26]. This phenomenon is termed as densification. Moisture apparently catalyzes this reaction particularly at higher temperatures [26]. Densification not only leads to lower permeability but also causes embrittlement of the silica film that compromises selectivity. In this work, we have developed modified porous glass membranes that provide unprecedented selectivities for the species involved with no attendant lowering of permeability.

4.2 Experimental Details

The porous Vycor membrane was modified using several methods. The details of each of these methods is provided below.

4.2.1 Membrane Modification Methods

4.2.1.1 Sol-Gel Processing

The sol-gel method was developed from Kitao et al. [3] and involved the preparation of three solutions, A, B, and C with TEOS, H_2O and HNO_3 in the ratio 1:10:0.1, 1:50:0.05 and 1:100:0.005 respectively. Reagent A was obtained by boiling solution A for 0.33 h and reagent B by boiling solution B for 0.16 h. Solution C was used as prepared. The tube (with ends capped with stoppers to prevent coating the inside of the tube) was dipped successively in A, B, and C, followed by wiping the tube to remove excess gel, washed with distilled water, dried at 473 K for 2 h (β= 1 K min^{-1}) and calcined at 723 K for 1 h (β= 1 K min^{-1}). The process of dipping and heating was repeated several times.

4.2.1.2 Polymerization of silica precursor

The process adopted from Li [27] involved the polymerization of a silica precursor, trichloromethylsilane (Aldrich 97 %) within the pores of the Vycor tube. The shell and tube sides were isolated from each other using stoppers and mounted as shown in Figure 4.1. The membrane section (outer tube side) was wrapped with absorbent tissue and held together with elastic bands. A solution prepared by diluting 2.8 cm^3 of ammonia solution (Fisher, 29.9% assay) with 12.2 cm^3 of H_2O, was injected in the shell side while simultaneously 15 cm^3 of trichloromethylsilane was injected in the tube side. The assembly was rotated using a motor at 4 rpm and was maintained at 265 K using a constant temperature bath (prepared by dissolving NaCl in ice + water). After 10 h, the inner tube was removed, dried in O_2 for 12 h at 343 K (β= 1 K min^{-1}), then heated to 693 K (β= 2 K min^{-1}) and maintained at this temperature for 8 h.

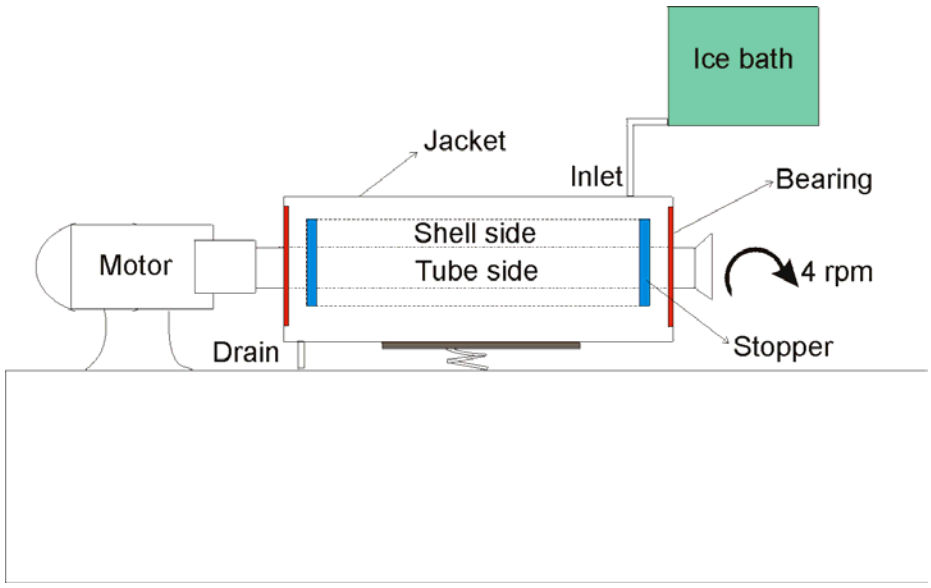

Figure 4.1 Experimental Setup for Modification of the Vycor Membrane using Polymerization of a Silica Precursor

4.2.1.3 Silica Sol Processing

This method adopted from de Lange [28] involved refluxing a solution of TEOS, H_2O, C_2H_5OH, and HNO_3 (in the ratio 1:1:26:11.76) at 353 K for 2 h. A sample of the solution was diluted with C_2H_5OH (1:18) and the membrane dipped (with ends sealed to prevent the solution from coating the inner side of the tube) for a few seconds. It was then dried at 393 K for 3 h (β= 1 K min^{-1}) and calcined at 673 K for 3 h (β= 1 K min^{-1}). The dipping was repeated a second time with the dilution being 1:180.

4.2.1.4 Chemical Vapor Deposition of TEOS at 473 K

This procedure was adopted from Okubo and Inoue [14]. Figure 4.2 shows the experimental setup used to modify the porous glass membrane. The reactor assembly with a 4 cm porous glass section (no catalyst) was heated to 473 K with Ar flow on both the shell and tube side (100 μmol s^{-1}). Tetraethyl orthosilicate (TEOS, Aldrich, 98%) was introduced through a bubbler (at 298 K) using Ar (3 μmol s^{-1}) as the carrier gas. This was premixed with O_2 (5 μmol s^{-1}) to facilitate the decomposition of TEOS at the lower temperature. This was mixed with the tube side Ar stream before introduction in the tube side. The TEOS-Ar-O_2 stream was allowed to flow for 80 h after which the reactor was cooled in Ar.

4.2.1.5 Chemical Vapor Deposition of TEOS at 873 K

The experimental setup was similar to the one adopted for the CVD of TEOS at 473 K. The reactor assembly with a 4 cm porous glass section (no catalyst) was heated to 873 K with Ar flow on both the shell (20 μmol s^{-1}) and tube (8 μmol s^{-1}) side. Tetraethyl orthosilicate (TEOS, Aldrich, 98%) was introduced through a bubbler (at 298 K) using Ar (3 μmol s^{-1}) as the carrier gas. This stream was premixed with additional Ar to provide the required TEOS concentration before introduction in the tube side. The TEOS-Ar stream was allowed to flow for different time periods (12, 24, and 48 h) after which the reactor was cooled in Ar. Ar was also introduced in the shell side as a sweep gas.

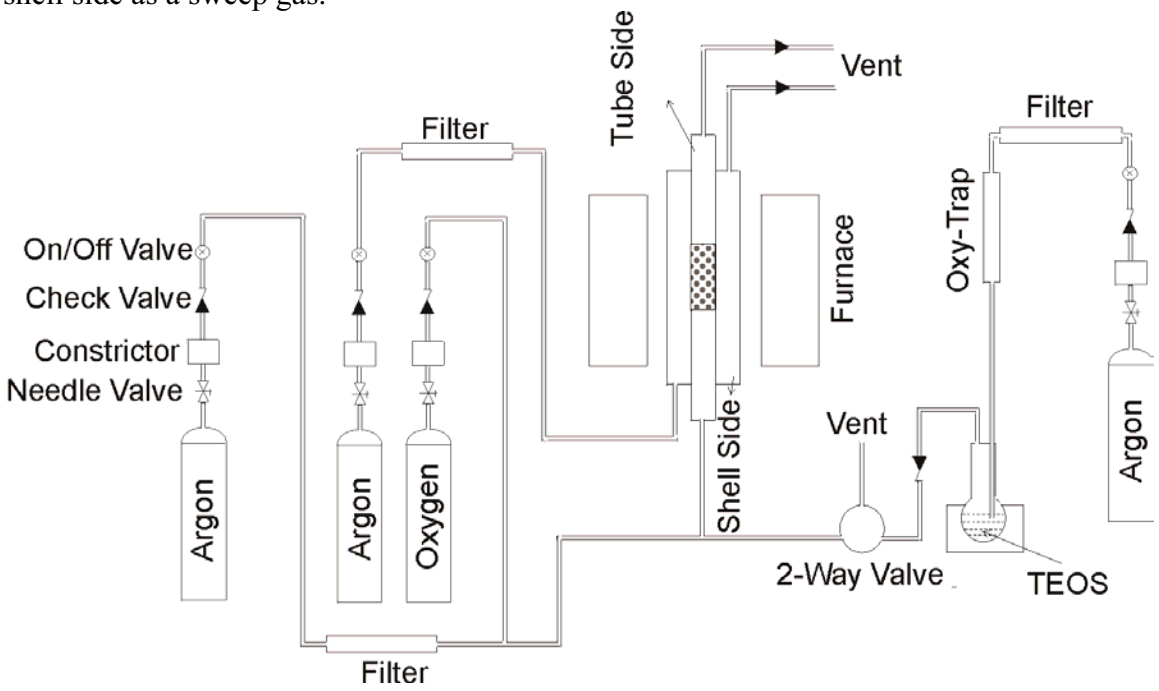

Figure 4.2 Experimental Setup for the CVD of TEOS at 473 and 873 K

4.2.2 Membrane Characterization

Both the fresh and used modified porous glass membranes were characterized by N_2 physisorption in a volumetric unit (Micromeritics ASAP 2000 series) using 0.4-0.6 g of the sample. The sample was first degassed under vacuum at 393 K. This was followed by measurement of both the adsorption and desorption amounts of N_2 at 77 K up to a $P/P_0 \sim 0.99$. The pore size distribution was determined from the desorption isotherm using the Barrett, Joyner and Halenda (BJH) method [29].

4.2.3 Isotope Exchange Studies

Figure 4.3 shows the experimental setup for isotope exchange studies. An equimolar mixture of H_2 and D_2 (5 μmol s^{-1}) premixed with Ar (7 μmol s^{-1}) was passed through the shell side of the reactor. N_2 (29 μmol s^{-1}) was used as the sweep gas on the tube side. A sample from the tube side was analyzed online using a mass spectrometer (Dycor Model) for masses 1, 2, 3, and 4. This was repeated for several temperatures. These studies were conducted for the original porous Vycor glass membrane and the modified Nanosil membrane.

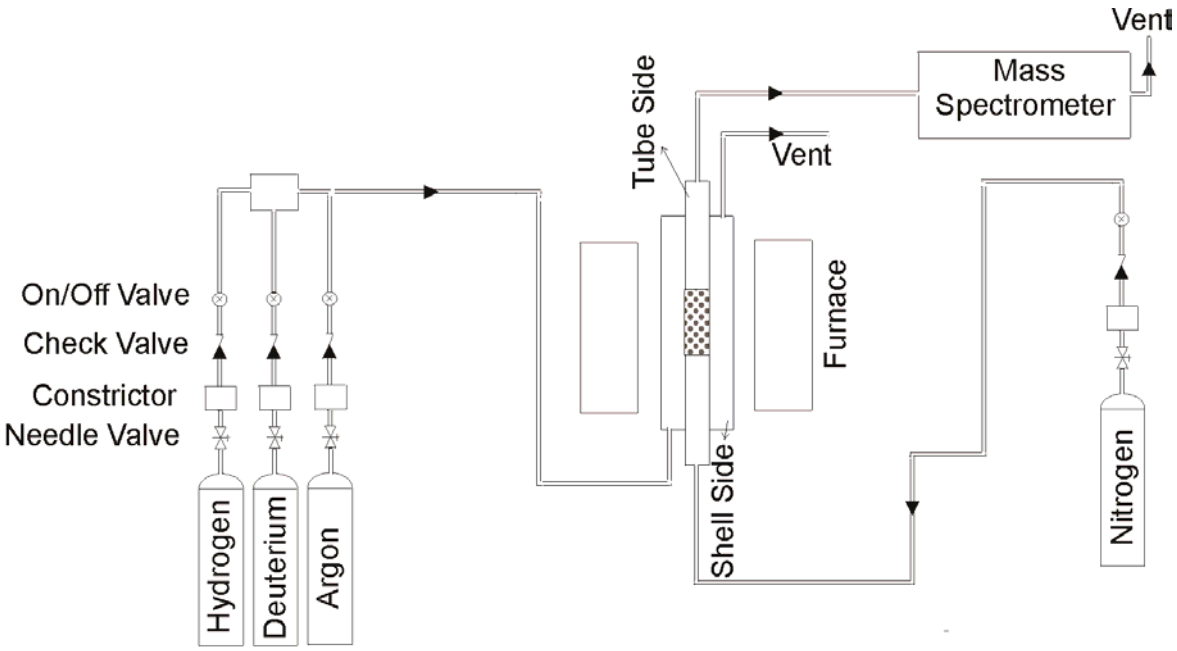

Figure 4.3 Experimental Setup to Determine Mechanism of Separation in the Nanosil Membrane

4.2.4 Catalyst Reactivity Studies

The reactor setup and experimental details are provided in Chapter 2 on catalyst results.

4.2.5 Permeability Studies

The permeability experiments are detailed in Chapter 3. Permeability coefficients were calculated from

$$P_i = \frac{Q}{A\Delta P} \qquad (1)$$

where P_i is the permeability coefficient (mol m^{-2} s^{-1} Pa^{-1}), Q is the flow rate on the tube side (mol s^{-1}), A is the cross sectional area (m^2) of the membrane available for diffusion, and ΔP is the pressure difference (Pa) between the shell and tube side. Separation factors were calculated from the ratios of individual gas permeabilities.

4.2.6 Hydrothermal Stability Experiments

For hydrothermal stability tests, the membrane system was heated to 873 K in Ar, followed by introduction of water (to make up 10% H_2O in Ar) through a syringe pump (Orion, Model 341B). The membrane was maintained at this temperature for a total of over 120 h. Permeability data was measured by stopping the moisture introduction at appropriate intervals, allowing 0.25 h to flush the system and conducting H_2 permeability studies. After determining the permeability, water was re-introduced and this process repeated several times.

4.3 Results and Discussion

The permeability coefficients for the different species were determined by flowing the pure gas on the shell side under pressure and measuring the tube side flow rate as described in Chapter 3. The hydrogen permeability coefficient Q_{H_2} for the Vycor sample was 1.8×10^{-8} mol m^{-2} s^{-1} Pa^{-1} at 873 K. However, in the literature values of 2.4×10^{-8} [30], 3.6×10^{-8} [2], 4.0×10^{-8} [10], 4.0×10^{-8} [11] and 5.4×10^{-8} mol m^{-2} s^{-1} Pa^{-1} [12] have been reported for Vycor glass at 873 K (values in mol m^{-2} s^{-1} Pa^{-1} can be converted to cm^3 cm^{-2} s^{-1} Pa^{-1} by multiplying by 2.24). Boyd and Thompson [31] have reported a value of 0.90×10^{-14} mol m^{-2} s^{-1} Pa^{-1} for solid glass at this temperature. The separation factors listed in the earlier chapter were obtained in the temperature range 300 – 973 K. The predominant mode of transport of all species in the Vycor membrane was shown to be molecular.

The porous glass membrane was modified by several methods the details of which are provided in the experimental section. Figure 4.4 compares the H_2/CH_4 separation ratios for the

membranes prepared by the modification of the original porous glass membrane by polymerization, dip coating, silica sols and CVD of TEOS (at 473 K). There was no enhancement in selectivities by modifying the porous membrane with any of these methods. The H_2 permeabilities were at or lower than the permeability of the original support material. There was also breakage of the membrane during the modification process, particularly with the sol-gel and silica sol methods. Also, with silica sol processing and polymerization, it was difficult to ensure repeatability due to the inherent nature of these processes.

The porous glass membrane was then modified by the chemical vapor deposition of TEOS at 873 K as described in the experimental section. The deposition was conducted on different samples for 48, 24, and 12 h. Figure 4.5 compares the permeabilities of these membranes with the original porous glass membrane. It is evident, that the diffusion mechanism changed from a Knudsen mode to an activated process. The 48 and 24 h deposited membranes have lower permeability than the support Vycor material. However, the 12 h deposited membrane had permeability comparable to the support material. Table 4.1 compares the selectivities of the porous glass membrane with that of the 12 h membrane. The modified membrane offered unprecedented selectivity (~ 100 %) to hydrogen with H_2/CH_4, H_2/CO, and H_2/CO_2 separation factors of at least 27000, 87000, and 8200 respectively, while retaining a high permeability (see Figure 4.5), comparable to the support material.

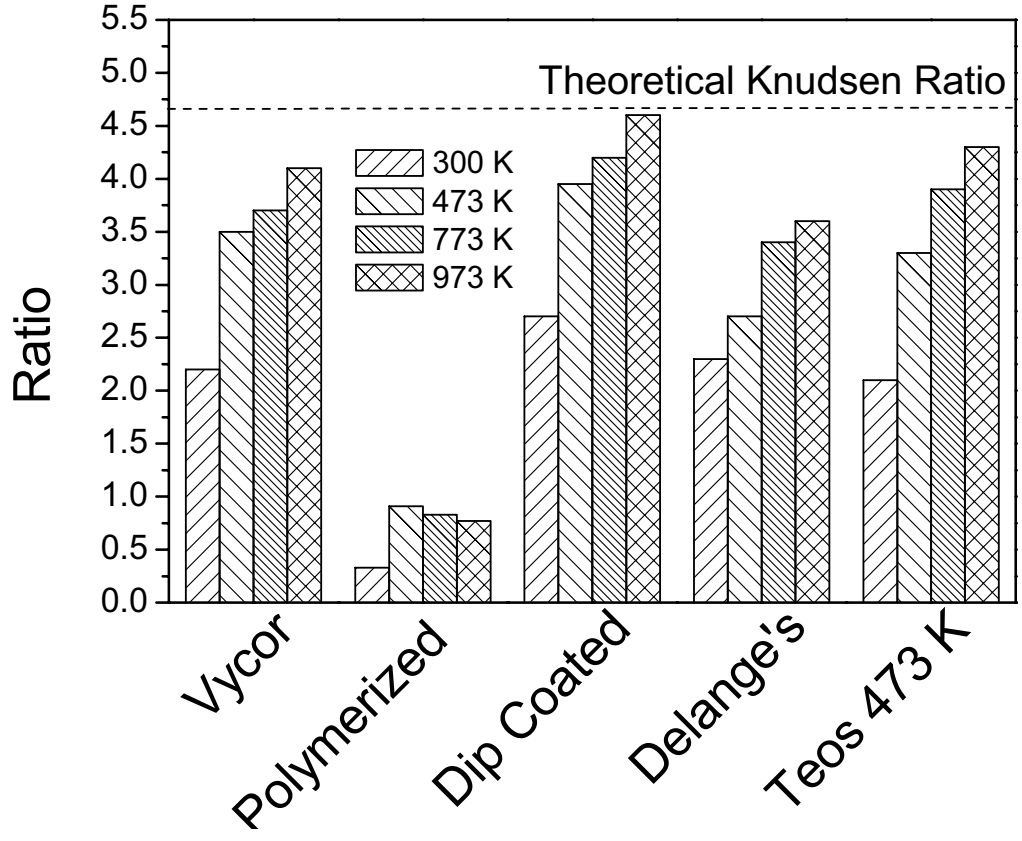

Figure 4.4 H_2/CH_4 Separation Ratios for the Membranes Developed by the Different Modification Methods

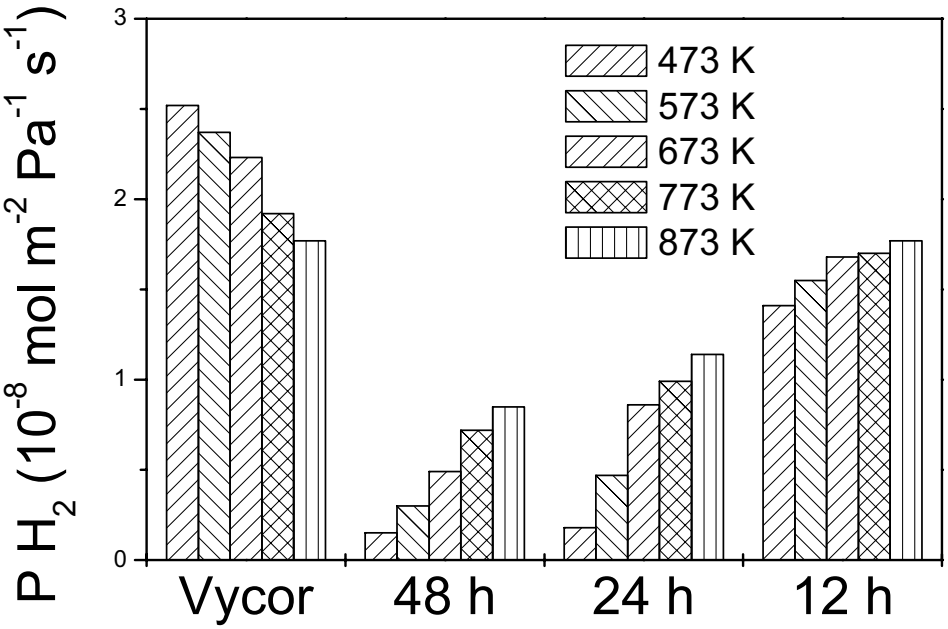

Figure 4.5 Comparison of H_2 Permeabilities of the Vycor and Nanosil Membranes

Table 4.1 Selectivity Factors for Porous Glass and Nanosil Membranes

Temp (K)	H_2/CH_4			H_2/CO			H_2/CO_2		
			Nanosil			Nanosil			Nanosil
	Theo	Expt		Theo	Expt		Theo	Expt	
473	2.83	2.76	23000	3.74	3.62	72000	4.69	4.26	6700
573			24000			76000			7400
773			27000			85000			8100
873			27000			87000			8200
973			27000			82000			7300

Isotope exchange experiments with deuterium were carried out in order to understand the mode of hydrogen transport. Table 4.2 lists the results of the studies with a hydrogen-deuterium mixture.

Table 4.2 H_2-D_2 Exchange Experiments for Porous Glass and Nanosil Membranes

Temperature (K)	mass 1/mass 2	mass 3/mass 4
873	0.72	0.57
898	0.73	0.55
923	0.72	0.55
948	0.71	0.55
973	0.72	0.57

Temperature (K)	mass 1/mass 2	mass 3/mass 4
873	0.74	0.98
898	0.73	0.85
923	0.73	0.79
948	0.72	0.80
973	0.73	0.89

The top section shows the results of reference measurements carried out with the porous Vycor glass membrane. The observation of mass 1 and mass 3 species in this case where only molecular hydrogen transport occurred was due to the fragmentation and recombination of hydrogen species in the mass spectrometer ionizer, and can be considered as a blank level for these species. The bottom section summarizes the results for the Nanosil membrane. The most important result is that the ratio of mass 3/mass 4 is substantially above the blank level indicating that HD (mass 3) has been formed by passage through the membrane. Meanwhile the ratio mass 1/mass 2 remains substantially unchanged since any fragmentation of HD contributes equal quantities of H and D. The results indicate that the mode of transport of hydrogen was atomic. The dissociation of molecular hydrogen by highly dispersed silica to form surface OH groups has been reported at temperatures as low as 393 –473 K [32]. A recent study [30] used a statistical permeance model to explain the diffusion mechanism in the Nanosil membrane. This work proposed that molecular jumps via adsorption sites that accommodate these species provide for transport across the membrane. The process was reported to involve molecular hydrogen and not atomic. In view of this, an alternative explanation for the finding of mass 3 species in the present work is needed. The observation of this species could have been due to exchange between gas-phase hydrogen and surface hydroxyl groups on the silica.

The apparent activation energy calculated from permeability data was 2 kJ mol^{-1} with the low activation energy for the process consistent with a surface diffusion mechanism. Boyd and Thompson [31] have reported E_a = 20-41 kJ mol^{-1} for solid glass while Altemose [33] has reported a value of E_a = 32 kJ mol^{-1} for non-porous glass. This was also lower than most reported values [2-5, 8-13, 15-17, 19-25]. A possible explanation can be offered by considering the mechanism of diffusion of hydrogen through silica to be a two-step process as shown below:

$$H_2 + 2^* \underset{E_{true}}{\overset{\Delta H}{\rightleftharpoons}} 2H^*$$

$$H^* \longrightarrow$$

The first step is the equilibrated adsorption of hydrogen followed by the irreversible step (surface diffusion of hydrogen on silica). This provides for $E_{app} = (E_{true} - \frac{\Delta H}{2})$ which can explain the low activation energy as calculated from the experimental data.

The Nanosil membranes were characterized by N_2 physisorption experiments. Figure 4.6 shows the adsorption and desorption isotherms (BJH method) for the fresh and used Nanosil samples.

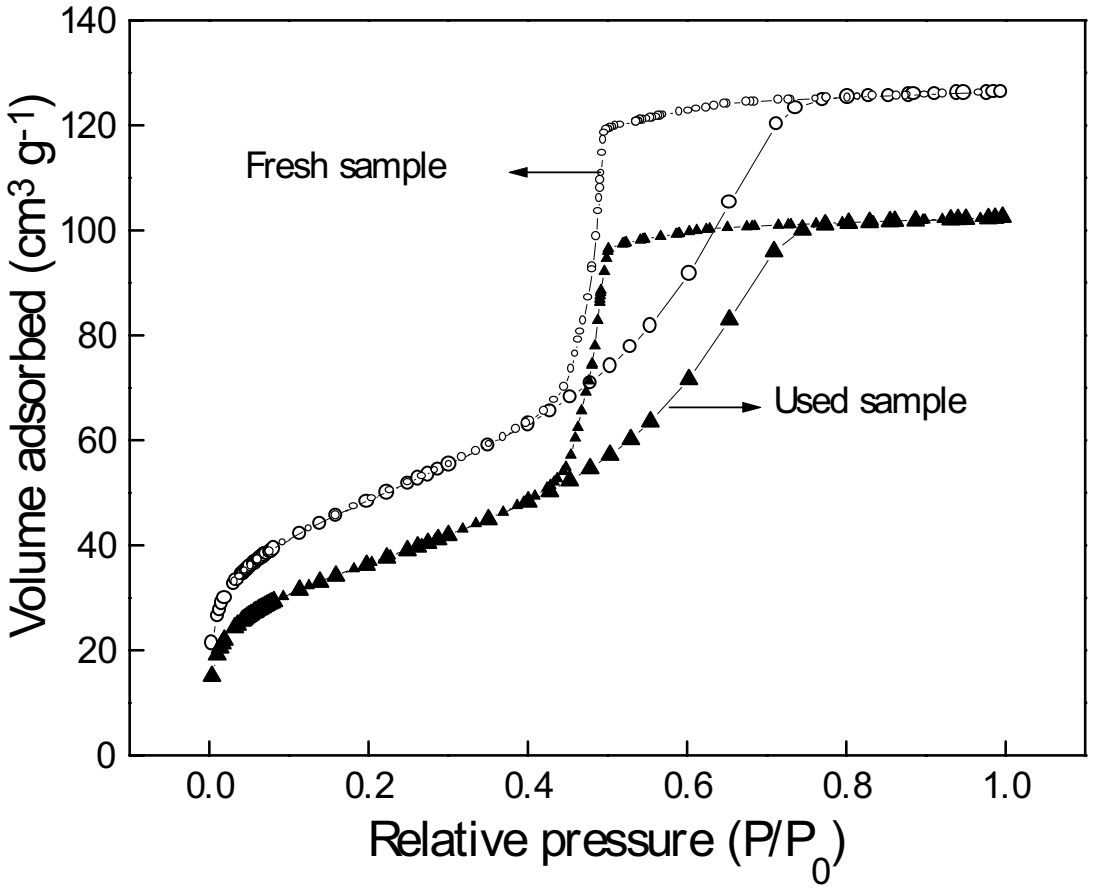

Figure 4.6 Adsorption-Desorption Isotherms for the Fresh and Used Nanosil Membranes

The isotherms obtained were similar those obtained for the porous glass samples. The used sample however, indicated shrinking of the total pore volume since the total area encompassed by the used sample was smaller than that of the fresh sample. However, as is evident from Figure 4.7, there was no appreciable change in the pore size for both the samples (average pore size of 3.6 nm).

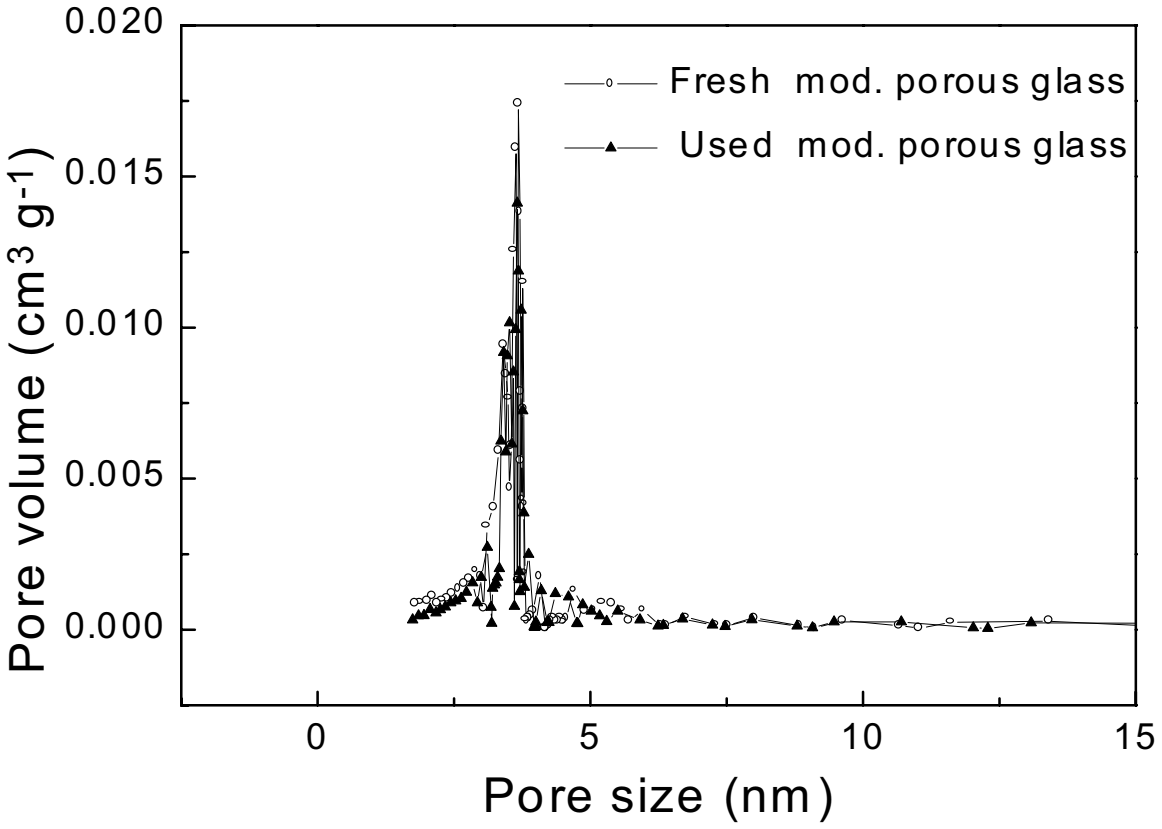

Figure 4.7 Pore Size Distribution of the Fresh and Used Nanosil Membranes

Most researchers have reported lowering of permeability (sometimes > 50 %) of silica modified membranes on exposure to moisture. Figure 4.8 shows the stability plot for the Nanosil membrane on exposure to moisture (10 % H_2O in Ar). There was only a 3 % drop in permeability in the first 12 h with no further drop in permeability for up to 120 h. This demonstrated the stability of the Nanosil membrane towards densification in the presence of moisture.

Reactivity experiments with Rh/Al_2O_3 have been described in Chapter 2. The performance of the porous Vycor membrane and its limitations was also detailed in Chapter 3. This limitation was overcome by the selective removal of only hydrogen without any loss of reactants. Figure 4.9 compares the methane conversions in the three reactor configurations: fixed-bed, porous glass membrane, and Nanosil membrane. Both the membrane configurations provided methane conversions that was higher than equilibrium conversion levels. The Nanosil membrane reactor however, provided conversions higher than the Vycor membrane reactor configuration. Experimental observations indicated that H_2 separation by the Nanosil membrane was comparable to the porous glass membrane with the added advantage of providing almost 100 % pure H_2 separation (within the limits of analytical detection).

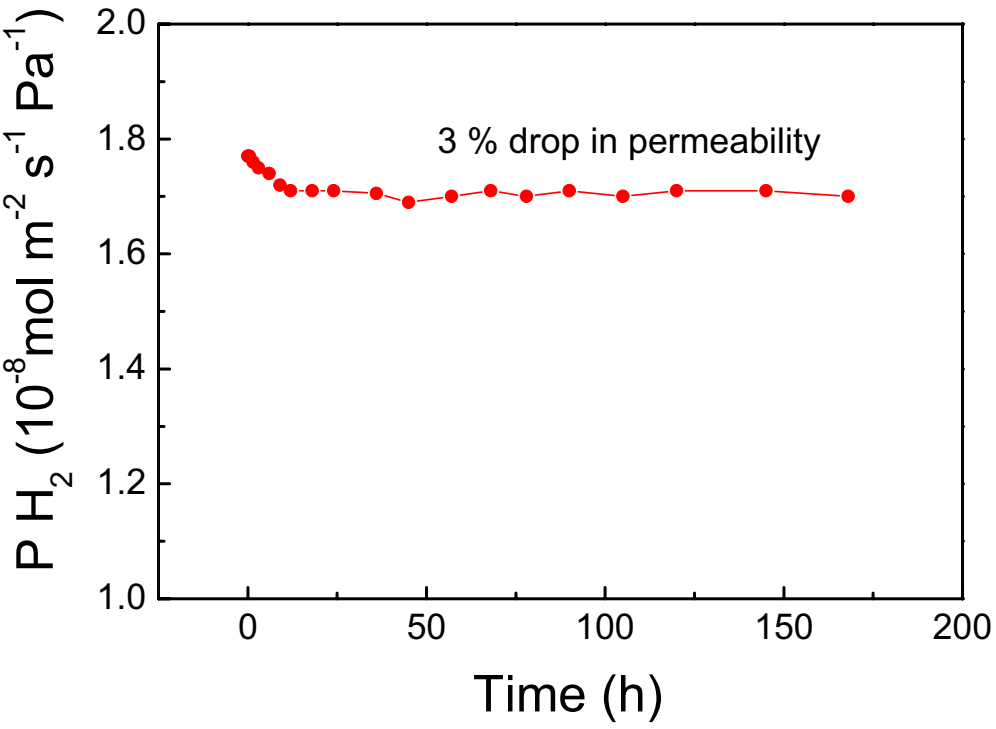

Figure 4.8 Hydrodynamic Stability of the Nanosil Membrane

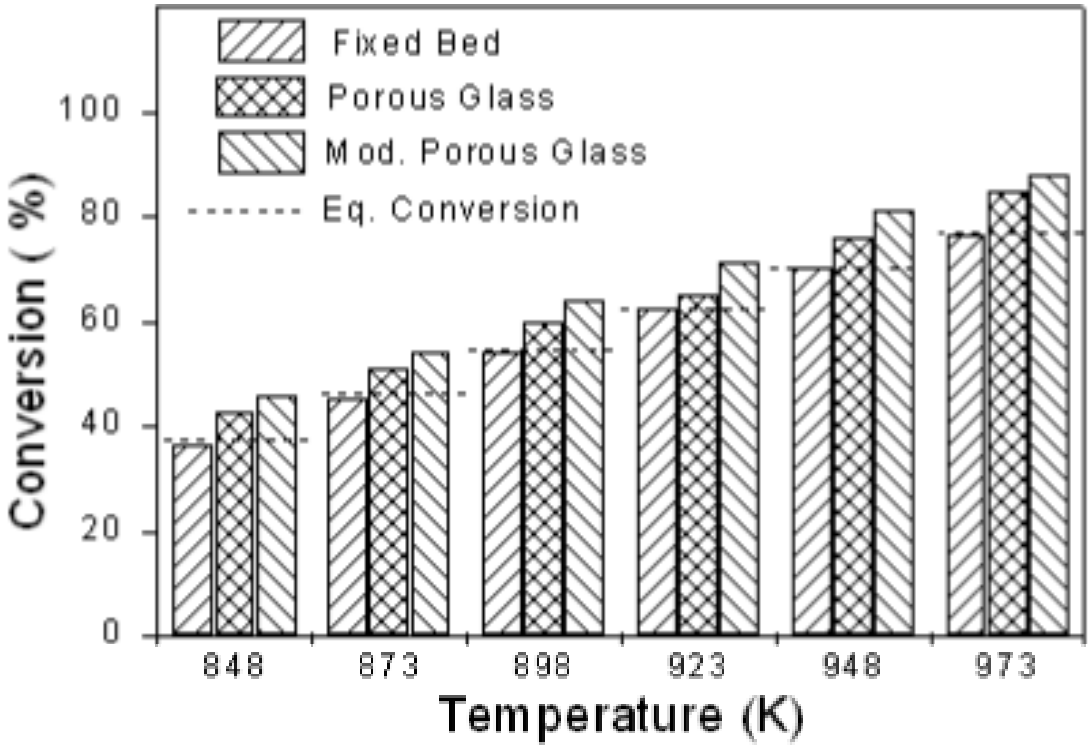

Figure 4.9 Methane Conversions in the 3 Reactor Configurations

4.4 Conclusions

The limitations imposed by thermodynamics on methane conversion have been circumvented by the use of membranes to preferentially remove a species during reaction. The shortcoming of the Knudsen mode of diffusion, was overcome by the development of a modified porous glass membrane. The Nanosil membrane developed here was remarkable considering that most studies report lowering of permeability with any improvement of selectivity. Also, as is evident from Table 4.1, such high selectivities for the species studied here have not been reported. The membrane was also stable under hydrothermal stresses.

REFERENCES

[1] S. Kim, G. R. Gavalas, Ind. Eng. Chem Res. 34 (1995) p. 168.

[2] S. Kitao, M. Asaeda, Key Engg Materials, 61 & 62 (1991) p. 267.

[3] S. Kitao, H. Kameda, M. Asaeda, Membrane 15(4) (1990) p. 222.

[4] R. A. Levy, C. Ravindranath, L. N. Krasnoperov, J. Opyrchal, E. S. Ramos, J. Electrochem. Soc. 144 (1997) p. 349.

[5] S. Morooka, S. S. Kim, S. Yan, K. Kusukabe, M. Watanabe, Int. J. Hydrogen Energy 21 (1996) p. 183.

[6] G. R. Gavalas, C. E. Megris, S. W. Nam, Chem. Eng. Sci. 44 (1989) p. 1829.

[7] H. Y. Ha, S. W. Nam, S-A. Hong, W. K. Lee, J. Membr. Sci., 85 (1993) p. 279.

[8] T. Ioannides, X. E. Verykios, Catal. Lett., 36 (1996) p. 165.

[9] B-K. Sea, M. Watanabe, K. Kusakabe, S. Morooka, S-S. Kim, Gas Sep. Purif. 10 (1996) p. 187.

[10] M. Tsapatsis, G. R. Gavalas, J. Membr. Sci. 87 (1994) p. 281.

[11] S. Jiang, Y. Yan, G. R. Gavalas, J. Membr. Sci. 103 (1995) p. 211.

[12] S. W. Nam, G. R. Gavalas, AIChE Symp. Series. 85(268) (1989) p. 68.

[13] H. Ohya, S. Sato, A. Ishii, Y. Negishi, K. Matsumoto, Int. J. Hydrogen Energy 18 (1993) p. 475.

[14] T. Okubo, H. Inoue, J. Membr. Sci., 42 (1989) p. 109.

[15] T. Okubo, H. Inoue, AIChE J. 35 (1989) p. 845.

[16] M. Tsapatsis, S. Kim, S. W. Nam, G. R. Gavalas, Ind. Eng. Chem. Res. 30 (1991) p. 2152.

[17] G. Meunier, J. P. Manaud, Int. J. Hydrogen Energy 17 (1992) p. 599.

[18] S. Uemiya, Y. Kude, K. Sugino, T. Matsuda, E. Kikuchi, Chem. Lett. (1988) p. 1687.

[19] S. Uemiya, N. Sato, H. Ando, Y. Kude, T. Matsuda, E. Kikuchi, J. Membr. Sci., 56 (1991) p. 303.

[20] J. C. S. Wu, H. Sabol, G. W. Smith, D. L. Flowers, P. K. T. Liu, J. Membr. Sci., 96 (1994) p. 275.

[21] S. Yan, H. Maseda, K. Kusakabe, S. Morooka, Ind. Eng. Chem. Res. 33 (1994) p. 2096.

[22] S. Morooka, S. Yan, K. Kusakabe, Y. Akiyama, J. Membr. Sci., 101 (1995) p. 89.

[23] R. S. A. de Lange, J. H. A. Hekkink, K. Keizer, A. J. Burggraaf, Microporous Materials 4 (1995) p. 169.

[24] R. S. A. de Lange, J. H. A. Hekkink, K. Kiezer, A. J. Burggraaf, Key Eng. Mater., 61 & 62 (1991) p. 77.

[25] R. M. de Vos, H. Verweij, Science, 279 (1998) p. 1710.

[26] R. K. Iler, The Chemistry of Silica, John Wiley & Sons, NY, NY (1979).

[27] D. Li, Ph. D. Dissertation, University of Cincinnati, Cincinnati (1991).

[28] R. S. A. de Lange, Ph. D. Dissertation, University of Twente, The Netherlands (1993).

[29] E. P. Barrett, L. G. Joyner, P. P. Halenda, J. Amer. Chem. Soc. 73 (1951) p. 373.

[30] D. Lee, S. T. Oyama, J. Memb. Sci. 210 (2002) p. 291.

[31] D. C. Boyd and D. A. Thompson, Glass, in Kirk-Othmer (Ed.), Encyclopedia of Chemical Technology, 3rd Ed. John Wiley & Sons, NY, NY Vol. II (1980) p. 807.

[32] V. K. Rajagopal, R. D. Guthrie, T. Fields, B. H. Davis, Catal. Today, 31 (1996) p. 57.

[33] V. O. Altemose, 7th Symposium on Art of Glassblowing, The American Scientific Glassblowing Society, Wilmington, DE (1962) p. 61.

5 MATHEMATICAL MODEL DEVELOPMENT

A mathematical model was developed to simulate a reactor operating with a fixed-bed and reactors incorporating the porous glass (Vycor brand from Corning, Inc.), and the totally selective modified porous glass (Nanosil) membranes. This study utilized reforming kinetics from Richardson and Paripatyadar [1] for a Rh/Al_2O_3 catalyst. Both the reforming reaction (1) and the reverse water-gas shift (RWGS) reaction (2) were included in the study.

$$CH_4 + CO_2 \rightarrow 2CO + 2H_2 \qquad \Delta H^0_{298} = 247 \text{ kJ mol}^{-1} \qquad (1)$$

$$CO_2 + H_2 \rightleftharpoons CO + H_2O \qquad \Delta H^0_{298} = 41 \text{ kJ mol}^{-1} \qquad (2)$$

The model was developed with the following assumptions:

A) steady state operation

B) plug-flow behavior

C) negligible radial and intraparticle gradients.

The mode of separation in the porous glass membrane was assumed to be predominantly by Knudsen diffusion (also experimentally demonstrated). For the modified membrane developed in this study, experiments conducted (described in chapter 4) indicated that activated diffusion was the mechanism of separation. Hence, this was used to describe diffusion in the modified porous glass (Nanosil) reactor model.

5.1 Model Development

The equations describing the combined reaction and separation flow system were developed following Wu and Liu [2], using the geometry shown in Figure 5.1. It was assumed that radial concentration gradients could be neglected. Appendix B uses correlations to verify that plug-flow conditions existed in the bed. The packed bed was held in the exterior annular region (shell side) of a concentric tubular system.

Material balance

A material balance on the shell side yielded (refer to Figure 5.1):

$$\frac{dQ_i}{dz} + 2\,\frac{D_i R_1 (P_i - P_i')}{(R_2^2 - R_1^2)} + \text{reaction rate} = 0 \qquad (3)$$

(primes refer to the tube side and for the reaction rate the + sign is assigned for reactants and – for products). The meaning of each of the symbols is given in the Nomenclature section at the end of this Chapter. Application of equation (3) to each species provided 7 equations as listed in Table 5.1.

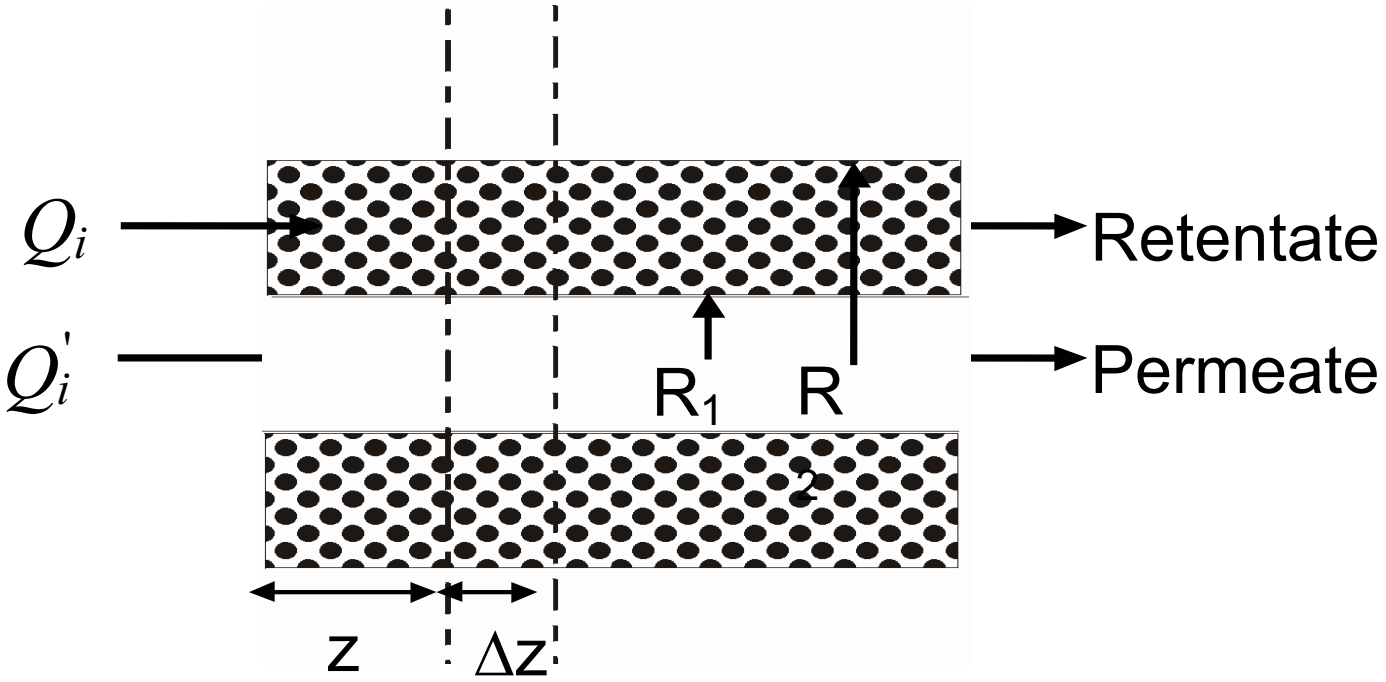

Figure 5.1 Schematic for Derivation of Material Balance

Table 5.1 Differential Equations from Mass Balance for each Species on the Shell Side

$\frac{dQ_{CH_4}}{dz} + \frac{2D_{CH_4} R_1 (P_{CH_4} - P'_{CH_4})}{(R_2^2 - R_1^2)}$ + Rate (CH_4)=0
$\frac{dQ_{CO_2}}{dz} + \frac{2D_{CO_2} R_1 (P_{CO_2} - P'_{CO_2})}{(R_2^2 - R_1^2)}$ + Rate (CO_2)= 0
$\frac{dQ_{CO}}{dz} + \frac{2D_{CO} R_1 (P_{CO} - P'_{CO})}{(R_2^2 - R_1^2)}$ - Rate (CO) = 0

$$\frac{dQ_{H_2}}{dz} + \frac{2D_{H_2}R_1(P_{H_2} - P'_{H_2})}{(R_2^2 - R_1^2)} \text{ - Rate } (H_2) = 0$$

$$\frac{dQ_{Ar}}{dz} + \frac{2D_{Ar}R_1(P_{Ar} - P'_{Ar})}{(R_2^2 - R_1^2)} = 0$$

$$\frac{dQ_{H_2O}}{dz} + \frac{2D_{H_2O}R_1(P_{H_2O} - P'_{H_2O})}{(R_2^2 - R_1^2)} \text{ - Rate } (H_2O) = 0$$

A similar balance on the tube side yielded:

$$\frac{dQ'_i}{dz} - \frac{2D_i(P_i - P'_i)}{R_1} = 0 \qquad (4)$$

Application of equation (4) to each species provided 7 equations as listed in Table 5.2.

Diffusion

For the porous glass membrane, the separation was assumed to be by Knudsen diffusion. Knudsen diffusivity (D_i) was defined as [2]

$$D_i = \frac{2r\varepsilon}{3\tau RTd}\sqrt{\frac{8000\,RT}{\pi M_i}} \qquad (5)$$

The mechanism of separation for the modified porous glass sample was activated, and the diffusion coefficient was given by [3]:

$$P = P_0 e^{(-\frac{E}{RT})} \qquad (6)$$

Partial pressure

The partial pressures of each component on the shell and tube side was expressed by the following:

$$P_i = \frac{Q_i}{\Sigma Q_i} P_t \qquad (7)$$

$$P_i' = \frac{Q_i'}{\sum Q_i'} P_t' \tag{8}$$

Table 5.2 Differential Equations from Mass Balance for each Species on the Tube Side

$\frac{dQ'_{CH_4}}{dz} - \frac{2D_{CH_4}(P_{CH_4} - P'_{CH_4})}{R_1} = 0$
$\frac{dQ'_{CO_2}}{dz} - \frac{2D_{CO_2}(P_{CO_2} - P'_{CO_2})}{R_1} = 0$
$\frac{dQ'_{CO}}{dz} - \frac{2D_{CO}(P_{CO} - P'_{CO})}{R_1} = 0$
$\frac{dQ'_{H_2}}{dz} - \frac{2D_{H_2}(P_{H_2} - P'_{H_2})}{R_1} = 0$
$\frac{dQ'_{Ar}}{dz} - \frac{2D_{Ar}(P_{Ar} - P'_{Ar})}{R_1} = 0$
$\frac{dQ'_{H_2O}}{dz} - \frac{2D_{H_2O}(P_{H_2O} - P'_{H_2O})}{R_1} = 0$

Pressure drop [4]

The shell side pressure drop was estimated from the Ergun equation (9) while the tube side pressure drop was calculated from the standard equation for flow through a pipe (10).

$$\frac{-dP_t}{dz} = \frac{150\mu_s v_z (1-\varepsilon)^2}{d_p^2 \varepsilon^3} + \frac{1.75\rho_s v_z^2 (1-\varepsilon)}{d_P \varepsilon^3} \tag{9}$$

$$\frac{-dP_t'}{dz} = \frac{8v_z' \mu_t}{R_1^2} \tag{10}$$

Kinetics

The kinetics developed by Richardson and Paripatyadar [1] for a Rh/Al_2O_3 were used in the model developed here. The effects of the RWGS reaction was included in determining the kinetics for the methane reforming reaction. The rate equations (forward rate) for the reforming and the RWGS were:

$$r_1 = k_1\left[\frac{K_{CO_2}K_{CH_4}P_{CO_2}P_{CH_4}}{(1+K_{CO_2}P_{CO_2}+K_{CH_4}P_{CH_4})^2}\right] \tag{11}$$

$$r_2 = k_2 P_{CO_2} \tag{12}$$

The reverse rate expressions were determined by the addition of a term to the forward rate equation such that at equilibrium, the net rate approached zero [1]. Using this, the net rates for the two reactions were:

$$\text{net rate of reaction 1} = k_1\left[\frac{K_{CO_2}K_{CH_4}P_{CO_2}P_{CH_4}}{(1+K_{CO_2}P_{CO_2}+K_{CH_4}P_{CH_4})^2}\right]\left[1-\frac{(P_{CO}P_{H_2})^2}{K_1 P_{CH_4}P_{CO_2}}\right] \tag{13}$$

$$\text{net rate of reaction 2} = k_2 P_{CO_2}\left[1-\frac{P_{CO}P_{H_2O}}{K_2 P_{CO_2}P_{H_2}}\right] \tag{14}$$

The independent variable was z and the dependent variables (total of 14) were Q_{CH_4}, Q_{CO_2}, Q_{CO}, Q_{H_2}, Q_{Ar}, Q_{H_2O}, Q'_{CH_4}, Q'_{CO_2}, Q'_{CO}, Q'_{H_2}, Q'_{Ar}, Q'_{H_2O}, P_t, P'_t. The total number of equations were 14 (6 for each species on the shell side, 6 for each species on the tube side and 2 from the pressure drop). The boundary conditions are listed in Tables 5.3 and 5.4. The differential equations were solved using the DIVPAG subroutine available in the IMSL Library in FORTRAN (for the fixed-bed mode, there was no contribution from diffusion), the details of which are given in Appendix A.

Table 5.3 Shell Side Boundary Conditions

$Q_{CH_4} = Q_{CH_4,0}$	$Q_{CO_2} = Q_{CO_2,0}$
$Q_{CO} = 0.0$	$Q_{H_2} = 0.0$
$Q_{Ar} = Q_{Ar,0}$	$Q_{H_2O} = 0.0$
$P_t = P_{t,0}$	

Table 5.4 Tube Side Boundary Conditions

$Q'_{CH_4} = 0.0$	$Q'_{CO_2} = 0.0$
$Q'_{CO} = 0.0$	$Q'_{H_2} = 0.0$
$Q'_{Ar} = Q_{Ar,0}$	$Q'_{CO} = 0.0$
$P'_t = P'_{t,0}$	

Energy balance

An extra equation was developed to account for axial thermal gradients (due to the strong endothermicity of the reforming reaction) for the fixed-bed configuration only. As will be clear from the results presented later, the axial temperature change was minimal so as not to present significant gradients in the reactor. Therefore, only the isothermal operation was considered for the two membrane configurations. An energy balance [5] on the reactor resulted in:

$$\frac{dT}{dz} = \frac{U + [-Rate(CO_2)][-\Delta H_R(T)_1 - \Delta H_R(T)_2]}{F_{CO_{2,0}}\left[\sum \Theta_i C_{p_i} + (X_1 \Delta C_{p_1}) + (X_2 \Delta C_{p_2})\right]} \quad (15)$$

where

$$\mathrm{U} = \frac{2\pi L k_q (Temp - T)}{\ln(R_{out}/R_2)} + 2\pi R_{out} L \sigma (Temp^4 - T^4)\,[6]$$

$$\Delta H_R(T)_1 = \sum H_1^0(298) + \int_{298}^{T} \Delta C_{p_1}$$

$$\Delta H_R(T)_2 = \sum H_2^0(298) + \int_{298}^{T} \Delta C_{p_2}$$

For this case, the system of differential equations system consisted of an additional equation with one additional variable, temperature. The solution was developed as before using the DIVPAG subroutine in FORTRAN.

5.2 Results and Discussion

Figure 5.2 compares the results from the model for the fixed-bed reactor in the adiabatic mode of operation and the one with an external heat source (such as a furnace) at 873 K.

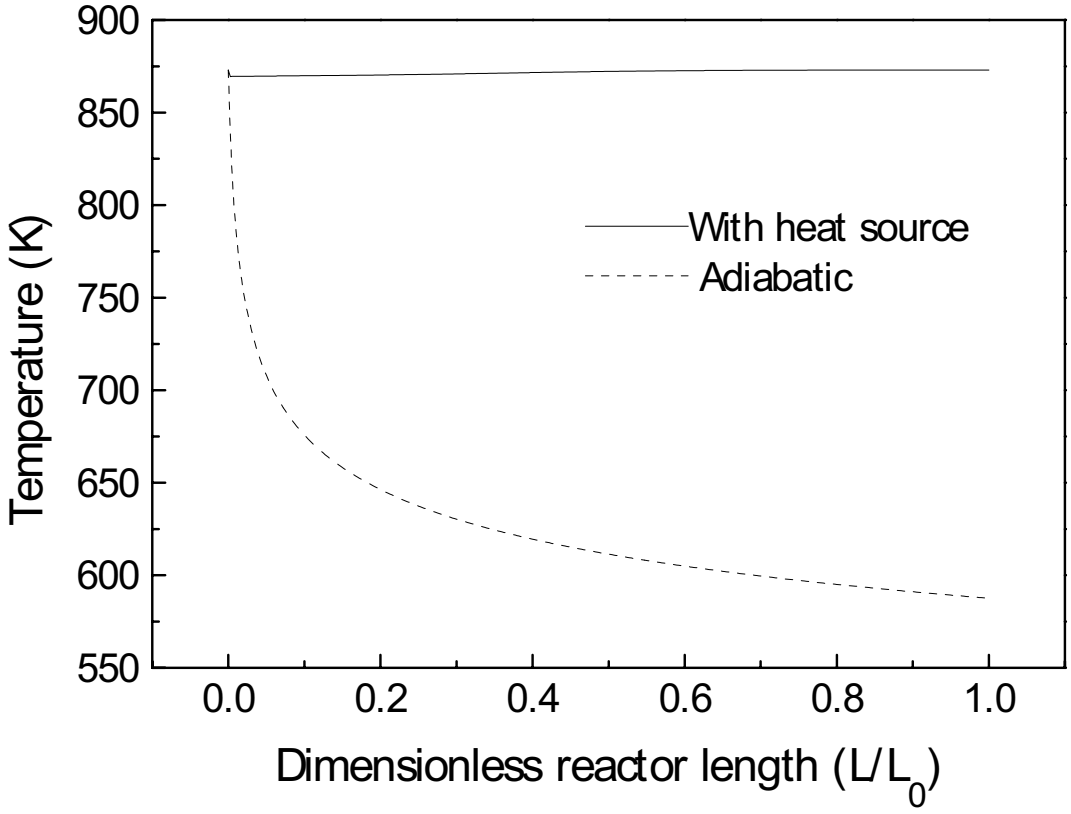

Figure 5.2 Temperature Profile along the Length of the Reactor

For the former, there is a clear drop in temperature with consequent quenching of the reaction, while the latter shows no appreciable change in axial temperature. As an additional check, correlations from [7- 10] were used to establish the fact that radial and intraparticle gradients if any, were small (see Appendix B). The energy balance term was not included for the membrane configurations in view of the fact that the fixed-bed model predicted negligible axial gradients in temperature.

Figure 5.3 shows the pressure drop on the shell side for the fixed bed configuration. The pressure drop through the fixed-bed was negligible (about 0.5 Pa), compared to the total pressure of the system, 101 kPa.

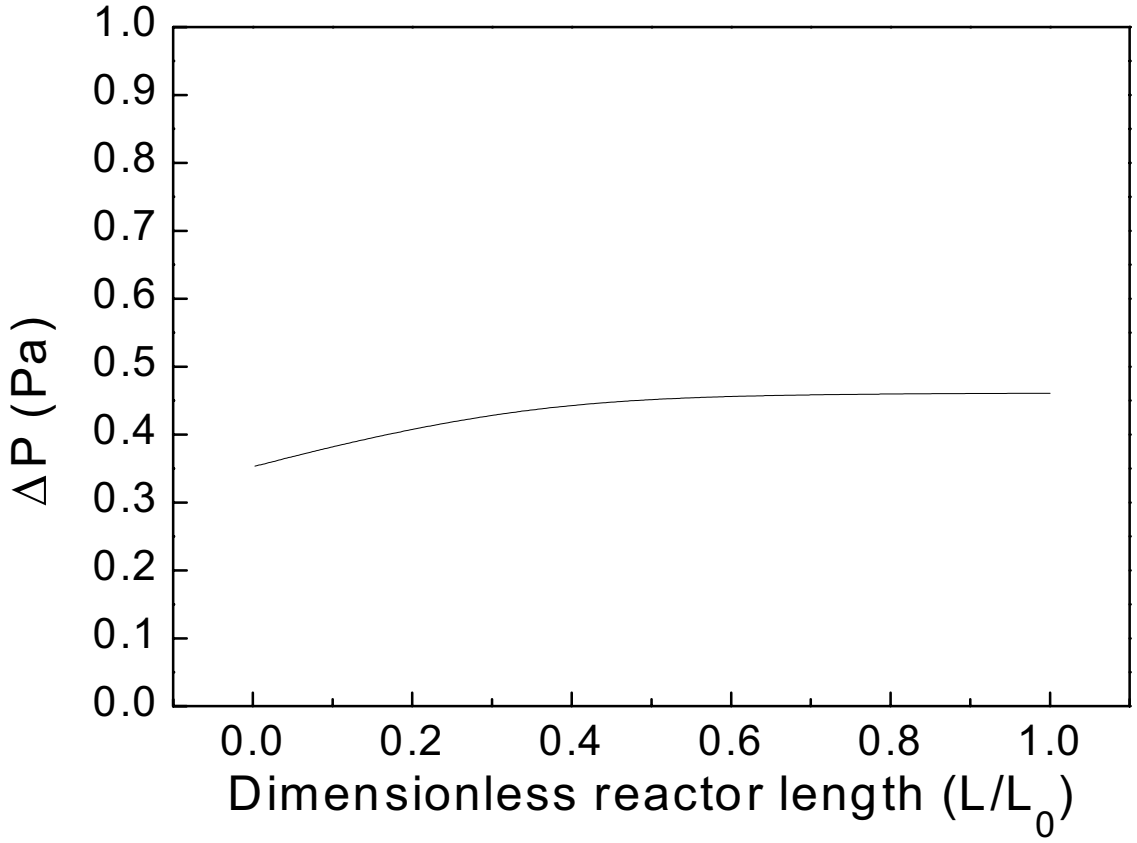

Figure 5.3 Pressure Drop in the Fixed Bed Mode

Figure 5.4 shows the predicted flows of CH_4, CO_2 and H_2 in the three reactor configurations at 973 K. The topmost panel (Fig 5.4 a) shows the flow rate of these species in the fixed bed mode of operation. The CO_2 and CH_4 flows decrease from inlet to outlet since they are the reactants. The CO_2 flow is lower because it is consumed by the RWGS reaction. The H_2 flow rate gradually increases down the length of the reactor, and becomes constant around 0.6 L/L_0. The next two panels show the flow rates of the species in the reactor with the Vycor membrane. On the shell side (Fig 5.4 b), the flows are similar to that in the fixed bed. CH_4 and CO_2 decrease from inlet to outlet, CO_2 more because of the RWGS reaction. H_2 increases along the reactor as it is a product of the dry reforming reaction. On the tube side (Fig 5.4 c), CH_4 and CO_2 appear immediately because they are present at high concentrations as reactants, and because the Vycor membrane is poorly selective. H_2 then appears and grows down the reactor.

The final two panels show the flow rates of the species in the reactor with the Nanosil membrane. On the shell side (Fig 5.4 d), the flows are similar to those in the fixed bed and Vycor membrane configuration. On the tube side (Fig 5.4 e), in contrast to the findings with the Vycor membrane, only hydrogen appears and grows along the length of the reactor. CH_4 and CO_2 do not appear since this membrane is selective to only H_2 and does not permit transport of these species. This is an important result as it shows the possibility of providing pure H2 without contamination by other species.

Figure 5.5 provides a similar plot for species to include CO_2, CO, H_2, and H_2O. The model developed provided a better understanding of the nature of the reacting streams and the individual concentrations of each species along the length of the reactor.

Figure 5.6 compares the tube side molar flows of hydrogen in the porous glass membrane and Nanosil membrane reactors. The molar flows are comparable which agrees with our experimental observation of similar hydrogen flow rates (in the tube side) with the original and modified membranes.

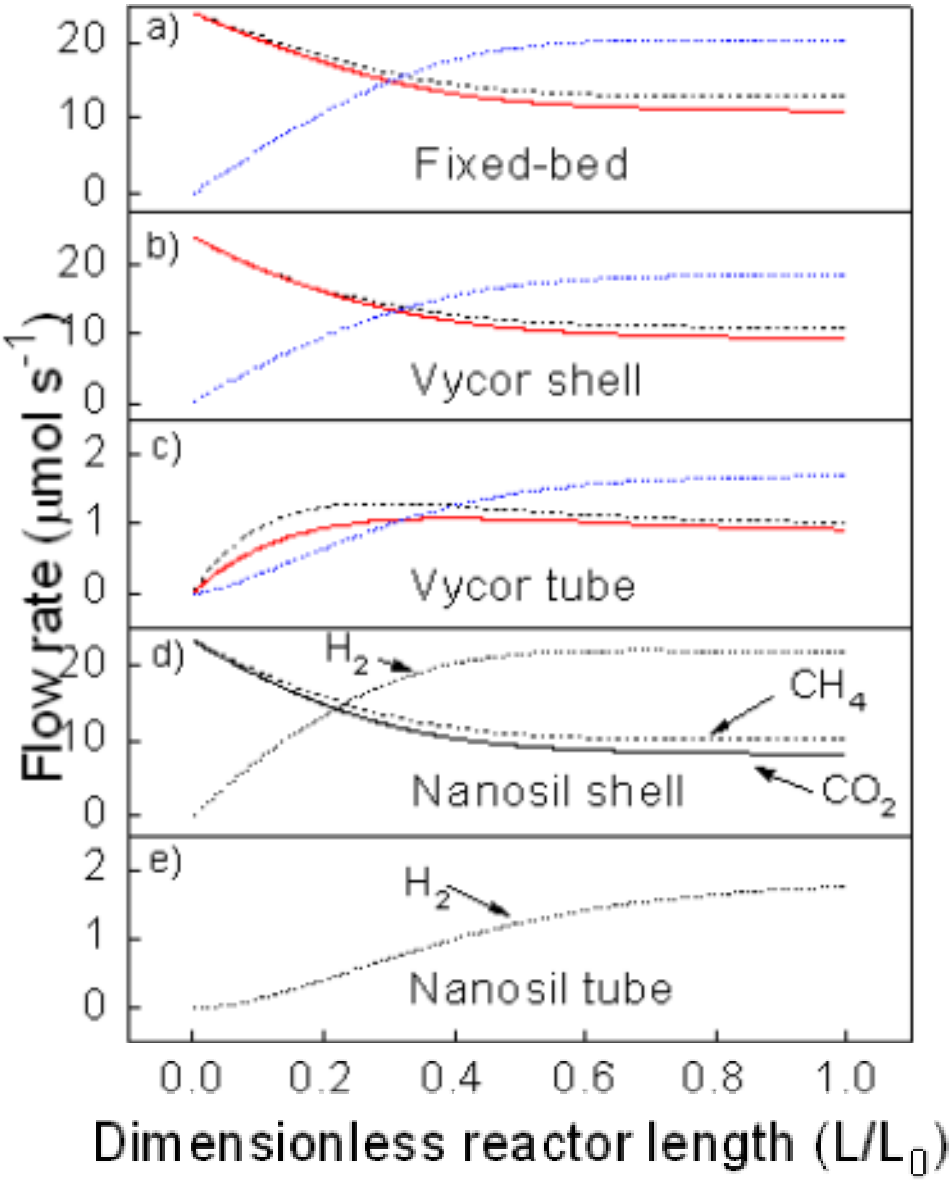

Figure 5.4 Flow Profiles for CH_4, CO_2 and H_2 Derived from the Mathematical Model at 973 K

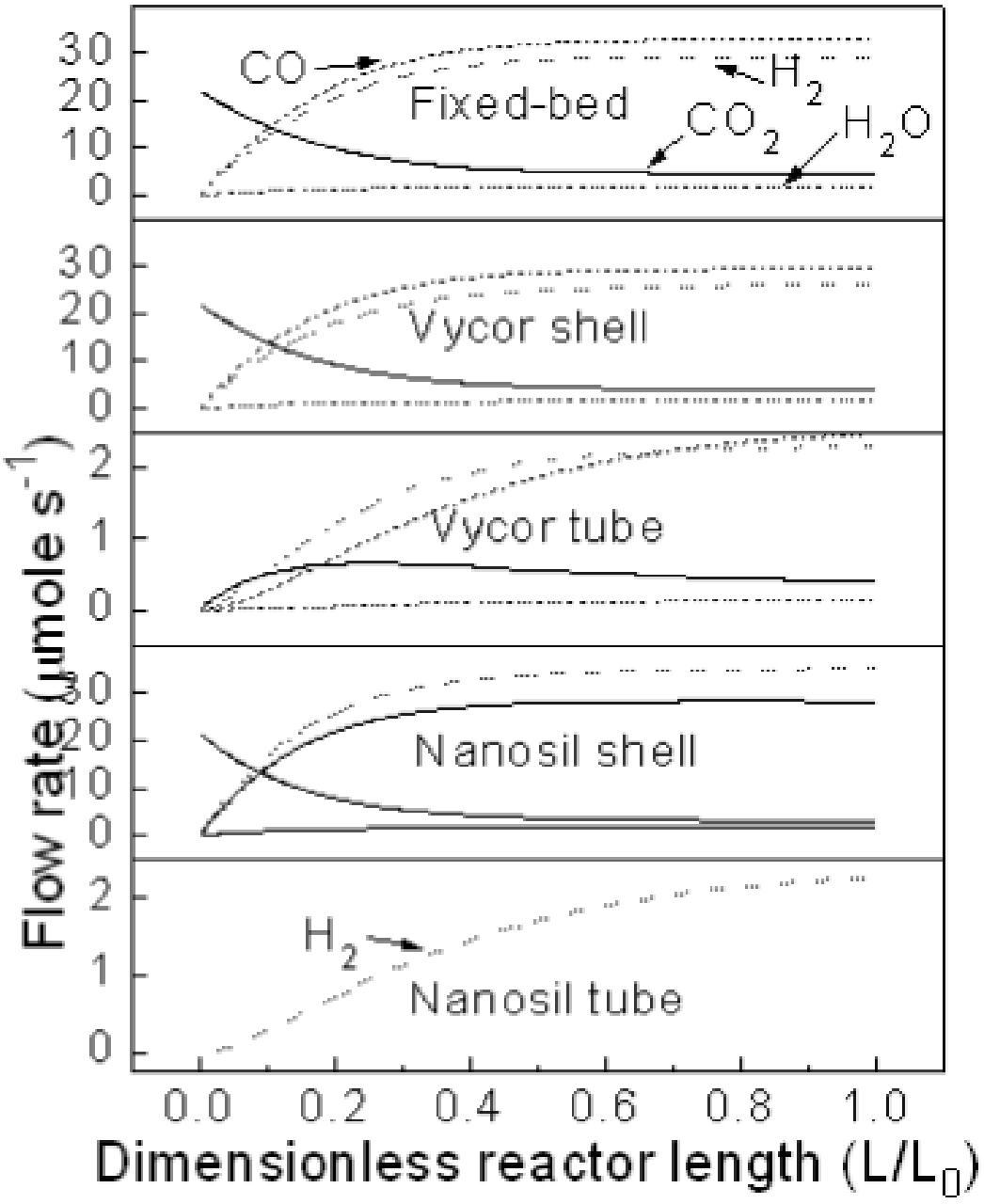

Figure 5.5 Flow Profiles for CO_2 CO, H_2 and H_2O Derived from the Mathematical Model at 973 K

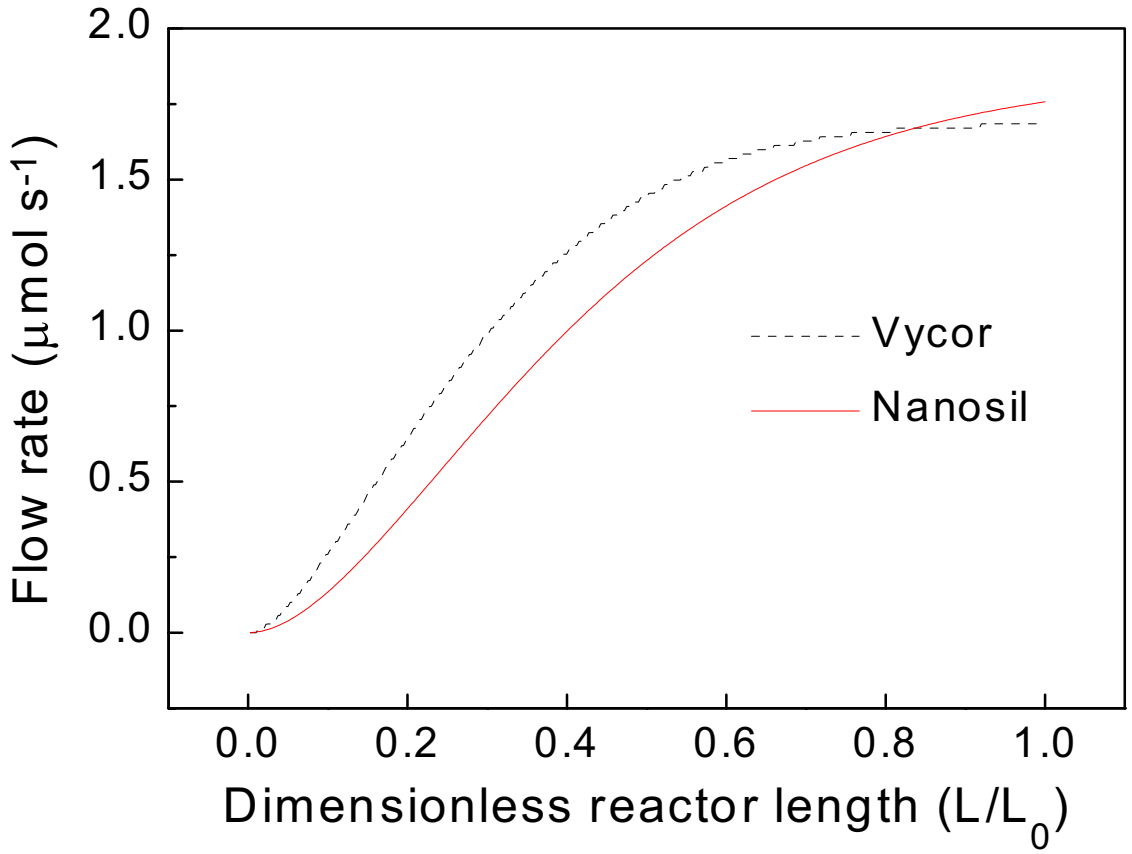

Figure 5.6 Comparison of Tube Side H_2 Flow Rate for the Two Membrane Configurations

Table 5.5 compares the theoretical and experimental values of the equilibrium constants (K_1 and K_2) for the reforming and the RWGS reactions respectively. Theoretical values were calculated from [11]:

$$\ln K_1 = \frac{-28657.2}{T} + 6.091\ln(T) - 8.168\times10^{-3}\frac{T}{2} + 2.164\times10^{-6}\frac{T^2}{6} + \frac{126100}{2T^2} - 6.88612 \quad (16)$$

$$\ln K_2 = \frac{5872.37}{T} - 1.86\ln(T) + 5.4\times10^{-4}\frac{T}{2} + \frac{116400}{2T^2} + 18.0133 \quad (17)$$

The experimental values were calculated from the mole fractions of all the species in the three configurations (also listed in Table 5.5). There is close agreement between the experimental and theoretical values of the equilibrium constants.

Table 5.5 Comparison of Theoretical and Experimental Values of the Equilibrium Constants (873 K)

Fixed Bed Reactor

Theoretical		Experimental		Mole fraction				
K_1	K_2	K_1	K_2	CH_4	CO_2	CO	H_2	H_2O
0.18	0.37	0.18	0.36	0.14	0.11	0.26	0.20	0.03

Vycor Membrane Reactor

Theoretical		Experimental		Mole fraction				
K_1	K_2	K_1	K_2	CH_4	CO_2	CO	H_2	H_2O
0.18	0.37	0.17	0.44	0.12	0.09	0.24	0.18	0.03

Nanosil Membrane Reactor

Theoretical		Experimental		Mole fraction				
K_1	K_2	K_1	K_2	CH_4	CO_2	CO	H_2	H_2O
0.18	0.37	0.19	0.39	0.13	0.10	0.27	0.19	0.03

Table 5.6 compares the results from the mathematical model with the experimental results for all three reactor systems. The table also provides theoretical methane conversions from thermodynamic calculations. The simulated results track the experimental values fairly well at all conditions for all the reactor configurations. Close examination indicates that the model is marginally higher than experimental for the fixed bed configuration but is mostly lower than the experimental values for the membrane configurations.

Table 5.6 Theoretical and Experimental Methane Conversions in the Three Different Reactor Systems

		Fixed bed		Porous Vycor		Nanosil	
Temp (K)	Thermodynamic (%)	Model (%)	Experimental (%)	Model (%)	Experimental (%)	Model (%)	Experimental (%)
848	37.5	37.8	36.70	41.9	42.7	44.0	46.0
873	45.7	46.3	45.2	50.1	51.3	53.2	54.1
898	54.2	54.9	54.3	58.3	59.9	62.2	64.2
923	62.5	63.1	62.6	65.9	65.3	70.2	71.5
948	70.0	70.4	70.2	75.7	76.1	79.2	81.4

5.3 Nomenclature

C_{p_i} = heat capacity of species i (J mol^{-1} K^{-1})

d_p = particle diameter (m)

D_i = effective permeability of species i (mol m^{-2} Pa^{-1} s^{-1})

E = activation energy (J mol^{-1})

$F_{CO_{2,0}}$ = initial molar flow rate of CO_2 (mol s^{-1})

k_q = thermal conductivity of quartz (J m^{-1} s^{-1} K^{-1})

k_b = thermal conductivity of the bed (J m^{-1} s^{-1} K^{-1})

k_1 = rate constant for (1) (mol g_{cat}^{-1} s^{-1})

k_2 = rate constant for (2) (mol g_{cat}^{-1} s^{-1})

K_{CO_2} = adsorption equilibrium constant of CO_2 (Pa^{-1})

K_{CH_4} = adsorption equilibrium constant of CH_4 (Pa^{-1})

L = length of the reactor (m)

L_0 = total length of reactor (m)

M_i = molecular weight of species i (g mol^{-1})

n = number of moles in stagnant reactor (mol)

N_{Re_P} = particle Reynold's number

P = permeability coefficient (mol m^{-2} s^{-1} Pa^{-1})

P_o = permeability constant (mol m^{-2} s^{-1} Pa^{-1})

P_i = partial pressure of species i on shell side (Pa)

P_i' = partial pressure of species i on tube side (Pa)

P_t = total pressure on shell side (Pa)

P_t' = total pressure on tube side (Pa)

Q_i = molar flux of species i on shell side (mol m^{-2} s^{-1})

Q_i' = molar flux of species i on tube side (mol m^{-2} s^{-1})

r = pore radius of the membrane (m)

r_R = hydraulic radius (m)

r' = rate of reaction with inert quartz particles (mol s^{-1} m^{-3})

R = gas constant (Pa m^3 mol^{-1} K^{-1})

R_1 = outer radius of the tube (m)

R_2 = inner radius of the shell (m)

R_{in} = inner radius of the tube (m)

R_{out} = outer radius of shell (m)

t = membrane thickness (m)

T = shell temperature (K)

$Temp$ = furnace temperature (K)

U = heat generated by furnace (J s^{-1})

μ_s = viscosity of the mixture on the shell side (N s m^{-2})

μ_t = viscosity of the mixture in the tube side (N s m^{-2})

x = conversion

X_1, X_2 = conversion of CO_2 from reaction 1 and 2 respectively

ΔCp = sum of heat capacities (J mol^{-1} K^{-1})

ΔH = heat of reaction (J mol^{-1})

$\Delta H_R(T)_1$ = heat of reaction for reaction 1 (J mol^{-1})

$\Delta H_R(T)_2$ = heat of reaction for reaction 2 (J mol^{-1})

τ = tortuosity of the membrane

ε = porosity of the packed bed

ε_p = porosity of the membrane

ρ_s = density of the mixture on the shell side (kg m^{-3})

ρ_t = density of the mixture on the tube side (kg m^{-3})

σ = Stefan-Boltzmann constant (W m^{-2} K^{-4})

v_z = shell side mixture velocity (m)

v_z' = tube side mixture velocity (m)

Θ_i = stoichiometric ratio of species i [5]

Values used for computation:

$C_{p_{CH_4}} = 14.15 + 0.0755T - 1.799 \times 10^{-5} T^2$ (J mol^{-1} K^{-1}) [11]

$C_{p_{CO_2}} = 45.37 + 8.688 \times 10^{-3} T - 961929.8 T^{-2}$ (J mol^{-1} K^{-1}) [11]

$C_{p_{CO}} = 28.068 + 4.631 \times 10^{-3} T - 25773.4 T^{-2}$ (J mol^{-1} K^{-1}) [11]

$C_{p_{H_2}} = 27.012 + 3.508 \times 10^{-3} T + 69006.2 T^{-2}$ (J mol^{-1} K^{-1}) [11]

$C_{p_{Ar}} = 20.79$ (J mol^{-1} K^{-1}) [11]

$C_{p_{H_2O}} = 28.85 + 0.012T + 100599.4 T^{-2}$ (J mol^{-1} K^{-1}) [11]

$d_p = 0.326 \times 10^{-3}$ (m)

E = 1900 (J mol^{-1}) [12]

$k = 2.7755$ (J m^{-1} s^{-1} K^{-1}) [6]

k_q = 0.15 at 973 K (J m^{-1} s^{-1} K^{-1}) [6]

$k_b = 4.4 \times 10^{-2}$ for Ar at 873 K (J m^{-1} s^{-1} K^{-1}) [6]

$k_1 = 1290 \times \exp\left[\frac{-102065}{R \times T}\right]$ (mol g_{cat}^{-1} s^{-1}) [13]

k_2 $= 1.875 \times \exp\left[\frac{-73105}{R \times T}\right]$ (mol g_{cat}^{-1} s^{-1}) [13]

K_{CO_2} $= 2.64 \times 10^3 \times \exp\left[\frac{37641}{R \times T}\right]$ (Pa^{-1}) [13]

K_{CH_4} $= 2.63 \times 10^3 \times \exp\left[\frac{40684}{R \times T}\right]$ (Pa^{-1}) [13]

L_0 = 0.04 (m)

P_o = 2.3 (mol m^{-2} s^{-1} Pa^{-1}) [12]

r $= 4.0 \times 10^{-9}$ (m)

r_R = 2×10^{-3} (m)

R = 8.314 (Pa m^3 mol^{-1} K^{-1}) [11]

R_1 $= 5.0 \times 10^{-3}$ (m)

R_2 $= 7.0 \times 10^{-3}$ (m)

R_{in} = 4.0×10^{-3} (m)

R_{out} $= 8.0 \times 10^{-5}$ (m)

t $= 1.0 \times 10^{-3}$ (m)

τ = 3.0 [14]

ε = 0.6

ε_p = 0.4 [14]

σ = 5.67×10^{-8} (W m^{-2} K^{-4}) [6]

REFERENCES:

[1] J. T. Richardson, S. A. Paripatyadar, Appl. Catal. 61 (1990) p. 293.

[2] J. C. S. Wu, P. K. T. Liu, Ind. Eng. Chem. Res. 31 (1992) p. 323.

[3] A. K. Prabhu, S. T. Oyama, J. Memb. Sci. 176 (2000) p. 233.

[4] R. B. Bird, W. E. Stewart, E. N. Lightfoot, Transport Phenomena, John Wiley & Sons, New York, NY (1960).

[5] H. S. Fogler, Elements of Chemical Reaction Engineering, 2nd Ed., Prentice-Hall Inc., New Jersey (1992) p. 410.

[6] F. P. Incropera, D. P. De Witt, Fundamentals of Heat and Mass Transfer, 2nd Ed. John Wiley & Sons, New York, NY (1985) p. 760.

[7] C. N. Satterfield, Heterogeneous Catalysis in Industrial Practice, 2nd Ed. McGraw Hill Inc., Singapore (1993) p. 492.

[8] F. M. Dautzenburg, Symp. Div. of Petr. Chem. and the D-32 Committee of ASTM at the 196th National Meeting of the ACS, Los Angeles, CA (1988).

[9] D. E. Mears, Ind. Eng. Chem. Process Des. Dev. 10 (1971) p. 541.

[10] D. E. Mears, The role of axial dispersion in trickle-flow laboratory reactors, Chem Eng. Sci. 26 (1971) p. 1361.

[11] J. M. Smith, H. C. van Ness, Introduction to Chemical Engineering Thermodynamics, 4th Ed., McGraw-Hill Co., New York, NY (1987) p. 106.

[12] A. K. Prabhu, S. T. Oyama, J. Memb. Sci. 176 (2000) p. 233.

[13] J. T. Richardson, S. A. Paripatyadar, Appl. Catal. 61 (1990) p. 293.

[14] Data for Vycor Glass 7930, Corning Inc., NY.

6. CONCLUSIONS AND FUTURE WORK

6.1 Conclusions

Both Ni and Rh catalysts developed in this work provided high activity and were stable for tens of hours of operation with no appreciable deactivation. The conversions provided were also at or close to thermodynamic equilibrium levels. To overcome equilibrium limitations, a commercially available porous Vycor membrane reactor was utilized to selectively remove the products from the reaction chamber. However, due to its poor selectivity, there was some loss of reactants to the tube side, providing only marginal improvements in performance. To overcome this drawback, a hydrogen-only selective membrane was developed using chemical vapor deposition of a silica precursor. This membrane termed Nanosil, provided unprecedented selectivities to H_2 compared to CH_4, CO_2 and CO with no attendant loss of permeability of the base substrate. The utilization of this new membrane allowed selective separation of only hydrogen thereby providing better performance than the Vycor membrane reactor. A mathematical model was developed to simulate the operation of the three different reactors. The results from theoretical modeling matched fairly well with those from experimental studies.

6.2 Future Work

Future work could involve items listed below:

a) Use of a higher permeability substrate. Modify this substrate using the process developed here to provide high selectivities together with high permeabilities (fluxes).
b) Use special techniques to probe the surface of the modified glass. Atomic Force Microscopy had been explored but provided no information on actual pore structure particularly for the Nanosil membrane.
c) Modify mathematical model to study if absolute separation efficiencies can be significantly improved to offset any lowering of conversions due to higher pressures.
d) Develop catalysts that could minimize contributions from the RWGS reaction. This will minimize any potential loss of permeability due to moisture.

APPENDIX A. FORTRAN PROGRAM DETAILS

The basic model developed was for the isothermal plug flow reactor (PFR). This was to provide comparison between the experimental plug flow reactor and the mathematical model developed under the assumptions listed in Chapter 5. To include non-isothermal effects, the energy equation was incorporated into the PFR model. This allowed the addition of heat to the reactor to compensate for the endothermic reactions prevailing in the reactor. Pressure drop terms were also incorporated into the models. The membrane model (porous glass model) was developed using standard Knudsen diffusion terms to account for mass transfer across the porous Vycor membrane. For the Nanosil membrane, only the mass transfer contributions were changed to reflect activated diffusion across the membrane (see Chapter 5). Overall, 4 models were developed:

a) Isothermal PFR
b) Non-isothermal PFR
c) Porous Vycor membrane reactor
d) Nanosil membrane reactor

PFR-ISOTHERMAL MODEL

The list below describe all variables used in the modeling of the PFR reactor for the isothermal case. This is a user-friendly model, which requires the initial gas flow rates, temperature and pressure of the system to be input from the screen. It allows the model to evaluate various conditions without the need for recompiling the code.

Description of program constants, variables, parameters, etc. (Common to both the Isothermal and Non-Isothermal cases):

NEQ = Number of differential equations
IDO = Flag indicating state of computation
IEND = Integer
METH = Method of analysis
INORM = Switch determining error
MXSTEP = Maximum number of steps
PARAM(NPARAM) = Vector of length 50(NPARAM) containing parameters
XEND = Value of X
Y(NEQ) = Differential equations

FCN, FCNJ = Programmer defined subroutines
DIVPAG, SSET = ISML subroutines
PARAM(1) = initial value of step size
PARAM(4) = Maximum number of steps
PARAM(10) = Switch determining error
PARAM(12) = Method of analysis

TEMPI = Initial Temperature (Kelvin)
PTOTAL = Total pressure (Pa)
VMETHI = Initial flux of methane in shell ($cm^3\ min^{-1}$)
VCARBDI = Initial flux of carbon dioxide in shell ($cm^3\ min^{-1}$)
VARGI = Initial flux of argon in shell ($cm^3\ min^{-1}$)
FLUXSH = Conversion factor [$cm^3\ min^{-1} \rightarrow mol\ m^{-2}\ s^{-1}$] for shell side

NMETHI = Initial flux of methane in shell ($mol\ m^{-2}\ s^{-1}$)
NCARBDI = Initial flux of carbon dioxide in shell ($mol\ m^{-2}\ s^{-1}$)
NARGI = Initial flux of argon in shell ($mol\ m^{-2}\ s^{-1}$)

RADTUBE = Outer radius of tube (m)
RADSHELL = Inner radius of tube (m)
AREASHELL = Area of the shell (m^2)

X = Distance down the reactor (m)
R = gas constant ($J\ mol\ K^{-1}$)
Y(1) = Methane in shell ($mol\ m^{-2}\ s^{-1}$)
Y(2) = Carbon dioxide in shell ($mol\ m^{-2}\ s^{-1}$)
Y(3) = Carbon monoxide in shell ($mol\ m^{-2}\ s^{-1}$)
Y(4) = Hydrogen in shell ($mol\ m^{-2}\ s^{-1}$)
Y(5) = Argon in shell ($mol\ m^{-2}\ s^{-1}$)
Y(6) = Water in shell ($mol\ m^{-2}\ s^{-1}$)
Y(7) = Pressure of shell (Pa)

TOL = Tolerance of error
CONV = Conversion of methane
CONVCO = Conversion of carbon dioxide
WCAT = Mass of the catalyst in the reactor (g)
PI = constant = 3.14159265359

RCR = The rate constant for reaction 1 ($gmol\ gcat^{-1}\ s^{-1}$)
RCS = The rate constant for reaction 2 ($gmol\ gcat^{-1}\ s^{-1}$)
KCO2R, KCH4R =Appropriate adsorption equilibrium constants for reaction 1 (atm^{-1})
KR = Equilibrium constant for reaction 1
KS = Equilibrium constant for reaction 2
KX = RCR × KCO2R × KCH4R

NTOTAL = Total flux in the shell ($mol\ m^{-2}\ s^{-1}$)
PMETH = Partial pressure of methane in the shell (Pa)
PCARBD = Partial pressure of carbon dioxide in the shell (Pa)
PCARBM = Partial pressure of carbon monoxide in the shell (Pa)
PHYD = Partial pressure of hydrogen in the shell (Pa)
PARG = Partial pressure of argon in the shell (Pa)
PWAT = Partial pressure of water in the shell (Pa)

VELSHELL = Velocity of gases in the shell (m s^{-1})

PCO = Partial pressure of carbon monoxide in the shell (Pa)
PH2 = Partial pressure of hydrogen in the shell (Pa)
PCO2 = Partial pressure of carbon dioxide in the shell (Pa)
PCH4 = Partial pressure of methane in the shell (Pa)
PH2O = Partial pressure of water in the shell (Pa)

MOLFR(1) = Mole fraction of methane in shell
MOLFR(2) = Mole fraction of carbon dioxide in shell
MOLFR(3) = Mole fraction of carbon monoxide in shell
MOLFR(4) = Mole fraction of hydrogen in shell
MOLFR(5) = Mole fraction of argon in shell
MOLFR(6) = Mole fraction of water in shell

MW(1) = Molecular weight of methane (g $mole^{-1}$)
MW(2) = Molecular weight of carbon dioxide (g $mole^{-1}$)
MW(3) = Molecular weight of carbon monoxide (g $mole^{-1}$)
MW(4) = Molecular weight of hydrogen (g $mole^{-1}$)
MW(5) = Molecular weight of argon (g $mole^{-1}$)
MW(6) = Molecular weight of water (g $mole^{-1}$)

VIS(1) = Viscosity of methane in the reactor (N s m^{-2})
VIS(2) = Viscosity of carbon dioxide in the reactor (N s m^{-2})
VIS(3) = Viscosity of carbon monoxide in the reactor (N s m^{-2})
VIS(4) = Viscosity of hydrogen in the reactor (N s m^{-2})
VIS(5) = Viscosity of argon in the reactor (N s m^{-2})
VIS(6) = Viscosity of water in the reactor (N s m^{-2})
MWAVG = Molecular weight of the gas mixture (g mol^{-1})
DENAVG = Density of the gas mixtures (g m^{-3})

RRF = Forward rate expression for reaction 1
RSF = Forward rate expression for reaction 2
RR = Net rate expression for reaction 1
RS = Net rate expression for reaction 2
RCH4 = Methane reaction rate (gmol $gcat^{-1}$ s^{-1})
RCO2 = Carbon dioxide reaction rate (gmol $gcat^{-1}$ s^{-1})
RCO = Carbon monoxide reaction rate (gmol $gcat^{-1}$ s^{-1})
RH2 = Hydrogen reaction rate (gmol $gcat^{-1}$ s^{-1})
RH2O = Water reaction rate (gmol $gcat^{-1}$ s^{-1})

POR = Porosity of the bed
VOID = Void space in the bed
DP = Average diameter of the catalyst particles (m)
G = Superficial mass velocity
gc = Constant

YPRIME(1) = Change in flux of methane (mol m^{-3} s^{-1})
YPRIME(2) = Change in flux of carbon dioxide (mol m^{-3} s^{-1})
YPRIME(3) = Change in flux of carbon monoxide (mol m^{-3} s^{-1})
YPRIME(4) = Change in flux of hydrogen (mol m^{-3} s^{-1})
YPRIME(5) = Change in flux of argon (mol m^{-3} s^{-1})
YPRIME(6) = Change in flux of water (mol m^{-3} s^{-1})
YPRIME(7) = Pressure drop defined by Ergun equation (Pa)

ACTUAL PROGRAM

```
C       This program solves for molar flux of each species, pressure, and
C       conversion of methane as a function of reactor length It uses the
C       IMSL subroutine DIVPAG found in the DMATH5A library to solve the
C       set of ODEs.  This is the isothermal PFR model for the user specified flow rates,
C       temperature and pressure
C
C
C       *****DECLARATION OF VARIABLES*****
C
        INTEGER NEQ, NPARAM, NMF,I,J,CHECK
        PARAMETER (NEQ=7,NPARAM=50,NMF=6)
        INTEGER IDO, IEND, METH, INORM, MXSTEP
        DOUBLE PRECISION A(1,1), FCN, FCNJ, HINIT, PARAM(NPARAM)
        DOUBLE PRECISION TOL, X, XEND, Y(NEQ), TEMPI, PTOTAL, PI
        DOUBLE PRECISION NMETHI, NCARBDI, NARGI, CONV, CONVCO
        DOUBLE PRECISION VMETHI, VCARBDI, VARGI, FLUXSH
        DOUBLE PRECISION AREASHELL, RADTUBE, RADSHELL
        COMMON TEMPI
C
C
C       *****DECLARATION OF FUNCTION*****
C
        EXTERNAL FCN, DIVPAG, SSET, FCNJ
        HINIT = 1.0D-4
        INORM = 0
        METH = 2
        MXSTEP = 500000
        OPEN (2, FILE = 'PFR.DAT')
C
C
        CALL SSET (NPARAM, 0.0, PARAM, 1)
        PARAM(1) = HINIT
        PARAM(4) = MXSTEP
        PARAM(10) = INORM
        PARAM(12) = METH
        IDO = 1
```

```
C
C
C
C       *****INPUT QUANTITIES INTO PROGRAM*****
C
        PRINT *
        PRINT *, 'This program solves for the molar flux of each species,
        + the pressure, and the conversion of methane and carbon dioxide as
        + a function of reactor length in an isothermal PFR.  The output is
        + stored in the file "pfr.dat".'
        PRINT *
        PRINT *, 'Enter the shell inlet volumetric flowrates (cm^3 min^-1).'
        PRINT *, '      for methane:'
        READ *, VMETHI
        PRINT *
        PRINT *, '      for carbon dioxide:'
        READ *, VCARBDI
        PRINT *
        PRINT *, '      for argon:'
        READ *, VARGI
        PRINT *
        PRINT *
        PRINT *, 'Enter the temperature in Kelvins.'
        READ *, TEMPI
        PRINT *
        PRINT * , ' Enter the pressure in Pascals'
        READ *, PTOTAL
C
C   *****ASSIGNMENT OF VALUE TO CONSTANTS *****
C
        PI = 3.14159265359D0
        RADSHELL = 7.0D-3
        RADTUBE = 5.0D-3
        AREASHELL=PI*((RADSHELL**2.0)-(RADTUBE**2.0))
        FLUXSH=(273.0D0)/(TEMPI*22400.0D0*60.0D0*AREASHELL)
        R= 8.314D0
C
C
C   *****CONVERT VOLUMETRIC FLOWS TO FLUX *****
C
        NMETHI = VMETHI*FLUXSH
        NCARBDI = VCARBDI*FLUXSH
        NARGI = VARGI*FLUXSH
C
C
C    ***** INITIAL CONDITIONS *****
```

```
C
      AREASHELL=PI*((RADSHELL**2.0)-(RADTUBE**2.0))
      X = 0.0D0
      Y(1) = NMETHI
      Y(2) = NCARBDI
      Y(3) = 0.000000D0
      Y(4) = 0.000001D0
      Y(5) = NARGI
      Y(6) = 0.000000D0
      Y(7) = PTOTAL
      TOL = 1.0D-6
      CONV = 0.0D0
      C0NVCO = 0.0D0
      WRITE(2,90) X,CONV
      90 FORMAT (15F18.7)
C
C
C     *****NESTED LOOP AND SUBROUTINE INVOCATION SECTION*****
C
      I=1
      J=1
      DO 10 IEND =1,4000
      XEND = DFLOAT(IEND)/100000.0D0
      CALL DIVPAG (IDO, NEQ, FCN, FCNJ, A, X, XEND, TOL, PARAM, Y)
      CONV = (NMETHI-Y(1))/NMETHI
      CONVCO = (NCARBDI-Y(2))/NCARBDI
      CHECK= INT (I/10)
      IF (J .EQ. (CHECK*10)) THEN
      WRITE(2,100) X,CONV
      END IF
      I=I+1
      J=J+1
  10  CONTINUE
C
C
      IDO = 3
      CALL DIVPAG (IDO, NEQ, FCN, FCNJ, A, X, XEND, TOL, PARAM, Y)
 100  FORMAT (15F20.7)
      END
C
C
C     *****SUBROUTINE DEFINITION*****
C
C     SUBROUTINE DEFINED
      SUBROUTINE FCN (NEQ, X, Y, YPRIME)
      INTEGER NEQ, NMF
```

```
      PARAMETER (NMF=6)
      DOUBLE PRECISION X, Y(NEQ),YPRIME(NEQ),NTOTAL
      DOUBLE PRECISION PMETH, PCARBD, PCARBM, PHYD, PWAT, PARG
      DOUBLE PRECISION VELSHELL, TEMPI, PI
      DOUBLE PRECISION RADSHELL, RADTUBE, AREASHELL
      DOUBLE PRECISION MOLFR(NMF), MW(NMF), VIS(NMF), MWAVG,
      DOUBLE PRECISION VISNUM, VISDEN, VISMIX, DENAVG
      DOUBLE PRECISION G, DP, VOID, POR, gc
      DOUBLE PRECISION PCO,PH2,PCO2,PCH4,PH2O,RCR,RCS,R
      DOUBLE PRECISION KCO2R,KCH4R,KX,KR,KS
      DOUBLE PRECISION RCH4,RCO2,RCO,RH2,RH2O,RR,RS
      COMMON TEMPI
C
C     *****DEFINE VARIABLES*****
C
      R=8.314D0
      RCR=(1290.0D0)*EXP(-102065.0D0/(R*TEMPI))
      KCO2R=(2.61D-2)*EXP(37641.0D0/(R*TEMPI))
      KCH4R=(2.60D-2)*EXP(40684.0D0/(R*TEMPI))
      KX=RCR*KCO2R*KCH4R
      RCS=(1.857D0)*EXP(-73105.0D0/(R*TEMPI))
      KR=0.181381D0
      KS=0.368844D0
      PI = 3.14159265359D0
      RADSHELL = 7.0D-3
      RADTUBE = 5.0D-3
      AREASHELL = PI*((RADSHELL**2.0)-(RADTUBE**2.0))
C
C     *****PARTIAL PRESSURE ON SHELL SIDE*****
C
      NTOTAL = Y(1)+Y(2)+Y(3)+Y(4)+Y(5)+Y(6)
      PMETH  = (Y(1)/NTOTAL)*Y(7)
      PCARBD =(Y(2)/NTOTAL)*Y(7)
      PCARBM =(Y(3)/NTOTAL)*Y(7)
      PHYD = (Y(4)/NTOTAL)*Y(7)
      PARG = (Y(5)/NTOTAL)*Y(7)
      PWAT = (Y(6)/NTOTAL)*Y(7)
      VELSHELL = NTOTAL*0.0224D0*TEMPI/273.0D0
C
C     *****CONVERT PRESSURE TO ATM*****
C
      PCO=PCARBM/1000.0D0/101.33D0
      PH2=PHYD/1000.0D0/101.33D0
      PCO2=PCARBD/1000.0D0/101.33D0
      PCH4=PMETH/1000.0D0/101.33D0
      PH2O=PWAT/1000.0D0/101.33D0
```

```
C
C       *****MOLE FRACTIONS *****
C
        MOLFR(1) = Y(1)/NTOTAL
        MOLFR(2) = Y(2)/NTOTAL
        MOLFR(3) = Y(3)/NTOTAL
        MOLFR(4) = Y(4)/NTOTAL
        MOLFR(5) = Y(5)/NTOTAL
        MOLFR(6) = Y(6)/NTOTAL
C
C       ***** MOLECULAR WEIGHT OF INDIVIDUAL SPECIES *****
C
        MW(1) = 16.04D0
        MW(2) = 44.00D0
        MW(3) = 28.00D0
        MW(4) = 2.02D0
        MW(5) = 39.948D0
        MW(6) = 18.02D0
C
C       *****VISCOCITY OF MIXTURE*****
C
        VIS(1) = -3.45D-12*(TEMPI)**2.0 + 3.02D-8*TEMPI + 2.31D-6
        VIS(2) = 1.31D-12*(TEMPI)**2.0 + 4.88D-8*TEMPI + 1.02D-5
        VIS(3) = -5.95D-12*(TEMPI)**2.0 + 4.00D-8*TEMPI + 7.59D-6
        VIS(4) = -2.38D-12*(TEMPI)**2.0 + 1.84D-8*TEMPI + 4.00D-6
        VIS(5) = -4.29D-12*(TEMPI)**2.0 + 4.88D-8*TEMPI + 1.02D-5
        VIS(6) = 4.76D-13*(TEMPI)**2.0 + 36.77D-8*TEMPI - 2.00D-6
C
        VISNUM = (MOLFR(1)*VIS(1)*(MW(1)**0.5)) +
        $(MOLFR(2)*VIS(2)*(MW(2)**0.5)) + (MOLFR(3)*VIS(3)*(MW(3)**0.5))
        $+ (MOLFR(4)*VIS(4)*(MW(4)**0.5)) + (MOLFR(5)*VIS(5)*(MW(5)**0.5))
        $ + (MOLFR(6)*VIS(6)*(MW(6)**0.5))
C
        VISDEN = (MOLFR(1)*(MW(1)**0.5)) + (MOLFR(2)*(MW(2)**0.5))
        $   +    (MOLFR(3)*(MW(3)**0.5)) + (MOLFR(4)*(MW(4)**0.5))
        $   +    (MOLFR(5)*(MW(5)**0.5)) + (MOLFR(6)*(MW(6)**0.5))
        VISMIX = VISNUM/VISDEN
C
C       *****DENSITY OF MIXTURE*****
C
        MWAVG = (MOLFR(1)*MW(1)) + (MOLFR(2)*MW(2)) + (MOLFR(3)*MW(3))
        +(MOLFR(4)*MW(4)) + (MOLFR(5)*MW(5)) + $ (MOLFR(6)*MW(6))
C
        DENAVG = (MWAVG*Y(7))/(8.314D0*TEMPI)
C
C       *****REACTION TERMS*****
```

```
C
      RRF=(KX*PCO2*PCH4)/((1+KCO2R*PCO2+KCH4R*PCH4)**2)
      RSF=RCS*PCO2
      RR=RRF*(1.0D0-(((PCO*PH2)**2)/(KR*PCH4*PCO2)))
      RS=RSF*(1.0D0-((PCO*PH2O)/(KS*PCO2*PH2)))
      RCH4=RR*0.15D0
      RCO2=(RR+RS)*0.15D0
      RCO=(2*RR+RS)*0.15D0
       RH2=(2*RR-RS)*0.15D0
      RH2O=RS*0.15D0
C
C     *****PARAMETERS FOR THE ERGUN EQUATION *****
C
      POR = 0.60D0
      VOID = 1.0D0 - POR
      DP = 3.625D-4
      G =DENAVG*VELSHELL
      gc = 1.0D0
C
C     *****ODE'S*****
C
      YPRIME(1) = -(RCH4)/(0.08D0*AREASHELL)
      YPRIME(2) = -(RCO2)/(0.08D0*AREASHELL)
      YPRIME(3)=  RCO/(0.08D0*AREASHELL)
      YPRIME(4)=  RH2/(0.08D0*AREASHELL)
      YPRIME(5) = 0.0D0
      YPRIME(6) = RH2O/(0.08D0*AREASHELL)
      YPRIME(7) =-(G/(DENAVG*gc*DP))*(VOID/POR**3.0)*
     +  ((150.0*VOID*VISMIX/DP) + 1.75*G)
      RETURN
      END
C
      SUBROUTINE FCNJ (N, X, Y, DYPDY)
      INTEGER N
      DOUBLE PRECISION X, Y(N), DYPDY(N,*)
      RETURN
      END
```

NON-ISOTHERMAL PLUG FLOW REACTOR

The list below included only those terms not defined above.

Y(8) = Temperature in the reactor (K)
Temp = Temperature in the reactor (K)
FCO2 = Initial carbon dioxide molar flow rate (mol s^{-1})

CONV1 = Conversion of carbon dioxide from the first reaction
CONV2 = Conversion of carbon dioxide from the second reaction
INICH4 = Initial methane in the shell (mol m^{-2} s^{-1})
INICO2 = Initial carbon dioxide in the shell (mol m^{-2} s^{-1})
L = Length of the reactor (m)
K = Thermal Conductivity of quartz (J m^{-1} s^{-1} K^{-1})
ROUT = Shell outside radius (m)
RIN = Shell inside radius (m)
CH4A, CH4B, CH4C = Coefficient of heat capacity for methane
CO2A, CO2B, CO2D = Coefficient of heat capacity for carbon dioxide
COA, COB, COD = Coefficient of heat capacity for carbon monoxide
H2A, H2B, H2D = Coefficient of heat capacity for hydrogen
ARA = Coefficient of heat capacity for argon
H2OA, H2OB, H2OD = Coefficient of heat capacity for water
CPCH4 = Heat capacity for methane (J mol^{-1} K^{-1})
CPCO2 = Heat capacity for carbon dioxide (J mol^{-1} K^{-1})
CPH2 = Heat capacity for hydrogen (J mol^{-1} K^{-1})
CPCO = Heat capacity for carbon monoxide (J mol^{-1} K^{-1})
CPH2O = Heat capacity for water (J mol^{-1} K^{-1})
CPAR = Heat capacity for argon (J mol^{-1} K^{-1})
DA1, DB1, DC1, DD1 = Coefficient of sum heat capacity for reaction 1
DA2, DB2, DC2, DD2 = Coefficient of sum heat capacity for reaction 2
DCP1 = Sum heat capacity for reaction 1 (J mol^{-1} K^{-1})
DCP2 = Sum heat capacity for reaction 2 (J mol^{-1} K^{-1})
HR1 = Heat of reaction for reaction 1 (J mol^{-1})
HR2 = Heat of reaction for reaction 2 (J mol^{-1})
Q = Heat generated by furnace (J s^{-1})
P = Heat consumed by reaction (J s^{-1})
RATIO = The ratio of initial carbon dioxide and argon feed rate
SUM = Sum of initial feed species heat capacity (J mol^{-1} K^{-1})
YPRIME(8) = Change in temperature (K)

ACTUAL FORTRAN PROGRAM

```
C       This program solves for molar flux of each species, pressure, and
C       conversion of methane as a function of reactor length It uses the
C       IMSL subroutine DIVPAG found in the DMATH5A library to solve the
C       set of ODEs.  This is the nonisothermal PFR model.
C
C
        INTEGER NEQ, NPARAM, NMF,I,J,K
        PARAMETER (NEQ=8,NPARAM=50,NMF=7)
        INTEGER IDO, IEND, METH, INORM, MXSTEP
        DOUBLE PRECISION A(1,1), FCN, FCNJ, HINIT, PARAM(NPARAM)
        DOUBLE PRECISION TOL, X, XEND, Y(NEQ), TEMPI, PTOTAL, PI
        DOUBLE PRECISION NMETHI, NCARBDI, NARGI, CONV, CONVCO
        DOUBLE PRECISION VMETHI, VCARBDI, VARGI, FLUXSH
```

```
      DOUBLE PRECISION AREASHELL, RADTUBE, RADSHELL
      DOUBLE PRECISION TEMP,FCO2,CONV1,CONV2,INICO2,INICH4
      COMMON TEMPI,FCO2,TEMP,CONV1,CONV2
      COMMON NARGI,NCARBDI
C
      EXTERNAL FCN, DIVPAG, SSET, FCNJ
      HINIT = 1.0D-4
      INORM = 0
      METH = 2
      MXSTEP = 500000
      OPEN (2, FILE = 'NONISOTHERMAL.DAT')
C
      CALL SSET (NPARAM, 0.0, PARAM, 1)
      PARAM(1) = HINIT
      PARAM(4) = MXSTEP
      PARAM(10) = INORM
      PARAM(12) = METH
      IDO = 1
C
C     ***** USER DEFINED VARIABLES *****
C
      PRINT *
      PRINT *, 'This program solves for the molar flux of each species,
      + the pressure, and the conversion of methane and carbon dioxide as
      + a function of reactor length in an isothermal PFR.  The output is
       + stored in the file "nonisothermal.dat".'
      PRINT *
      PRINT *, 'Enter the shell inlet volumetric flowrates (cc/min).'
      PRINT *, '      for methane:'
      READ *, VMETHI
      PRINT *
      PRINT *, '      for carbon dioxide:'
      READ *, VCARBDI
      PRINT *
      PRINT *, '       for argon:'
      READ *, VARGI
      PRINT *
      PRINT *
      PRINT *, 'Enter the temperature in Kelvins.'
      READ *, TEMPI
      PRINT *
      PRINT * , ' Enter the pressure in Pascals'
      READ *, PTOTAL
C
C       ***** CONSTANTS *****
C
```

```
      PI = 3.14159265359D0
      RADSHELL = 7.0D-3
      RADTUBE = 5.0D-3
      AREASHELL=PI*((RADSHELL**2.0)-(RADTUBE**2.0))
      FLUXSH=(273.0D0)/(TEMPI*22400.0D0*60.0D0*AREASHELL)
      R= 8.314D0
C
C     *****CONVERT VOLUMETRIC FLOWS TO FLUX *****
C
      NMETHI = VMETHI*FLUXSH
      NCARBDI = VCARBDI*FLUXSH
      NARGI = VARGI*FLUXSH
C
C     ***** INITIAL CONDITIONS *****
C
      AREASHELL=PI*((RADSHELL**2.0)-(RADTUBE**2.0))
C
      X = 0.0D0
      Y(1) = NMETHI
      Y(2) = NCARBDI
      Y(3) = 0.000000D0
      Y(4) = 0.000001D0
      Y(5) = NARGI
      Y(6) = 0.000000D0
      Y(7) = PTOTAL
      Y(8) = TEMPI
      TEMP = Y(8)
      FCO2 = NCARBDI * AREASHELL
      CONV1 = 0.0D0
      CONV2 = 0.0D0
      INICO2 = NCARBDI
      INICH4 = NMETHI
      TOL = 1.0D-6
      CONV = 0.0D0
      C0NVCO = 0.0D0
      WRITE(2,100) X,TEMP
   90 FORMAT (10F10.7)
C
      I=1
      J=1
      DO 10 IEND =1,4000
      XEND = DFLOAT(IEND)/100000.0D0
      CALL DIVPAG (IDO, NEQ, FCN, FCNJ, A, X, XEND, TOL, PARAM, Y)
      CONV = (NMETHI-Y(1))/NMETHI
      CONVCO = (NCARBDI-Y(2))/NCARBDI
      TEMP = Y(8)
```

```
      CONV1 = (INICH4-Y(1))/INICH4
      CONV2 = (INICO2-Y(2))/INICO2-CONV1
      INICH4=Y(1)
      INICO2=Y(2)
      CHECK= INT (I/10)
      IF (J .EQ. (CHECK*10)) THEN
      WRITE(2,100) X,TEMP
      END IF
      I=I+1
      J=J+1
   10 CONTINUE
C
      IDO = 3
      CALL DIVPAG (IDO, NEQ, FCN, FCNJ, A, X, XEND, TOL, PARAM, Y)
  100 FORMAT (10F12.7)
      END
C
      SUBROUTINE FCN (NEQ, X, Y, YPRIME)
      INTEGER NEQ, NMF
      PARAMETER (NMF=7)
      DOUBLE PRECISION X, Y(NEQ),YPRIME(NEQ),NTOTAL
      DOUBLE PRECISION PMETH, PCARBD, PCARBM, PHYD, PWAT, PARG
      DOUBLE PRECISION VELSHELL, TEMPI, PI
      DOUBLE PRECISION RADSHELL, RADTUBE, AREASHELL
      DOUBLE PRECISION MOLFR(NMF), MW(NMF), VIS(NMF), MWAVG
      DOUBLE PRECISION DENAVG, VISNUM, VISDEN, VISMIX
      DOUBLE PRECISION G, DP, VOID, POR, gc
      DOUBLE PRECISION PCO,PH2,PCO2,PCH4,PH2O,RCR,RCS,R
      DOUBLE PRECISION KCO2R,KCH4R,KX,KR,KS
      DOUBLE PRECISION RCH4,RCO2,RCO,RH2,RH2O,RR,RS
      DOUBLE PRECISION FCO2,TEMP,CONV1,

      DOUBLE PRECISION HR1,HR2,RATIO,SUM,NARGI,NCARBDI,CPCO,P, Q
      DOUBLE PRECISION H2OD,DA1,DB1,DC1,DD1,DA2,DB2
      DOUBLE PRECISION COA,COB,COD,H2A,H2B,H2D,ARA,H2OA,H2OB
      DOUBLE PRECISION CPH2,CPAR,CPH2O,CH4A,CH4B,CH4C
      DOUBLE PRECISION DC2,DD2,DCP1,DCP2, CO2A,CO2B, CO2D
      DOUBLE PRECISION CONV2,L,K,ROUT,CPCH4,CPCO2
      COMMON TEMPI,FCO2,TEMP,CONV1,CONV2,NARGI,NCARBDI
C
C     *****DEFINE VARIABLES*****
C
      R=8.314D0
      RCR=(1290.0D0)*EXP(-102065.0D0/(R*TEMP))
      KCO2R=(2.61D-2)*EXP(37641.0D0/(R*TEMP))
      KCH4R=(2.60D-2)*EXP(40684.0D0/(R*TEMP))
```

```
      KX=RCR*KCO2R*KCH4R
      RCS=(1.857D0)*EXP(-73105.0D0/(R*TEMP))
      KR=.181381D0
      KS=0.368844D0
      PI = 3.14159265359D0
      RADSHELL = 7.0D-3
      RADTUBE = 5.0D-3
      AREASHELL = PI*((RADSHELL**2.0)-(RADTUBE**2.0))
      L=1.0D-5
      K=2.78D0
      ROUT=8.0D-3
      CH4A=14.15D0
      CH4B=0.0755D0
      CH4C=-1.799D-5
      CO2A=45.370D0
      CO2B=8.688D-3
      CO2D=-961929.8D0
      COA=28.068D0
      COB=4.631D-3
      COD=-25773.4D0
      H2A=27.012D0
      H2B=3.508D-3
      H2D=69006.2D0
      ARA=4.97D0*4.184197D0
      H2OA=28.85D0
      H2OB=0.012D0
      H2OD=100599.4D0
C
C     *****PARTIAL PRESSURE ON SHELL SIDE*****
C
      NTOTAL = Y(1)+Y(2)+Y(3)+Y(4)+Y(5)+Y(6)
      PMETH  = (Y(1)/NTOTAL)*Y(7)
      PCARBD =(Y(2)/NTOTAL)*Y(7)
      PCARBM =(Y(3)/NTOTAL)*Y(7)
      PHYD = (Y(4)/NTOTAL)*Y(7)
      PARG = (Y(5)/NTOTAL)*Y(7)
      PWAT = (Y(6)/NTOTAL)*Y(7)
      VELSHELL = NTOTAL*0.0224D0*TEMPI/273.0D0
C
C     *****CONVERT PRESSURE TO ATM*****
C
      PCO=PCARBM/1000.0D0/101.33D0
      PH2=PHYD/1000.0D0/101.33D0
      PCO2=PCARBD/1000.0D0/101.33D0
      PCH4=PMETH/1000.0D0/101.33D0
      PH2O=PWAT/1000.0D0/101.33D0
```

```
C
C       *****MOLE FRACTIONS *****
C
        MOLFR(1) = Y(1)/NTOTAL
        MOLFR(2) = Y(2)/NTOTAL
        MOLFR(3) = Y(3)/NTOTAL
        MOLFR(4) = Y(4)/NTOTAL
        MOLFR(5) = Y(5)/NTOTAL
        MOLFR(6) = Y(6)/NTOTAL
C
C       ***** MOLECULAR WEIGHT OF INDIVIDUAL SPECIES *****
C
        MW(1) = 16.04D0
        MW(2) = 44.00D0
        MW(3) = 28.00D0
        MW(4) = 2.02D0
        MW(5) = 39.948D0
        MW(6) = 18.02D0
C
C       *****VISCOSITY OF MIXTURE*****
C
        VIS(1) = -3.45D-12*(TEMP)**2.0 + 3.02D-8*TEMP + 2.31D-6
        VIS(2) = 1.31D-12*(TEMP)**2.0 + 4.88D-8*TEMP + 1.02D-5
        VIS(3) = -5.95D-12*(TEMP)**2.0 + 4.00D-8*TEMP + 7.59D-6
        VIS(4) = -2.38D-12*(TEMP)**2.0 + 1.84D-8*TEMP + 4.00D-6
        VIS(5) = -4.29D-12*(TEMP)**2.0 + 4.88D-8*TEMP + 1.02D-5
        VIS(6) = 4.76D-13*(TEMP)**2.0 + 36.77D-8*TEMP - 2.00D-6
C
        VISNUM = (MOLFR(1)*VIS(1)*(MW(1)**0.5)) +
        $(MOLFR(2)*VIS(2)*(MW(2)**0.5)) + (MOLFR(3)*VIS(3)*(MW(3)**0.5))
        $+ (MOLFR(4)*VIS(1)*(MW(4)**0.5)) + (MOLFR(5)*VIS(5)*(MW(5)**0.5))
        $ + (MOLFR(6)*VIS(6)*(MW(6)**0.5))
C
        VISDEN = (MOLFR(1)*(MW(1)**0.5)) + (MOLFR(2)*(MW(2)**0.5))
        $   +    (MOLFR(3)*(MW(3)**0.5)) + (MOLFR(4)*(MW(4)**0.5))
        $   +    (MOLFR(5)*(MW(5)**0.5)) + (MOLFR(6)*(MW(6)**0.5))
        VISMIX = VISNUM/VISDEN
C
C       *****DENSITY OF MIXTURE*****
C
        MWAVG = (MOLFR(1)*MW(1)) + (MOLFR(2)*MW(2)) + (MOLFR(3)*MW(3))
        $ +(MOLFR(4)*MW(4)) + (MOLFR(5)*MW(5)) + (MOLFR(6)*MW(6))
C
        DENAVG = (MWAVG*Y(7))/(8.314D0*TEMP)
C
C       *****REACTION TERMS*****
```

```
C
      RRF=(KX*PCO2*PCH4)/((1+KCO2R*PCO2+KCH4R*PCH4)**2)
      RSF=RCS*PCO2
      RR=RRF*(1.0D0-(((PCO*PH2)**2)/(KR*PCH4*PCO2)))
      RS=RSF*(1.0D0-((PCO*PH2O)/(KS*PCO2*PH2)))
      RCH4=RR
      RCO2=RR+RS
      RCO=2*RR+RS
      RH2=2*RR-RS
      RH2O=RS
C
C     *****PARAMETERS FOR THE ERGUN EQUATION *****
C
      POR = 0.60D0
      VOID = 1.0D0 - POR
      DP = 3.625D-4
      G =DENAVG*VELSHELL
      gc = 1.0D0
C
C     *****HEAT CAPACITY TERMS*****
C
      CPCH4 = CH4A+CH4B*TEMP+CH4C*(TEMP**2)
      CPCO2 = CO2A+CO2B*TEMP+CO2D/(TEMP**2)
      CPH2  = H2A+H2B*TEMP+H2D/(TEMP**2)
      CPH2O = H2OA+H2OB*TEMP+H2OD/(TEMP**2)
      CPCO  = COA+COB*TEMP+COD/(TEMP**2)
      CPAR  = ARA
      DA1   = 2*COA+2*H2A-CH4A-CO2A
      DB1   = 2*COB+2*H2B-CH4B-CO2B
      DC1   = -CH4C
      DD1   = 2*COD+2*H2D-CO2D
      DA2   = COA+H2OA-CO2A-H2A
      DB2   = COB+H2OB-CO2B-H2B
      DC2   = 0.0D0
      DD2   = COD+H2OD-CO2D-H2D
      DCP1  = DA1+DB1*TEMP+DC1*(TEMP**2)+DD1/(TEMP**2)
      DCP2  = DA2+DB2*TEMP+DC2*(TEMP**2)+DD2/(TEMP**2)
C
C    ********HEAT OF REACTION TERMS**********************
C
      HR1 = 246979.0D0+DA1*(TEMP-298.0D0)+(DB1/2.0D0)*
      $ (TEMP**2-298.0D0**2)+(DC1/3.0D0)*(TEMP**3-298.0D0**3)
      $ -DD1*(1/TEMP-1/298.0D0)
      HR2 = 41166.0D0+DA2*(TEMP-298.0D0)+(DB2/2.0D0)*
      $ (TEMP**2-298.0D0**2)+(DC2/3.0D0)*(TEMP**3-298.0D0**3)
      $ -DD2*(1/TEMP-1/298.0D0)
```

```
C
C       *****HEAT GENERATED BY FURNANCE*****
C
        P=(RR*1.25D-4)*(-HR1)+(RS*1.25D-4)*(-HR2)
C
C       *****PART OF DENOMINATOR TERM FOR USE IN YPRIME(8)*****
C
        RATIO = NARGI/NCARBDI
        SUM = (CH4A+CO2A+RATIO*ARA)+(CH4B+CO2B)*TEMP
        $ +(CH4C)*(TEMP**2)+(CO2D)/(TEMP**2)
C
C       *****ODE'S*****
C
        YPRIME(1) = -(RCH4)/(0.08D0*AREASHELL)
        YPRIME(2) = -(RCO2)/(0.08D0*AREASHELL)
        YPRIME(3) = RCO/(0.08D0*AREASHELL)
        YPRIME(4) = RH2/(0.08D0*AREASHELL)
        YPRIME(5) = 0.0D0
        YPRIME(6) = RH2O/(0.08D0*AREASHELL)
        YPRIME(7) = -(G/(DENAVG*gc*DP))*(VOID/POR**3.0)*
     +  ((150.0*VOID*VISMIX/DP) + 1.75*G)
        YPRIME(8) = (P)/(FCO2*(SUM+CONV1*DCP1+CONV2*DCP2)))/L
        RETURN
        END
C
        SUBROUTINE FCNJ (N, X, Y, DYPDY)
        INTEGER N
        DOUBLE PRECISION X, Y(N), DYPDY(N,*)
        RETURN
        END
```

POROUS VYCOR MEMBRANE REACTOR

KSTAR = Term used to calculate Knudsen diffusion
KCH4 = Effective permeability of methane (mol m^{-2} $Pa^{-1}s^{-1}$)
KCO2 = Effective permeability of carbon dioxide (mol m^{-2} $Pa^{-1}s^{-1}$)
KCO = Effective permeability of carbon monoxide (mol m^{-2} $Pa^{-1}s^{-1}$)
KH2 = Effective permeability of hydrogen (mol m^{-2} $Pa^{-1}s^{-1}$)
KAR = Effective permeability of argon (mol m^{-2} $Pa^{-1}s^{-1}$)
KH2O = Effective permeability of water (mol m^{-2} $Pa^{-1}s^{-1}$)

DCH4 = Methane diffused through membrane in the shell side (mol m^{-3} s^{-1})
DCO2 = Carbon dioxide diffused through membrane in the shell side (mol m^{-3} s^{-1})
DCO = Carbon monoxide diffused through membrane in the shell side (mol m^{-3} s^{-1})
DH2 = Hydrogen diffused through membrane in the shell side (mol m^{-3} s^{-1})
DH2O = Water diffused through membrane in the shell side (mol m^{-3} s^{-1})
DAR = Argon diffused through membrane in the shell side (mol m^{-3} s^{-1})
DTCH4 = Methane diffused through membrane in the tube side (mol m^{-3} s^{-1})
DTCO2 = CO_2 diffused through membrane in the tube side (mol m^{-3} s^{-1})
DTCO = CO_2 diffused through membrane in the tube side (mol m^{-3} s^{-1})
DTH2 = Hydrogen diffused through membrane in the tube side (mol m^{-3} s^{-1})
DTH2O = Water diffused through membrane in the tube side (mol m^{-3} s^{-1})
DTAR = Argon diffused through membrane in the tube side (mol m^{-3} s^{-1})
T1, T2, T3 = terms used in the Ergun equation calculation

ACTUAL FORTRAN PROGRAM

```
C     This program solves for molar flux of each species, pressure, and
C     conversion of methane as a function of reactor length It uses the
C     IMSL subroutine DIVPAG found in the DMATH5A library to solve the
C     set of ODEs.  This is the vycor membrane model.
C
C
      INTEGER NEQ, NPARAM, NMF,I,J,CHECK
      PARAMETER (NEQ=14,NPARAM=50,NMF=13)
      INTEGER IDO, IEND, METH, INORM, MXSTEP
      DOUBLE PRECISION A(1,1), FCN, FCNJ, HINIT, PARAM(NPARAM)
      DOUBLE PRECISION TOL, X, XEND, Y(NEQ), TEMPI, PTOTAL, PI
      DOUBLE PRECISION NMETHI, NCARBDI, NARGI, CONV, CONVCO, T1
      DOUBLE PRECISION VMETHI, VCARBDI, VARGI, FLUXSH,FLUXSHT,T2
      DOUBLE PRECISION AREASHELL, RADTUBE, RADSHELL,M1,M2,M3,T3
      DOUBLE PRECISION VTARGI,NTARGI,PTTOTAL,AREATUBE,M4,M5,M6
      COMMON TEMPI
C
      EXTERNAL FCN, DIVPAG, SSET, FCNJ
      HINIT = 1.0D-4
      INORM = 0
      METH = 2
      MXSTEP = 5000000
      OPEN (2, FILE = 'VYCOR.DAT')
C
      CALL SSET (NPARAM, 0.0, PARAM, 1)
      PARAM(1) = HINIT
      PARAM(4) = MXSTEP
      PARAM(10) = INORM
      PARAM(12) = METH
```

```
      IDO = 1
C
C     ***** USER DEFINED VARIABLES *****
C
      PRINT *
      PRINT *, 'This program solves for the molar flux of each species,
     + the pressure, and the conversion of methane and carbon dioxide as
     + a function of reactor length in an isothermal PFR.  The output is
     + stored in the file "vycor.dat".'
      PRINT *
      PRINT *, 'Enter the shell inlet volumetric flowrates (cc/min).'
      PRINT *, '      for methane:'
      READ *, VMETHI
      PRINT *
      PRINT *, '      for carbon dioxide:'
      READ *, VCARBDI
      PRINT *
      PRINT *, '      for argon:'
      READ *, VARGI
      PRINT *
      PRINT *
      PRINT *, 'Enter the temperature in Kelvins.'
      READ *, TEMPI
      PRINT *
      PRINT * , ' Enter the pressure in Pascals'
      READ *, PTOTAL
      PRINT *
      PRINT *, 'Enter the tube inlet volumetric flowrates (cc/min).'
      PRINT *, '      for argon:'
      READ *, VTARGI
C
C     ***** CONSTANTS *****
C
      PI = 3.14159265359D0
      RADSHELL = 7.0D-3
      RADTUBE = 5.0D-3
      AREASHELL=PI*((RADSHELL**2.0)-(RADTUBE**2.0))
      AREATUBE=PI*(4.0D-3**2.0)
      FLUXSH=(273.0D0)/(TEMPI*22400.0D0*60.0D0*AREASHELL)
      FLUXSHT=(273.0D0)/(TEMPI*22400.0D0*60.0D0*AREATUBE)
      R= 8.314D0
C
C     ***** CONVERT VOLUMETRIC FLOWS TO FLUX *****
C
      NMETHI = VMETHI*FLUXSH
      NCARBDI = VCARBDI*FLUXSH
```

```
      NARGI = VARGI*FLUXSH
      NTARGI = VTARGI*FLUXSHT
C
C     ***** INITIAL CONDITIONS *****
C
      AREASHELL=PI*((RADSHELL**2.0)-(RADTUBE**2.0))
      AREATUBE=PI*(4.0D-3**2.0)
      PTTOTAL = PTOTAL
      X = 0.0D0
      Y(1) = NMETHI
      Y(2) = NCARBDI
      Y(3) = 0.000000D0
      Y(4) = 0.000001D0
      Y(5) = NARGI
      Y(6) = 0.000000D0
      Y(7) = PTOTAL
      Y(8) = 0.000000D0
      Y(9) = 0.000000D0
      Y(10) = 0.000000D0
      Y(11) = 0.000000D0
      Y(12) = NTARGI
      Y(13) = 0.000000D0
      Y(14) = PTTOTAL
      T1 = 0.0D0
      T2 = 0.0D0
      T3 = 0.0 D0
      M1=0.0D0
      M2=0.0D0
      M3=0.0D0
      TOL = 1.0D-6
      CONV = 0.0D0
      C0NVCO = 0.0D0
      WRITE(2,100) X,CONV
   90 FORMAT (12F18.7)
C
      I=1
      J=1
      DO 10 IEND =1,4000
      XEND = DFLOAT(IEND)/100000.0D0
      CALL DIVPAG (IDO, NEQ, FCN, FCNJ, A, X, XEND, TOL, PARAM, Y)
      M1=NMETHI*AREASHELL
      M2=Y(1)*AREASHELL
      M3=Y(8)*AREATUBE
      M4=NCARBDI*AREASHELL
      M5=Y(2)*AREASHELL
      M6=Y(9)*AREATUBE
```

```
      CONV = (M1-(M2+M3))/M1
      CONVCO = (M4-(M5+M6))/M4
      CHECK= INT (I/10)
      IF (J .EQ. (CHECK*10)) THEN
      WRITE(2,100) X,CONV
      END IF
      I=I+1
      J=J+1
   10 CONTINUE
C
      IDO = 3
      CALL DIVPAG (IDO, NEQ, FCN, FCNJ, A, X, XEND, TOL, PARAM, Y)
  100 FORMAT (10F10.7)
      END
C
      SUBROUTINE FCN (NEQ, X, Y, YPRIME)
      INTEGER NEQ, NMF
      PARAMETER (NMF=13)
      DOUBLE PRECISION X, Y(NEQ),YPRIME(NEQ),NTOTAL
      DOUBLE PRECISION PMETH, PCARBD, PCARBM, PHYD, PWAT, PARG
      DOUBLE PRECISION VELSHELL, TEMPI, PI
      DOUBLE PRECISION RADSHELL, RADTUBE, AREASHELL
      DOUBLE PRECISION MOLFR(NMF),MW(NMF),VIS(NMF),MWAVG
      DOUBLE PRECISION VISNUM, VISDEN, VISMIX, DENAVG
      DOUBLE PRECISION G, DP, VOID, POR, gc
      DOUBLE PRECISION PCO,PH2,PCO2,PCH4,PH2O,PAR,RCR,RCS,R
      DOUBLE PRECISION KCO2R,KCH4R,KX,KR,KS,PTARG
      DOUBLE PRECISION RCH4,RCO2,RCO,RH2,RH2O,RR,RS,PTWAT
       DOUBLE PRECISION NTOTTUBE, PTMETH, PTCARBD,
      DOUBLE PRECISION VELTUBE,PTCO,PTH2,PTCO2,PTCH4,PTH2O,PTAR
      DOUBLE PRECISION VISMIXT,VISNUMT,VISDENT,DENAVGT
      DOUBLE PRECISION T1,T2,T3,KSTAR,KCH4,KCO2,KCO,KH2,KAR,KH2O
      DOUBLE PRECISION DTCH4,DTCO2,DTCO,DTH2,DTH2O,DTAR
      DOUBLE PRECISION DCH4,DCO2,DCO,DH2,DH2O,DAR
      DOUBLE PRECISION MWAVGT, PTCARBM,PTHYD
      COMMON TEMPI
C
C     *****DEFINE VARIABLES*****
C
      R=8.314D0
      RCR=(1290.0D0)*EXP(-102065.0D0/(R*TEMPI))
      KCO2R=(2.61D-2)*EXP(37641.0D0/(R*TEMPI))
      KCH4R=(2.60D-2)*EXP(40684.0D0/(R*TEMPI))
      KX=RCR*KCO2R*KCH4R
      RCS=(1.857D0)*EXP(-73105.0D0/(R*TEMPI))
      KR=0.181381D0
```

```
      KS=0.368844D0
      PI = 3.14159265359D0
      RADSHELL = 7.0D-3
      RADTUBE = 5.0D-3
      AREASHELL = PI*((RADSHELL**2.0)-(RADTUBE**2.0))
      AREATUBE=PI*(4.0D-3**2.0)
C
C     *****PARTIAL PRESSURE ON SHELL SIDE*****
C
      NTOTAL = Y(1)+Y(2)+Y(3)+Y(4)+Y(5)+Y(6)
      PMETH  = (Y(1)/NTOTAL)*Y(7)
      PCARBD =(Y(2)/NTOTAL)*Y(7)
      PCARBM =(Y(3)/NTOTAL)*Y(7)
      PHYD = (Y(4)/NTOTAL)*Y(7)
      PARG = (Y(5)/NTOTAL)*Y(7)
      PWAT = (Y(6)/NTOTAL)*Y(7)
      VELSHELL = NTOTAL*0.0224D0*TEMPI/273.0D0
C
C     *****PARTIAL PRESSURE ON TUBE SIDE*****
C
      NTOTTUBE = Y(8)+Y(9)+Y(10)+Y(11)+Y(12)+Y(13)
      PTMETH = (Y(8)/NTOTTUBE)*Y(14)
      PTCARBD =(Y(9)/NTOTTUBE)*Y(14)
      PTCARBM =(Y(10)/NTOTTUBE)*Y(14)
      PTHYD = (Y(11)/NTOTTUBE)*Y(14)
      PTARG = (Y(12)/NTOTTUBE)*Y(14)
      PTWAT = (Y(13)/NTOTTUBE)*Y(14)
      VELTUBE = NTOTTUBE*0.0224D0*TEMPI/273.0D0
C
C     *****CONVERT PRESSURE TO ATM*****
C
      PCO=PCARBM/1000.0D0/101.33D0
      PH2=PHYD/1000.0D0/101.33D0
      PCO2=PCARBD/1000.0D0/101.33D0
      PCH4=PMETH/1000.0D0/101.33D0
      PH2O=PWAT/1000.0D0/101.33D0
      PAR = PARG/1000.0D0/101.33D0
      PTCO=PTCARBM/1000.0D0/101.33D0
      PTH2=PTHYD/1000.0D0/101.33D0
      PTCO2=PTCARBD/1000.0D0/101.33D0
      PTCH4=PTMETH/1000.0D0/101.33D0
      PTH2O=PTWAT/1000.0D0/101.33D0
      PTAR = PTARG/1000.0D0/101.33D0
C
C     *****MOLE FRACTIONS ON SHELL SIDE*****
C
```

```
      MOLFR(1) = Y(1)/NTOTAL
      MOLFR(2) = Y(2)/NTOTAL
      MOLFR(3) = Y(3)/NTOTAL
      MOLFR(4) = Y(4)/NTOTAL
      MOLFR(5) = Y(5)/NTOTAL
      MOLFR(6) = Y(6)/NTOTAL
C
C     *****MOLE FRACTIONS ON TUBE SIDE******
C
      MOLFR(8) = Y(8)/NTOTTUBE
      MOLFR(9) = Y(9)/NTOTTUBE
      MOLFR(10) = Y(10)/NTOTTUBE
      MOLFR(11) = Y(11)/NTOTTUBE
      MOLFR(12) = Y(12)/NTOTTUBE
      MOLFR(13) = Y(13)/NTOTTUBE
C
C     ***** MOLECULAR WEIGHT OF INDIVIDUAL SPECIES *****
C
      MW(1) = 16.04D0
      MW(2) = 44.00D0
      MW(3) = 28.00D0
      MW(4) = 2.02D0
      MW(5) = 39.948D0
      MW(6) = 18.02D0
C
C     *****VISCOCITY *****
C
      VIS(1) = -3.45D-12*(TEMPI)**2.0 + 3.02D-8*TEMPI + 2.31D-6
      VIS(2) = 1.31D-12*(TEMPI)**2.0 + 4.88D-8*TEMPI + 1.02D-5
      VIS(3) = -5.95D-12*(TEMPI)**2.0 + 4.00D-8*TEMPI + 7.59D-6
      VIS(4) = -2.38D-12*(TEMPI)**2.0 + 1.84D-8*TEMPI + 4.00D-6
      VIS(5) = -4.29D-12*(TEMPI)**2.0 + 4.88D-8*TEMPI + 1.02D-5
      VIS(6) = 4.76D-13*(TEMPI)**2.0 + 36.77D-8*TEMPI - 2.00D-6
C
C     ***** VISCOCITY OF MIXTURE ON SHELL SIDE *****
C
      VISNUM = (MOLFR(1)*VIS(1)*(MW(1)**0.5)) +
     $(MOLFR(2)*VIS(2)*(MW(2)**0.5)) + (MOLFR(3)*VIS(3)*(MW(3)**0.5))
     $+ (MOLFR(4)*VIS(4)*(MW(4)**0.5)) + (MOLFR(5)*VIS(5)*(MW(5)**0.5))
     $ + (MOLFR(6)*VIS(6)*(MW(6)**0.5))
C
      VISDEN = (MOLFR(1)*(MW(1)**0.5)) + (MOLFR(2)*(MW(2)**0.5))
     $  +   (MOLFR(3)*(MW(3)**0.5)) + (MOLFR(4)*(MW(4)**0.5))
     $  +   (MOLFR(5)*(MW(5)**0.5)) + (MOLFR(6)*(MW(6)**0.5))
      VISMIX = VISNUM/VISDEN
C
```

```
C       ***** VISCOCITY OF MIXTURE ON TUBE SIDE *****
C
        VISNUMT = (MOLFR(8)*VIS(1)*(MW(1)**0.5)) +
        $(MOLFR(9)*VIS(2)*(MW(2)**0.5)) + (MOLFR(10)*VIS(3)*(MW(3)**0.5))
        $+ (MOLFR(11)*VIS(4)*(MW(4)**0.5)) + (MOLFR(12)*VIS(5)*
        $  (MW(5)**0.5)) + (MOLFR(13)*VIS(6)*(MW(6)**0.5))
C
        VISDENT = (MOLFR(8)*(MW(1)**0.5)) + (MOLFR(9)*(MW(2)**0.5))
        $  + (MOLFR(10)*(MW(3)**0.5)) + (MOLFR(11)*(MW(4)**0.5))
        $  + (MOLFR(12)*(MW(5)**0.5)) + (MOLFR(13)*(MW(6)**0.5))
        VISMIXT = VISNUMT/VISDENT
C
C       ******DENSITY OF MIXTURE ON SHELL SIDE*****
C
        MWAVG = (MOLFR(1)*MW(1)) + (MOLFR(2)*MW(2)) + (MOLFR(3)*MW(3))
        +(MOLFR(4)*MW(4)) + (MOLFR(5)*MW(5)) + (MOLFR(6)*MW(6))
C
        DENAVG = (MWAVG*Y(7))/(8.314D0*TEMPI)
C
C       ***** DENSITY OF MIXTURE ON TUBE SIDE *****
C
        MWAVGT = (MOLFR(8)*MW(1)) + (MOLFR(9)*MW(2)) + (MOLFR(10)*MW(3))
        +(MOLFR(11)*MW(4)) + (MOLFR(12)*MW(5)) + (MOLFR(13)*MW(6))
C
        DENAVGT = (MWAVGT*Y(14))/(8.314D0*TEMPI)
C
C       *****REACTION TERMS*****
C
        RRF=(KX*PCO2*PCH4)/((1+KCO2R*PCO2+KCH4R*PCH4)**2)
        RSF=RCS*PCO2
        RR=RRF*(1.0D0-(((PCO*PH2)**2)/(KR*PCH4*PCO2)))
        RS=RSF*(1.0D0-((PCO*PH2O)/(KS*PCO2*PH2)))
        RCH4=RR*0.15D0/(0.08D0*AREASHELL)
        RCO2=(RR+RS)*0.15D0
        RCO=(2*RR+RS)*0.15D0
        RH2=(2*RR-RS)*0.15D0
        RH2O=RS*0.15D0
C
C       ***** PARAMETERS FOR THE ERGUN EQUATION *****
C
        POR = 0.60D0
        VOID = 1.0D0 - POR
        DP = 3.625D-4
        G =DENAVG*VELSHELL
        gc = 1.0D0
        T1 = LOG(RADTUBE/RADSHELL)
```

```
      T2 = RADSHELL**2+RADTUBE**2
      T3 = RADSHELL**2-RADTUBE**2
C
C     ***** PARAMETERS FOR THE DIFFUSION TERM *****
C
       KSTAR = (2.0D0*(40.0D-10)*0.50D0)*SQRT(8000.0D0*R*TEMPI/PI)
      /(1.0D0*3.0D0*R*TEMPI*(1.0D-3))
      KCH4 = KSTAR/SQRT(MW(1))
      KCO2 = KSTAR/SQRT(MW(2))
      KCO = KSTAR/SQRT(MW(3))
      KH2 = KSTAR/SQRT(MW(4))
      KAR = KSTAR/SQRT(MW(5))
      KH2O = KSTAR/SQRT(MW(6))
C
C     *****DIFFUSION TERMS ON THE SHELL SIDE *****
C
      DCH4 = (2.0D0*KCH4*RADTUBE*(PMETH-PTMETH))/T3
      DCO2 = (2.0D0*KCO2*RADTUBE*(PCARBD-PTCARBD))/T3
      DCO = (2.0D0*KCO*RADTUBE*(PCARBM-PTCARBM))/T3
      DH2 = (2.0D0*KH2*RADTUBE*(PHYD-PTHYD))/T3
      DH2O = (2.0D0*KH2O*RADTUBE*(PWAT-PTWAT))/T3
      DAR = (2.0D0*KAR*RADTUBE*(PARG-PTARG))/T3
C
C     *****DIFFUSION TERMS ON THE TUBE SIDE *****
C
      DTCH4 = (2.0D0*KCH4*(PTMETH-PMETH))/RADTUBE
      DTCO2 = (2.0D0*KCO2*(PTCARBD-PCARBD))/RADTUBE
      DTCO = (2.0D0*KCO*(PTCARBM-PCARBM))/RADTUBE
      DTH2 = (2.0D0*KH2*(PTHYD-PHYD))/RADTUBE
      DTH2O = (2.0D0*KH2O*(PTWAT-PWAT))/RADTUBE
      DTAR = (2.0D0*KAR*(PTARG-PARG))/RADTUBE
C
C     *****ODE'S*****
C
      YPRIME(1) = -(RCH4)-DCH4
      YPRIME(2) = -(RCO2)/(0.08D0*AREASHELL)-DCO2
      YPRIME(3)=  RCO/(0.08D0*AREASHELL)-DCO
      YPRIME(4)=  RH2/(0.08D0*AREASHELL)-DH2
      YPRIME(5) = 0.0D0-DAR
      YPRIME(6) = RH2O/(0.08D0*AREASHELL)-DH2O
      YPRIME(7) = -(G/(DENAVG*gc*DP))*(VOID/POR**3.0D0)*
      + ((150.0D0*VOID*VISMIX/DP) + 1.75D0*G)
      YPRIME(8) = -DTCH4
      YPRIME(9) = -DTCO2
      YPRIME(10) = -DTCO
      YPRIME(11) = -DTH2
```

```
      YPRIME(12) = -DTAR
      YPRIME(13) = -DTH2O
      YPRIME(14) = -(8.0D0*VISMIXT*VELTUBE*T1)/((T1*T2)+T3)
      RETURN
      END
C
      SUBROUTINE FCNJ (N, X, Y, DYPDY)
      INTEGER N
      DOUBLE PRECISION X, Y(N), DYPDY(N,*)
      RETURN
      END
```

NANOSIL MEMBRANE REACTOR

The only terms that are different in this program are the diffusion terms. Since all components except hydrogen have been demonstrated experimentally to have negligible diffusion across the Nanosil membrane, the diffusion terms for all species except hydrogen, have been set to be small (the Knudsen terms have been reduced by 10^{-6}). The diffusion term for hydrogen is the one that has been determined experimentally (see Chapter 5). Except for these changes, the program is the same as that for the porous Vycor membrane reactor.

APPENDIX B. CORRELATIONS FOR PFR OPERATION

When a Plug Flow Reactor (PFR) is operated as an integral reactor with substantial conversion from entrance to exit, concentration and temperature gradients may exist in both the radial and axial directions. The most difficult requirement to achieve is isothermality in both the radial and axial directions. If this is attained, radial concentration gradients will seldom be significant [1].

RULE FOR ACCEPTABLE DEVIATION FROM PLUG FLOW

Dautzenberg has presented the following criterion[2]:

$$N_{Pe} > N_{Pe\min}$$

where:

$$N_{Pe} = 0.087 N_{\mathrm{Re}_P}^{0.23} \frac{L}{d_P}$$

$$N_{Pe\min} = 8n \ln \frac{1}{(1-\mathrm{x})}$$

$$N_{\mathrm{Re}_p} = \frac{u d_p \rho_f}{\mu_f}$$

$$\mathrm{u} = \frac{v}{A_{c.s.}} = \frac{6.05 \times 10^{-6}\, m^3 s^{-1}}{0.754 \times 10^{-4}\, m^2} = 0.08 \text{ m s}^{-1}$$

$$N_{\mathrm{Re}_p} = \frac{u d_p \rho_f}{\mu_f} = \frac{(0.08\, m s^{-1})(0.326 \times 10^{-3} m)(0.5\, kg m^{-3})}{3.0 \times 10^{-5}\, N s m^{-2}} = 0.43$$

$$N_{Pe} = 0.087 N_{\mathrm{Re}_P}^{0.23} \frac{L}{d_P} = (0.087)(0.43)^{0.23} \left(\frac{4.0 \times 10^{-2} m}{0.326 \times 10^{-3} m}\right) = 8.82$$

$$N_{Pe\min} = 8n \ln \frac{1}{(1-\mathrm{x})} = (8)(3.78 \times 10^{-5}) \left(\ln \frac{1}{1-0.728}\right) = 3.94 \times 10^{-4}$$

where n is the number of moles in the reactor under stagnant flow condition.

$$8.82 >> 3.94 \times 10^{-4}$$

which establishes the general rule for acceptable deviation from plug flow for our experiments.

Gradients in the reactor can be classified as [1]**:**

a) Intraparticle gradients
b) Interphase gradients
c) Intrareactor gradients

a) Intraparticle gradients

Intraparticle temperature gradients are negligible if [3]:

$$\frac{|-\Delta H|(-r)r_P^2}{k_P T_s} < \frac{RT_s}{E}$$

This criterion is valid whether or not diffusional limitations exist in the catalyst.

$$\frac{|-\Delta H|(-r)r_P^2}{k_P T_s} = \frac{(255.65\times10^3\, Jmol^{-1})(26.4\, mols^{-1}m^3)(1.63\times10^{-4}\, m)^2}{(10.0\,\mathrm{Jm^{-1}s^{-1}K^{-1}})(973\ K)} = 1.8429\times10^{-5}$$

$$\frac{RT_s}{E} = \frac{(8.314\, Jmol^{-1}K^{-1})(973\, K)}{20.0\times10^3\, Jmol^{-1}} = 0.40$$

$$1.8429\times10^{-5} << 0.40$$

$$\frac{|-\Delta H|(-r)r_P^2}{k_P T_s} < \frac{RT_s}{E}$$

This establishes that the radial temperature gradients are not severe within the catalyst pellet.

If both temperature and concentrations exist together, then the criterion is [1]:

$$\Phi_s < \frac{1}{|n-\gamma\beta|}$$

where:

$$\Phi_s = \frac{-\Delta H(-r)r_P^2}{\beta T_s k_P}$$

$$\gamma = \frac{E}{RT_s}$$

$$\Phi_s = \frac{-\Delta H(-r)r_P^2}{\beta T_s k_P} = \frac{-(255.65\times10^3\,Jmol^{-1})(26.4\,mols^{-1}m^3)(1.63\times10^{-4}\,m)^2}{(-0.1)(973\,K)(10.0\,Jm^{-1}s^{-1}K^{-1})} = 1.84\times10^{-4}$$

where $\beta = \pm 0.1$ for most reactions (- for endothermic reactions [1])

$$\gamma = \frac{E}{RT_s} = \frac{20.0\times10^3\,Jmol^{-1}}{(8.314\,Jmol^{-1}K^{-1})(973\,K)} = 2.5$$

$$\frac{1}{|n-\gamma\beta|} = \frac{1}{|0.5-(2.5)(-0.1)|} = 1.33$$

$$1.84\times10^{-4} << 1.33$$

$$\Phi_s < \frac{1}{|n-\gamma\beta|}$$

This establishes that both concentration and radial gradients are not significant within the catalyst particle.

b) Interphase gradients

Mears [4] has presented the following criterion for isothermality between the catalyst and the bulk fluid:

$$\frac{|-\Delta H|(-r)r_P}{hT} < 0.15\frac{RT_b}{E}$$

$$\frac{|-\Delta H|(-r)r_P}{hT} = \frac{(255.65\times10^3\,Jmol^{-1})(26.4\,mols^{-1}m^{-3})(1.63\times10^{-4}\,m)}{(920.2\,Wm^{-2}K^{-1})(\mathrm{T})} = \frac{1.20}{T}$$

$$\text{where Sh} \approx \text{Nu} \approx 0.07\,N_{\mathrm{Re}_P} = (0.07)(0.43) = 0.03$$

and

$$\text{Nu} = \frac{hd_P}{k_P} = \frac{(h)(0.326\times10^{-3}\,m)}{10.0\,Jm^{-1}s^{-1}K^{-1}} = 0.03$$

which gives:

$$h = 920.2\ \text{Wm}^{-2}\ \text{K}^{-1}$$

$$0.15\frac{RT_b}{E} = 0.15\frac{(8.314\,Jmol^{-1}K^{-1})(973\,K)}{20.0\times10^3\,Jmol^{-1}} = 0.061$$

which gives:

$$\frac{1.20}{T} < 0.061$$

or $$T \approx T_b$$

This establishes that any differences between the bulk temperature and catalyst surface temperature are small. Mears [4] also points out that generally, temperature gradients become the source of nonideality long before concentration gradients do so.

c) Intrareactor gradients

Axial gradients may exist by virtue of conversion. These effects can be minimized by selecting the appropriate ratio of catalyst bed length to particle size. Mears [5], and Lange and Busch [6] have established the following criterion for the minimum reactor $\frac{L}{d_p}$ necessary to avoid significant axial gradients.

$$\frac{L}{d_p} > 92.0 N_{\mathrm{Re}_P}^{-0.23} n \ln \frac{1}{(1-\mathrm{x})}$$

$$\frac{L}{d_P} = \frac{4.0\times10^{-2}\, m}{0.326\times10^{-3}\, m} = 122$$

$$N_{\mathrm{Re}_p} = \frac{u d_p \rho_f}{\mu_f} = \frac{(0.08 ms^{-1})(0.326\times10^{-3}\, m)(0.5 kgm^{-3})}{3.0\times10^{-5}\, Nsm^{-2}} = 0.43$$

$$92.0 N_{\mathrm{Re}_P}^{-0.23} n \ln \frac{1}{(1-x)} = (92.0)(0.43)^{-0.23}(3.78\times10^{-5})(\ln \frac{1}{1-0.728}) = 5.5\times10^{-3}$$

$$122 >> 5.5\times10^{-3}$$

$$\frac{L}{d_P} > 92.0 N_{\mathrm{Re}_P}^{-0.23} n \ln \frac{1}{(1-x)}$$

This establishes that axial gradients if any are small.

Intrareactor radial temperature gradients are minimized or eliminated by decreasing the reactor diameter or diluting the catalyst with inert particles. Mears [4] has presented the following condition for the observed reaction rate not to deviate more than 5 percent from the isothermal case (no inter- or intraparticle gradients). If this is attained, the radial concentration gradients (external to the catalyst particles) will usually be insignificant.

$$\frac{|-\Delta H|(-r')r_R^2}{k_b T_w} < 0.4 \frac{RT_w}{E}$$

$$\frac{|-\Delta H|(-r')r_R^2}{k_b T_w} = \frac{\left|255.65\times10^{\,Jmol^{-1}3}\right|(3.58\,mols^{-1}m^{-3})(2.0\times10^{-3}\,m)^2}{(4.4\times10^{-2}\,Jm^{-1}s^{-1}K^{-1})(973\,K)} = 0.08$$

$$0.4\frac{RT_w}{E} = 0.4\frac{(8.314\,Jmol^{-1}K^{-1})(973\,K)}{20\times10^3\,Jmol^{-1}} = 0.16$$

$$0.08 < 0.16$$

$$\frac{|-\Delta H|(-r')r_R^2}{k_b T_w} < 0.4\frac{RT_w}{E}$$

The value of the thermal conductivity (k_b) used in the above expression is for Argon at 973K. This is a very stringent condition when in reality, the actual thermal conductivity is a combination of the conductivities of the fluid, catalyst particles, and quartz particles. The validity of this inequality establishes the insignificance of radial temperature gradients. Mears [1] also points out that if this is attained, the radial concentration gradients (external to the catalyst particles) will usually be insignificant.

SYMBOLS AND VALUES USED

$A_{c.s.}$	area of cross section of the reactor = 0.754×10^{-4} m^2
d_P	catalyst particle size = 0.326×10^{-3} m
E	activation energy for the reaction = 20.0 kJmol^{-1}
h	heat transfer coefficient of the bed (Wm^{-2}K^{-1})
ΔH	enthalpy change on reaction = 255.65 kJmol^{-1}
k_b	thermal conductivity of the packed bed = 4.4×10^{-2} Jm^{-1}s^{-1}K^{-1} (at 973K for Argon)
k_P	thermal conductivity of the catalyst particle = 10.0 Jm^{-1}s^{-1}K^{-1}
L	length of the packed bed = 4×10^{-2} m
n	number of moles in the reactor = 3.78×10^{-5} mol
N_{Pe}	Peclet number
N_{Re_P}	particle Reynolds number
r	reaction rate = 26.4 mols^{-1}m^{-3}
r'	reaction rate with inert quartz particles = 3.58 mols^{-1}m^{-3}
r_P	radius of particle = 1.63×10^{-4} m
r_R	reactor hydraulic radius = 2×10^{-2} m
R	gas constant = 8.314 Jmol^{-1}K^{-1} [7]
R_1	O.D. of inner tube = 10.0×10^{-3} m
R_2	I.D. of outer tube = 14.0×10^{-3} m
T	temperature (K)
T_b	temperature of the bulk phase = 973 K
T_s	temperature at the outside surface of the particle (K)
T_w	temperature of the reactor wall = 973 K
u	superficial velocity = 1.66×10^{-2} ms^{-1}
v	inlet flow rate = 79.5×10^{-6} m^{3}s^{-1}
x	fraction of reactant consumed = 0.728
β	heat generation function = -0.1
μ_f	fluid viscosity = 3.0×10^{-5} Nsm^{-2} (at 973K for Argon)
ρ_f	fluid density = 0.5 kgm^{-3} (at 973K for Argon) [7]
Φ_s	Damkohler group II

REFERENCES:

[1] C. N. Satterfield, Heterogeneous Catalysis in Industrial Practice, 2nd Ed., McGraw-Hill Inc. (1991).

[2] F. M. Dautzenburg, Characterization and Catalyst Development, An Interactive Approach, Sym. of the Division of Petroleum Chemistry, Inc., and the D-32 Committee of ASTM at the 196th National Meeting of the ACS, Los Angeles, CA. (1988).

[3] J. B. Anderson, Chem. Eng. Sci. 18 (1963) P. 147.

[4] D. E. Mears, Ind. Eng. Chem. Process Des. Dev. 10 (1971) P. 541.

[5] D. E. Mears, Chem. Eng. Sci. 26 (1971) P. 1361.

[6] R. Lange, A. Busch, Chem. Technol. 31 (1979) P. 232.

[7] J. M. Smith, H. C. van Ness, Introduction to Chemical Engineering Thermodynamics, 4th Ed., McGraw-Hill Co., New York, NY (1987) p. 106.

VITA

The author, Anil Prabhu grew up in Bangalore, India. After an undergraduate degree in Mechanical Engineering from Mangalore University, he joined the Mechanical Engineering Department of Iowa State University and graduated with a Master's degree. In 1994, he enrolled in the doctoral program in Chemical Engineering at Virginia Tech. This dissertation has been completed as part of the graduation requirements for a Ph. D. degree. It deals with the study of the catalytic transformation of greenhouse gases in a hydrogen selective membrane reactor. He is expected to graduate from Virginia Tech in May 2003.